UNIVERSIDADE DE LISBOA

FACULDADE DE CIÊNCIAS

DEPARTAMENTO DE QUÍMICA E BIOQUÍMICA

A MOLECULAR IMAGING APPROACH TO CYSTIC FIBROSIS

VERA FILIPA CERQUEIRA FERREIRA

DISSERTAÇÃO

MESTRADO EM BIOQUÍMICA

ESPECIALIZAÇÃO EM BIOQUÍMICA

2012/2013

UNIVERSIDADE DE LISBOA

FACULDADE DE CIÊNCIAS

DEPARTAMENTO DE QUÍMICA E BIOQUÍMICA

A MOLECULAR IMAGING APPROACH TO CYSTIC FIBROSIS

VERA FILIPA CERQUEIRA FERREIRA

DISSERTAÇÃO

MESTRADO EM BIOQUÍMICA

ESPECIALIZAÇÃO EM BIOQUÍMICA

ORIENTADORES: DOUTORA FILIPA MENDES E PROFESSOR DOUTOR CARLOS FARINHA

2012/2013

ACKNOWLEDGEMENTS

À minha orientadora, Dra. Filipa Mendes, agradeço todo o apoio prestado durante o trabalho, a sua total disponibilidade para me ajudar, a simpatia, e sobretudo a calma transmitida, que foi muito importante nesta fase final. Ao meu orientador Prof. Dr. Carlos Farinha agradeço também a sua disponibilidade para me ajudar e simpatia com que sempre me recebeu.

À Prof. Dra. Isabel Santos agradeço o facto de me ter recebido no Grupo de Ciências Radiofarmacêuticas.

Ao Bruno agradeço por toda a ajuda que me deu no início do trabalho, que foi essencial para depois poder continuá-lo sozinha. Sem a tua ajuda teria sido tudo muito mais difícil. Obrigada por teres sido um excelente colega de laboratório e teres animado os meus dias de trabalho (até resolveres ir embora!).

Ao Dr. João Galamba Correia agradeço toda a ajuda prestada nos últimos tempos e a forma com que sempre se disponibilizou para esclarecer todas as minhas dúvidas.

À Dra. Célia agradeço a simpatia e boa disposição constante, e sobretudo a ajuda sempre que o HPLC resolvia não funcionar.

À Dra. Lurdes Gano agradeço toda a ajuda com as marcações dos anticorpos.

À Elisa agradeço os conhecimentos transmitidos, a ajuda no laboratório e por sempre ter respondido a todas as minhas perguntas. Agradeço também à Dra. Goreti pela ajuda e pela boa energia existente no nosso laboratório.

Ainda no ITN, não posso deixar de agradecer às duas pessoas que tornaram o meu ano muito mais divertido. À Letícia e ao Filipe, muito obrigado pelas boas horas de almoço, pela alegria e pela amizade que ficará.

Ao Doutor Joaquim Marçalo agradeço a realização dos espectros de massa apresentados neste trabalho.

Agradeço ainda a todos os meus colegas de trabalho pela forma simpática como me receberam e pela constante ajuda ao longo do ano.

Fora do laboratório, agradeço a todos os meus amigos, especialmente, à Carol e à Safira, as pessoas mais divertidas que já conheci, à Catarina pela amizade ao longo destes anos e ao Carlos por ter tornado os últimos dois anos de faculdade muito mais interessantes ☺

Por fim, agradeço à minha família, em especial aos meus pais, pelo apoio incondicional e pela paciência para aturarem o meu mau humor nos últimos tempos.

RESUMO

A Fibrose Quística (FQ) é a doença autossómica recessiva letal mais comum na população caucasiana. É caracterizada por um mau funcionamento ao nível pulmonar, pancreático, gastrointestinal e reprodutivo, embora a principal causa de morbilidade e mortalidade se deva à progressiva disfunção pulmonar. A elevada concentração de electrólitos no suor constitui também uma das principais características da doença, sendo o teste do suor utilizado no seu diagnóstico.

A FQ é causada por mutações no gene *CFTR* (*Cystic Fibrosis Transmembrane Conductance Regulator*) que codifica uma proteína, também denominada CFTR, expressa na membrana apical de células epiteliais. Esta proteína funciona maioritariamente como um canal de iões cloreto activado por AMP cíclico. Até à data, 1939 mutações no gene *CFTR* foram identificadas, embora para a maioria não exista uma evidência directa de que sejam causadoras de doença.

As mutações causadoras de doença podem provocar uma redução dos níveis de CFTR na membrana plasmática (por redução da sua síntese ou por defeito no seu tráfego intracelular) ou a perda de capacidade de abertura do canal (*gating*)/conductância de aniões, mas ambas as situações resultam na perda do transporte de iões cloreto mediado pela CFTR. A mutação causadora de doença mais comum consiste na delecção de um resíduo de fenilalanina na posição 508 (F508del), estando presente em cerca de 90% dos pacientes.

Embora a identificação do gene *CFTR* tenha contribuído para um melhor conhecimento da doença e para o seu diagnóstico, o tratamento de pacientes com FQ ainda é maioritariamente baseado na atenuação dos sintomas inerentes à doença.

Nos últimos anos, novas potenciais terapias baseadas em fármacos (moduladores) que corrigem os defeitos de tráfego e função da CFTR têm emergido. Os moduladores podem ser correctores, que corrigem o defeito de tráfego da CFTR, aumentando assim a quantidade de proteína expressa na membrana plasmática, ou potenciadores, que corrigem o defeito no *gating* do canal, estimulando a sua actividade. Vários correctores e potenciadores da CFTR têm sido identificados e recentemente um potenciador (ivacaftor) foi aprovado para uso clínico nos EUA. Adicionalmente, uma terapia combinada usando um corrector (lumacaftor) e um potenciador (ivacaftor) encontra-se em fase III de ensaios clínicos para pacientes homozigóticos para a mutação F508del.

Contudo, a eficácia da correcção farmacológica do defeito de tráfego da CFTR mutante é actualmente avaliada em relação a alterações na concentração de iões cloreto no suor,

diferença de potencial nasal ou função respiratória, não existindo qualquer método capaz de detectar a presença da CFTR na membrana plasmática em organismos vivos, após tratamento com correctores.

Assim, o desenvolvimento de um método não-invasivo capaz de detectar a presença da CFTR na membrana plasmática seria bastante vantajoso na medida em que permitiria a avaliação da eficácia de terapias usando correctores, mas também a avaliação de quais os pacientes indicados para receber uma terapia baseada em potenciadores.

A Imagiologia Molecular poderá ser a ferramenta necessária para colmatar a falta de um método capaz de detectar a CFTR na membrana plasmática. Esta é definida como a visualização, caracterização e quantificação *in vivo* de processos bioquímicos ou biológicos a nível molecular, permitindo a visualização não-invasiva de uma molécula alvo *in vivo* devido à sua interacção com uma sonda de imagiologia molecular.

Assim, o trabalho apresentado nesta tese teve como principal objectivo o desenvolvimento de sondas radioactivas não-invasivas capazes de detectar a expressão da CFTR normal e da CFTR F508del corrigida, na membrana plasmática de células epiteliais pulmonares humanas. Estas sondas radioactivas foram baseadas em dois anticorpos anti-CFTR específicos para uma zona extracelular da CFTR, ECL1 e MA1-935, e em duas pequenas moléculas orgânicas conhecidas por inibir a função da CFTR, $CFTR_{inh}$-172a e GP_{inh}-5a. O isótopo ^{99m}Tc foi o escolhido para a marcação das biomoléculas devido às suas excelentes propriedades físicas e ao seu baixo custo e fácil obtenção.

No geral, o trabalho foi dividido em duas grandes partes: marcação radioactiva de anticorpos anti-CFTR e marcação radioactiva de inibidores da CFTR.

Relativamente aos anticorpos anti-CFTR, inicialmente caracterizaram-se as soluções contendo os anticorpos por SDS-PAGE, tendo-se concluído que ambas as soluções de anticorpo necessitavam de uma purificação prévia antes da marcação radioactiva. Após a eficiente purificação do anticorpo ECL1 através de um sistema de purificação adequado para IgGs e, devido a várias questões metodológicas, o trabalho prosseguiu apenas com o estudo do anticorpo ECL1 como sonda radioactiva para a detecção da CFTR.

De seguida, procedeu-se à marcação do anticorpo ECL1 pelo método directo com ^{99m}Tc(I) através de grupos sulfidril presentes no anticorpo após redução. O anticorpo ECL1 reagiu com o precursor *fac*-$[^{99m}Tc(H_2O)_3(CO)_3]^+$, tendo sido testadas várias proporções relativas entre ambos. Contudo, o rendimento máximo obtido, de entre várias marcações, foi de apenas 11% após 4 horas de incubação.

Tendo em conta o insucesso na marcação do anticorpo ECL1 com ^{99m}Tc(I), uma estratégia alternativa foi adoptada: a marcação radioactiva também pelo método directo com

^{99m}Tc(IV), através do uso de um ligando competidor, o MDP, como agente transquelante. Para tal, inicialmente optimizaram-se as condições de marcação com ^{99m}Tc(IV) utilizando o anticorpo IOR-CEA1, uma imunoglobulina G, tal como o anticorpo ECL1. Observou-se que quanto mais elevada era a concentração de IOR-CEA1, mais elevado o rendimento de marcação, obtendo-se um rendimento máximo de 72% para a concentração de IOR-CEA1 mais elevada (0.33 mg/mL). Assim, concluiu-se que o rendimento de marcação era dependente da concentração de anticorpo utilizada.

De seguida, o anticorpo ECL1 foi marcado com ^{99m}Tc(IV), reproduzindo-se as condições de marcação do anticorpo IOR-CEA1 em que se obteve o rendimento de marcação mais elevado. Contudo, e ao contrário da marcação com ^{99m}Tc(I) em que se atingiu um rendimento de marcação de 11%, não foi observado qualquer anticorpo ECL1 marcado.

A segunda parte do trabalho consistiu na marcação radioactiva dos inibidores da CFTR, $CFTR_{inh}$-172a e GP_{inh}-5a, com a unidade *fac*-$[^{99m}Tc(CO)_3]^+$, através do método indirecto, utilizando a estratégia do ligando bifuncional. Para tal, sintetizou-se o ligando bifuncional **L1**, contendo uma unidade quelante pirazolo-diamina, um espaçador propilénico e um grupo funcional -NH_2 para posterior conjugação aos inibidores.

De seguida, conjugou-se o inibidor $CFTR_{inh}$-172a, contendo um grupo funcional -COOH, ao ligando **L1**, resultando no bioconjugado final **B1**. Este reagiu com os precursores do tipo *fac*-$[M(H_2O)_3(CO)_3]^+$ (M = Re/^{99m}Tc), de modo a obter complexos do tipo *fac*-$[M(CO)_3(\kappa^3$-**B1**$)]^+$ (M = Re/^{99m}Tc; **Re1**/ **Tc1**). O complexo **Re1** foi obtido com rendimento moderado (55%) e a coordenação tridentada da unidade quelante pirazolo-diamina ao metal confirmada por espectroscopia de ressonância magnética nuclear através do carácter diastereotópico apresentado pelos protões pertencentes a essa unidade quelante.

Contudo não foi possível obter o complexo **Tc1**, e tal foi confirmado através da comparação do perfil cromatográfico do complexo **Re1** com o produto obtido da marcação de **B1**. Tendo em conta que uma das causas para a falha na marcação poderia ser a degradação do bioconjugado **B1**, mais concretamente, a unidade correspondente ao inibidor $CFTR_{inh}$-172a, devido à elevada temperatura de marcação (100 °C), a estabilidade do inibidor $CFTR_{inh}$-172a a 100 °C foi avaliada. Foi possível concluir que a degradação do inibidor tende a aumentar com o aumento do tempo de incubação a 100 °C.

Paralelamente, o inibidor GP_{inh}-5a, contendo também um grupo funcional -COOH, foi conjugado ao ligando **L1**. Contudo, após várias tentativas de purificação, não foi possível a obtenção do bioconjugado final **B2** com elevada pureza. Consequentemente, não foi possível a síntese dos complexos do tipo *fac*-$[M(CO)_3(\kappa^3$-**B2**$)]^+$, tal como aconteceu para **B1**.

Em suma, o principal objectivo do trabalho, isto é, o desenvolvimento de sondas marcadas radioactivamente, baseadas em anticorpos anti-CFTR e em inibidores da CFTR, para detecção da expressão da CFTR, não foi totalmente atingido.

Relativamente à primeira parte do trabalho, embora a marcação do anticorpo ECL1 com ^{99m}Tc(I) e ^{99m}Tc(IV) não tenha sido bem sucedida, todos os resultados contribuíram para a optimização da marcação do anticorpo e serão bastante úteis em estudos futuros.

Embora a marcação radioactiva de ambos os inibidores com ^{99m}Tc(I) também não tenha sido atingida, vários objectivos intercalares foram atingidos, como a síntese e caracterização do ligando bifuncional **L1**, dos bioconjugados **B1** e **B2-Boc** e do complexo de rénio **Re1**.

ABSTRACT

Cystic Fibrosis is caused by mutations in the *CFTR* gene, which encodes the CFTR protein, a chloride channel expressed in the apical membrane of epithelial cells. Therapies based in drugs that correct the trafficking (correctors) or the gating (potentiatiors) defects of CFTR are emerging. However, there is no available methodology to detect the expression of normal and rescued CFTR at the membrane in living organisms, after treatment with correctors. Molecular Imaging can be the solution, since it allows the noninvasive visualization of a target molecule *in vivo* by virtue of its interaction with a molecular imaging probe.

The major goal of this thesis was the development of radiolabelled imaging probes for the detection of normal and rescued F508del-CFTR at the PM of human epithelial pulmonary cells. These probes were based on two anti-CFTR antibodies (ECL1 and MA1-935) and two CFTR inhibitors ($CFTR_{inh}$-172a and GP_{inh}-5a) and the ^{99m}Tc radioisotope was the chosen radionuclide.

In the first part of the work, ECL1 antibody was purified and radiolabelled by the direct method, either with ^{99m}Tc(I) or ^{99m}Tc(IV). In the radiolabelling with ^{99m}Tc(I), the highest radiolabelling yield obtained was 11%. Optimization of the radiolabelling with ^{99m}Tc(IV) was performed with the antibody IOR-CEA1, and the conditions presenting the highest radiolabelling yield reproduced for the ECL1 antibody. However, no radiolabelled ECL1 could be obtained.

In the second part, the bifunctional chelator **L1** was synthesized in order to radiolabel the CFTR inhibitors with ^{99m}Tc(I) using the bifunctional chelator approach. The inhibitors $CFTR_{inh}$-172a and GP_{inh}-5a were successfully conjugated to **L1**, yielding, respectively, the bioconjugates **B1** and **B2-Boc**.

The final bioconjugate **B1** reacted with the *fac*-$[M(H_2O)_3(CO)_3]^+$ (M = Re/^{99m}Tc) precursors, to give the complexes of the type *fac*-$[M(CO)_3(\kappa^3$-**B1**$)]^+$ (M = Re/^{99m}Tc; **Re1**/ **Tc1**), but only **Re1** was obtained.

Palavras-chave

Fibrose Quística

Imagiologia Molecular

Tecnécio

Anticorpos anti-CFTR

Inibidores da CFTR

Keywords

Cystic Fibrosis

Molecular Imaging

Technetium

Anti-CFTR antibodies

CFTR inhibitors

TABLE OF CONTENTS

Acknowledgements i

Resumo iii

Abstract vii

Palavras-chave ix

Keywords ix

Table of contents xi

Abbreviations xv

1. Introduction 1

1.1. Cystic Fibrosis 1

1.1.1. History 1

1.1.2. Clinical features 1

1.2. Cystic Fibrosis Transmembrane Conductance Regulator: from gene to function 1

1.2.1. *CFTR* gene 2

1.2.2. CFTR protein structure 4

1.2.3. CFTR folding and trafficking 5

1.2.4. CFTR channel function 6

1.3. Therapeutic strategies for CF 7

1.4. Molecular Imaging 8

1.4.1. Nuclear molecular imaging for diagnostic 9

1.4.2. Radiochemistry of technetium 10

1.4.2.1. Technetium 10

1.4.2.2. Coordination chemistry of ^{99m}Tc 12

1.4.2.3. The $[M(CO)_3]^+$ core (M = ^{99m}Tc, Re) 12

1.4.2.4. Design of targeted ^{99m}Tc-radiopharmaceuticals 13

1.4.2.4.1. Direct method 14

1.4.2.4.2. Indirect method 15

1.4.3. Molecular Imaging: an approach to CF 16

1.5. Objectives 19

2. Materials and Methods 21

2.1. Radiolabelling of molecular imaging probes based on anti-CFTR antibodies 21

2.1.1. Anti-CFTR antibodies 21

2.1.2. Protein quantification 22

2.1.3. Sodium dodecyl sulfate-polyacrylamide gel electrophoresis 22

2.1.4. Antibody purification 23
2.1.5. Size exclusion-high performance liquid chromatography 23
2.1.6. Antibody reduction 24
2.1.7. Determination of sulfhydryl groups 25
2.1.8. Radiolabelling methods 25
2.1.8.1. Manipulation of radioactive compounds 25
2.1.8.2. Reading of radioactivity of radioactive solutions 25
2.1.8.3. Preparation of the *fac*-[^{99m}Tc(CO)$_3$(H$_2$O)$_3$]$^+$ precursor 25
2.1.8.4. Radiolabelling with ^{99m}Tc 26
2.1.8.5. Instant thin-layer chromatography-silica gel 27
2.2. Radiolabelling of molecular imaging probes based on CFTR inhibitors 28
2.2.1. Solvents and reagents 28
2.2.2. Characterization and purification techniques 28
2.2.3. Synthesis and characterization of compounds 32
2.2.3.1. CFTR$_{inh}$-172a and GP$_{inh}$-5a 32
2.2.3.1.1. (Z)-4-((4-oxo-2-thioxo-3-(3-(trifluoromethyl)phenyl) thiazolidin-5-ylidene)methyl)benzoic acid (CFTR$_{inh}$-172a) 32
2.2.3.1.2. (7R,9S)-7,8-dihydroxy-3-(4-hydroxy-5-(hydroxymethyl)tetra hydrofuran-2-yl)-7,9-dimethyl-3,7,8,9-tetrahydropyrimido [1,2-i]purine-9-carboxylic acid (GP$_{inh}$-5a) 33
2.2.3.2. Bifunctional chelator L1 33
2.2.3.2.1. 1-(2-bromoethyl)-3,5-dimethyl-1*H*-pyrazole (1) 33
2.2.3.2.2. *Tert*-butyl 2-(2-(3,5-dimethyl-1*H*-pyrazol-1-yl)ethylamino) ethyl carbamate (2) 34
2.2.3.2.3. *Tert*-butyl 2-((2-(3,5-dimethyl-1H-pyrazol-1-yl)ethyl)(3-(1,3-dioxoisoindolin-2-yl)propyl)amino ethylcarbamate (3) 35
2.2.3.2.4. *Tert*-butyl 2-((3-aminopropyl)(2-(3,5-dimethyl-1*H*-pyrazol-1-yl) ethyl)amino)ethylcarbamate (L1) 35 37
2.2.3.3. Bioconjugates B1 and B2 .....
2.2.3.3.1. (Z)-tert-butyl 2-((2-(3,5-dimethyl-1H-pyrazol-1-yl) ethyl) (3-(4-((4-oxo-2-thioxo-3-(3-(trifluoromethyl)phenyl) thiazolidin -5-ylidene) methyl) benzamido) propyl)amino)ethylcarbamate (B1-Boc) 37
2.2.3.3.2. (Z)-N-(3-((2-aminoethyl)(2-(3,5-dimethyl-1H-pyrazol-1-yl)ethyl) amino)propyl)-4-((4-oxo-2-thioxo-3-(3-

(trifluoromethyl)phenyl) thiazolidin-5-ylidene)methyl)benzamide (B1) 38

2.2.3.3.3. *Tert*-butyl 2-((3-((7S,9S)-7,8-dihydroxy-3-(4-hydroxy-5-(hydroxyl-methyl)tetrahydrofuran-2-yl)-7,9-dimethyl-3,7,8,9-tetrahydro pyrimido[1,2-i] purine-9-carboxamido)propyl)(2-(3,5-dimethyl-1H-pyrazol-1-yl)ethyl)amino) ethylcarbamate (B2-Boc) 39

2.2.3.3.4. (7R,9R)-N-(3-((2-aminoethyl)(2-(3,5-dimethyl-1H-pyrazol-1-yl) ethyl)amino)propyl)-7,8-dihydroxy-3-(4-hydroxy-5-(hydroxymethyl)tetrahydrofuran-2-yl)-7,9-dimethyl-3,7,8,9-tetrahydropyrimido [1,2-i]purine-9-carboxamide (B2) 40

2.2.3.4. Rhenium complex - *fac*-$[Re(CO)_3(\kappa^3\text{-B1})]^+$ (Re1) 41

2.2.4. Radiolabelling of B1 with the *fac*-$[^{99m}Tc(CO)_3]^+$ core .....

3. Results and Discussion 45

3.1. Radiolabelling of molecular imaging probes based on anti-CFTR antibodies 45

3.1.1. Characterization and purification of antibodies 46

3.1.2. Antibody analysis by SE-HPLC 48

3.1.3. Radiolabelling with ^{99m}Tc by the direct method 51

3.1.3.1. Antibody reduction 51

3.1.3.2. Radiolabelling with $^{99m}Tc(I)$ 52

3.1.3.3. Radiolabelling with $^{99m}Tc(IV)$ 54

3.1.3.3.1. Radiolabelling optimization 54

3.1.3.3.2. Radiolabelling of ECL1 57

3.2. Radiolabelling of molecular imaging probes based on CFTR inhibitors 59

3.2.1. Synthesis and characterization of the bifunctional chelator L1 60

3.2.2. Synthesis and characterization of bioconjugates 63

3.2.2.1. Synthesis and characterization of B1 63

3.2.2.2. Synthesis and characterization of B2 67

3.2.3. Synthesis and characterization of the complex *fac*-$[Re(CO)_3(\kappa^3\text{-B1})]^+$ Re1 69

3.2.4. Radiolabelling with ^{99m}Tc by the indirect method 73

3. Concluding remarks 77

4. Future perspectives 83

5. References 85

Annexes 91

ABBREVIATIONS

A_{280nm} – absorbance at 280 nm

A_{412nm} – absorbance at 412 nm

A_{750nm} – absorbance at 750 nm

Ab – antibody

ABC – ATP-binding cassette

ACN – acetonitrile

ASL – airway surface liquid

ATP – adenosine triphosphate

BFC – bifunctional chelator

BM – biomolecule

Boc – *tert*-butoxycarbonyl

bs – broad singlet

BSA – bovine serum albumin

cAMP – cyclic adenosine monophosphate

CEA – carcinoembryonic antigen

CF – cystic fibrosis

CFC – CFTR folding consortium

CFFT – cystic fibrosis foundation therapeutics

CFTR – cystic fibrosis transmembrane conductance regulator

CT – computed tomography

d – day or doublet

del – deletion

DHB – 2,5-dihydroxybenzoic acid

DIPEA – *N*,*N*-diisopropylethylamine

DMF – *N,N*-dimethylformamide

DMSO – dimethyl sulfoxide

DTT – dithiothreitol

e^- – electron

ECL – extracellular loop

ER – endoplasmic reticulum

ESI – electrospray ionization

EtOAc – ethyl acetate

eV – electron volt

FEV – forced expiratory volume

gCOSY – gradient correlation spectroscopy

gHSQC – gradient heteronuclear single quantum coherence

h – hour

HBTU – *O*-(benzotriazol-1-yl)-*N,N,N',N'*-tetramethyluronium hexafluorophosphate

HIG – human polyclonal immunoglobulin

HPLC – high performance liquid chromatography

ICL – intracellular loop

Ig – immunoglobulin

ITLC – instant thin-layer chromatography

m – mass or multiplet

mAb – monoclonal antibody

MALDI-TOF – matrix-assisted laser desorption/ionization - time of flight

mCi – millicurie

MDP – methylene diphosphonate

MEK – methyl ethyl ketone

MeOH – methanol

min – minute

MRI – magnetic resonance imaging

MS – mass spectrometry

MSD – membrane-spanning domain

MW – molecular weight

NBD – nucleotide-binding domain

NMR – nuclear magnetic resonance

pAb – polyclonal antibody

PBS – phosphate buffered saline

PEG – polyethylene glycol

PET – positron emission tomography

PM – plasma membrane

ppm – parts per million

pz – pyrazole

q – quartet

QIT – quadrupole ion trap

quint – quintuplet

RD – regulatory domain

R_f – retention factor

RP-HPLC – reversed-phase-high performance liquid chromatography

r.t. – room temperature

R_t – retention time

s – singlet

SDS-PAGE – sodium dodecyl sulfate-polyacrylamide gel electrophoresis

SE – size exclusion

sep – septuplet

SG – silica-gel

SPECT – single photon emission computed tomography

t – triplet

$t_{1/2}$ – half-life

TBAB – tetrabutylammonium bromide

TFA – trifluoroacetic acid

TLC – thin-layer chromatography

TMS – tetramethylsilane

US – ultrasound

UV – ultraviolet

Vis – visible

wt – wild type

y – year

z – charge

2-ME – 2-mercaptoethanol

α – alpha

β – beta

β^+ – positron

γ – gamma

δ – chemical shift

η – yield

λ – wavelength

κ – denticity

1. INTRODUCTION

1.1. CYSTIC FIBROSIS

1.1.1. History

Cystic fibrosis (CF) is the most common lethal autosomic recessive disease in the Caucasian population, affecting 1 in 2000 to 6000 live births and having a carrier frequency of 1 in 25 to 30 individuals.[1]

CF was first recognized as a separate disease entity in 1938 by Dorothy Andersen, when autopsy studies of malnourished infants distinguished a disease with abnormal mucus plugging of the glandular ducts. Life expectancy was approximately 6 months and death often occurred from lung infection. CF was also recognized to be genetic in origin and transmitted in an autosomal recessive pattern. At that point, studies on the basic defect focused on abnormalities in mucus.[2]

In 1948, a curious elevation of electrolytes in the sweat of patients with CF (approximately a 5-fold excess of sodium and chloride) implied that CF was not only a disorder of mucus. The discovery of the sweat electrolyte defect, which was later attributed to a defect in the chloride transport in the sweat glands, offered a diagnostic test for sweat salt concentration, allowing the identification of milder cases of CF. This defective chloride transport was also detected in epithelial tissues in the lung, pancreas and intestine.[2]

Later, in 1989, Riordan *et al.* identified the gene responsible for CF disease. The gene and the protein that it encodes were named cystic fibrosis transmembrane conductance regulator (CFTR), due to its connection to salt and fluid transport across epithelia.[3]

The CFTR protein functions as a chloride channel at the cell surface and is expressed in epithelial tissue in the airways, pancreas, intestine, testis and exocrine glands, as well in some non-epithelial tissue, such as cardiac myocytes, smooth muscle and erythrocytes.[1,4]

1.1.2. Clinical features

In close connection to the CFTR-expressing epithelia, CF is a disease that is associated with lung, pancreatic, gastrointestinal and reproductive malfunctioning. Different mutations in

the *CFTR* gene result in different levels of functioning CFTR at the plasma membrane (PM) and, consequently, different levels of disease severity.[5]

Most of the current morbidity and mortality among CF patients results from impairment of the pulmonary system. Usually, mucociliary transport in airways is facilitated by hydration of the airway surface liquid (ASL), a periciliary and mucus layer that lines the airway tract. However, the absence or dysfunction of CFTR leads to ASL dehydration, increased mucoviscosity and impaired mucociliary transport. This obstruction of the airways, together with inflammation and bacterial infection, especially with *Pseudomonas aeruginosa*, *Staphylococcus aureus* and at a later stage *Burkholderia cepacia*, leads to degradation of the lung anatomy and function.[5-7]

Pancreatic insufficiency is another characteristic feature, thought to occur in 90 to 95% of CF patients due to the obstruction of pancreas ducts. Pancreatic abnormalities can also cause CF-related diabetes in approximately 25% of CF patients with age > 25 years.

Defective secretion of digestive enzymes and resulting fat malabsorption are observed in the gastrointestinal system leading to chronical malnutrition and, in approximately 10 to 15% of the cases, CF infants are born with an intestinal obstruction (*meconium ileus*), a fatal condition if left untreated.[7]

Nearly 99% of males with CF are infertile due to glandular obstruction or congenital bilateral absence of the vas deferens *in utero*. Although less common, infertility in females with CF is thought to occur, due to thickening of cervical mucus.[7]

The excessive secretion of sodium chloride by the sweat glands is a major characteristic in CF patients, exceeding 60 mmol/L in the majority of patients.[7] To date, the sweat test, which measures the concentration of Cl^- in a small sample of pharmacologically induced sweat, continues to be the major test in CF diagnosis.

1.2. CYSTIC FIBROSIS TRANSMEMBRANE CONDUCTANCE REGULATOR: FROM GENE TO FUNCTION

1.2.1. *CFTR* gene

The *CFTR* gene (ABCC7) encompasses approximately 180 kilobase pairs in the long arm of chromosome 7 position q31.2.[7] To date, 1939 mutations in the *CFTR* gene have been

identified, although for most of them there is no direct evidence that they are in fact disease-causing.[8] The most common CF-causing *CFTR* mutation consists in the deletion of the phenylalanine residue at position 508 (F508del or ΔF508) and is present in one or both alleles in approximately 90% of CF patients.[1,7]

Mutations in the *CFTR* gene are grouped into six classes according the mechanism by which they are believed to cause CF (**Figure 1**).

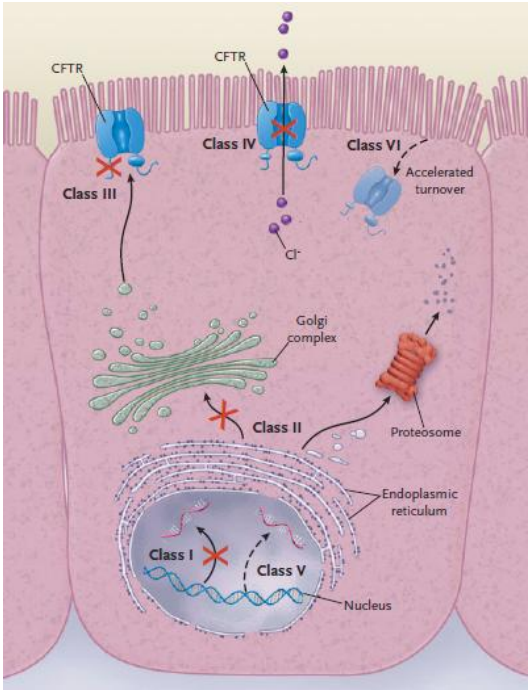

Figure 1: Different classes of CFTR mutations (from Rowe *et al.*, 2005).[9]

Class I and II mutations are characterized by a reduction in the amount of CFTR protein at the apical PM. Class I mutations can result from nonsense and frame-shift mutations, as well as mRNA splicing defects, leading to no protein synthesis. Class II mutations result in folding or maturation defects, which causes the protein to be retained at the endoplasmic reticulum (ER) and targeted to premature degradation.[7]

Class III and IV mutations encode full-length CFTR protein that is correctly PM located but lacks normal ion-channel activity. Class III mutations result in limited channel gating that arises from an abnormal function of a nucleotide-binding domain (NBD) that constitutes CFTR. CFTR with class IV mutations is able to open and close, but due to conductance defects, the ions are unable to pass through the channel as in the wild-type (wt) protein.[7,9]

In class V mutations, a reduced number of normal *CFTR* transcripts is produced, resulting in a reduced amount of normal CFTR protein at the cell surface.[7,9]

Finally, the recently introduced class VI is characterized by reduced stability of CFTR at the cell surface.[7,9]

F508del, the most common mutation, is considered a class II mutation. The mutant protein is not properly processed, which results in an almost absence of protein at the apical PM.[10] However, it was observed that after the correction of the processing defect of CFTR *in vitro* by incubation at low temperature[11] (see **Section 1.3. – Therapeutic strategies for CF**), the protein also displays a reduced activity as an ion channel,[12] and a decreased stability at the membrane.[13,14] For that reason, F508del can be also considered a class III and class VI mutation, respectively.

1.2.2. CFTR protein structure

CFTR protein is a cyclic adenosine monophosphate (cAMP)-regulated chloride channel, composed by 1480 amino acids and mainly expressed at the apical PM of epithelial cells. This protein belongs to the large adenosine triphosphate (ATP)-binding cassette (ABC) transporter superfamily, being the only member that functions as an ion channel.[15]

Each CFTR molecule is composed of five domains: two membrane-spanning domains (MSD1 and MSD2), two NBDs (NBD1 and NBD2) with two ATP-binding sites formed at the interface between the NBDs, and a regulatory domain (RD), which is a unique sequence that is not found in other ABC transporters (**Figure 2**).[7]

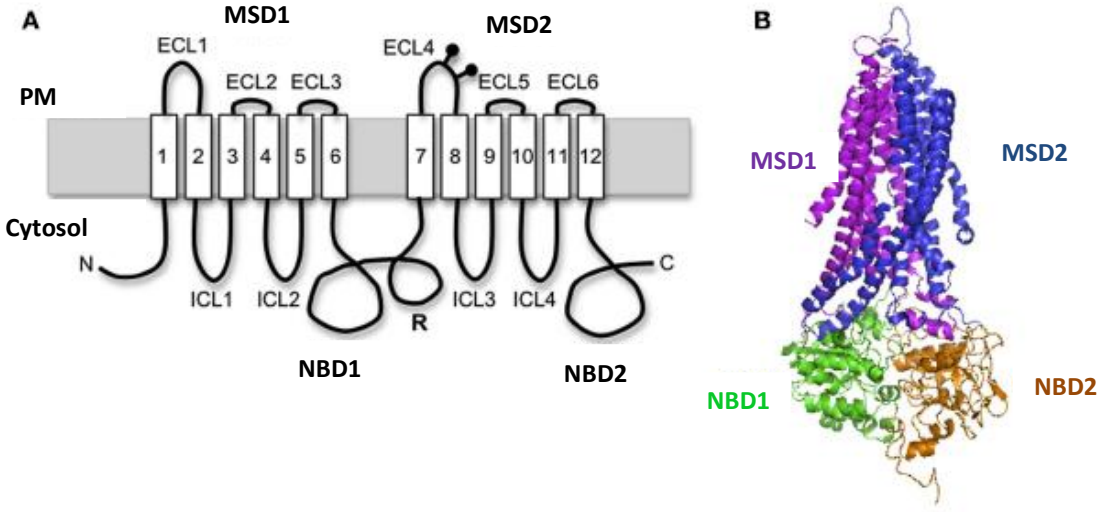

Figure 2: CFTR structural organization. (**A**) Schematic diagram of CFTR showing domain organization. (**B**) A predicted human CFTR structure based on homology model from the bacterial ABC transporter Sav1866 (adapted from Kim, 2012).[16]

Each MSD is constituted by six transmembrane segments connected by intra- and extracellular loops (ICLs and ECLs, respectively) that assemble to form the channel pore for anion transport. The RD contains multiple consensus phosphorylation sites and a large number of charged amino acids. It is thought that channel opening is promoted by the phosphorylation of the RD by the cAMP-dependent protein kinase A, although other kinases have also been implicated in the process.[4]

1.2.3. CFTR folding and trafficking

Given that CFTR is a membrane protein, it traffics through a series of membrane limited organelles until it reaches the PM, being this trafficking closely connected to its folding. However, due to its five domains, CFTR folding constitutes a complex process.

As occurs with membrane proteins, a new CFTR polypeptidic chain is inserted co-translationally in the ER membrane, while the nascent cytosolic domains associate with cytosolic molecular chaperones that help in the folding of CFTR. A branched 14-unit oligosaccharide, containing three glucose residues in one extremity, is added to the newly synthesized CFTR in the ECL4, in a process called *N*-glycosylation. Before the trimming of the *N*-glycosyl residues, they interact with calnexin, an ER membrane chaperone, promoting the folding of CFTR. CFTR is subjected to successive rounds of release-deglucosylation and rebinding-of-calnexin-reglucosylation, until it is folded.[17]

When CFTR is folded, it can exit the ER, proceeding through the secretory pathway. However, CFTR seems to have difficulties in achieving its native conformation. It is known that in most heterologously expressing cells, only 20 to 40% of newly synthesized CFTR nascent chain is converted in the mature CFTR, depending however on the cell model used.[1] The remaining misfolded CFTR does not escape the ER quality control and is disposed of by ER-associated degradation via the ubiquitin-proteasome pathway.[17]

The folding of F508del-CFTR is even more complex, since the phenylalanine residue at position 508 in NBD1 is not present, causing destabilization of NBD1 and compromising the overall domain assembly.[15] The mutant protein is retained at the early steps of its ER chaperone-dependent folding, recognized as misfolded by the ER quality control machinery, and degraded as described above.[17]

Under normal circumstances newly synthesized folded CFTR traffics from the ER to the Golgi apparatus in vesicles (**Figure 3**). Along the Golgi, the *N*-glycosylated immature CFTR

undergoes processing to produce mature CFTR - being these two forms clearly distinguishable by their different molecular weight (MW). Mature CFTR leaves the Golgi in secretory vesicles that can travel directly to the apical PM or to early/recycling endosomes. CFTR-containing vesicles traffic continually between early/recycling endosomes and PM. CFTR protein present in the PM can be also internalized (endocytosis) into early endosomes. Once in the early/recycling endosomes, CFTR can be recycled back to the PM or eventually targeted for degradation, following the late endosome-to-lysosome degradation pathway.[7,18]

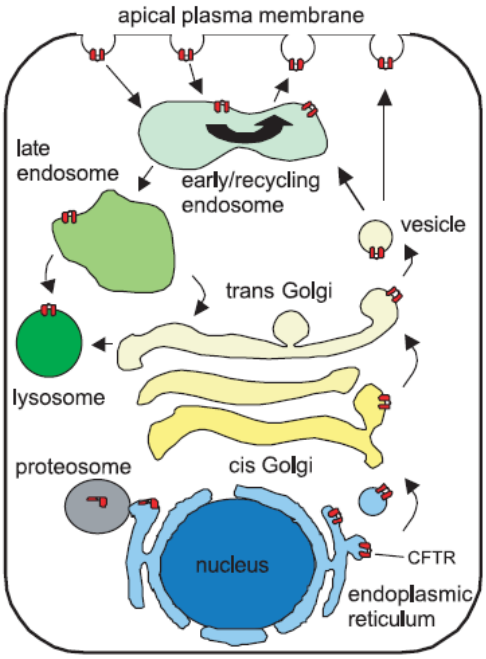

Figure 3: Trafficking of CFTR from the ER to the apical PM (from Bertrand *et al.*, 2003).[18]

1.2.4. CFTR channel function

Once at the cell surface, CFTR functions primarily as a chloride ion channel, but other anions can also pass through the channel, as the HCO_3^- ion.[19] Direct permeation of these anions through CFTR contributes to epithelial anion secretion. Besides being permeable to HCO_3^-, CFTR can also contribute indirectly to epithelial HCO_3^- secretion by stimulating Cl^-/HCO_3^- exchangers. Some epithelia that secrete HCO_3^- are affected by the loss of CFTR function, as the secretory epithelia of pancreatic duct, duodenum and airways, reflecting the importance of CFTR for the secretion of this ion.[20]

1.3. THERAPEUTIC STRATEGIES FOR CF

Identification of the defective gene responsible for CF has improved the understanding of CF disease and has helped diagnosis. However, a specific treatment for the CF basic defect still does not exist, and the symptomatic treatment remains the bedrock of CF patient care.

Nevertheless, in the last few years, specific CF therapies using drugs that target the basic defect in CF are emerging. These therapies are based on small organic molecules, known as modulators, which have been identified using high-throughput screenings. The modulators can be classified in correctors, designed to increase the amount of functional CFTR protein in the PM, and potentiators, which stimulate the chloride channel activity of the mutated protein.[7]

As previously mentioned, the F508del-CFTR is retained in the ER and undergoes premature degradation due to its instability and inefficient folding, resulting in an almost absence of protein inserted in the apical PM. However, it has been shown that F508del-CFTR can be rescued *in vitro* by incubation at low temperature (26 °C), evidencing that it can escape from the ER and reach the apical PM.[11] Nevertheless, when rescued, the mutated protein presents a shortened half-life and a reduced activity as an ion channel.[12-14] For that reason, a pharmacological treatment for F508del-CFTR should include a corrector and also a potentiator.

Recently, a new corrector, lumacaftor (VX-809, Vertex Pharmaceuticals, Cambridge, MA, USA), has proven to be more efficacious and selective for CFTR than all the previously reported correctors. Lumacaftor rescued F508del-CFTR to the PM, with the mutated CFTR protein exhibiting biochemical and functional characteristics similar to the normal CFTR.[21] In a phase IIa clinical study, lumacaftor was administered to adult patients homozygous for the F508del-CFTR mutation. Sweat chloride levels in lumacaftor-treated CF patients were modestly reduced and it was not observed an improvement in lung function or in CFTR-dependent nasal potential difference.[22] However, evidence of sweat chloride improvement, although small in magnitude, suggested that correction of the F508del-CFTR was possible.

Several potentiators have also been developed for CFTR. One of them, ivacaftor (Kalydeco, VX-770, Vertex Pharmaceuticals), which targets G551D-CFTR (a gating mutant that produces correctly localized but unfunctional protein) but also other gating mutants, was approved in 2012 by the Food and Drugs Administration in the USA, being the first drug targeting the molecular basis of CF. Since ivacaftor alone was not sufficient to meaningfully alter CFTR activity in patients homozygous for the F508del-CFTR mutation,[23] and to improve upon the effects of lumacafor alone, there is an ongoing clinical trial in phase III assessing the combined effect of ivacaftor with lumacaftor in F508del homozygous patients. The final results

of the phase II study have indicated that high doses of lumacaftor combined with ivacaftor significantly improved the forced expiratory volume (FEV).[24]

Currently, there is no available methodology to detect the presence of normal CFTR or rescued F508del-CFTR at the PM in living organisms (model animals or human subjects), after treatment with correctors. Thus, the development of a non-invasive method capable of detecting the presence of CFTR at the PM would be a great advantage for the follow up of the combined therapeutic approach using correctors and potentiators.

1.4. MOLECULAR IMAGING

Molecular imaging can be defined as the *in vivo* visualization, characterization and quantification of biological or biochemical processes at the molecular level. It allows the noninvasive visualization of a target molecule *in vivo* by virtue of its interaction with a molecular imaging probe.[25]

During the last decades, the field of molecular imaging has grown exponentially and to date, the predominant medical imaging modalities can be generally divided in two categories: structural and functional. Imaging modalities, such as computed tomography (CT), ultrasound (US) and magnetic resonance imaging (MRI) provide structural and anatomical information of normal or pathologic processes. On the other hand, techniques like positron emission tomography (PET), single photon emission computed tomography (SPECT) and optical imaging (bioluminescence and fluorescence) allow the visualization and characterization of biochemical pathways *in vivo* (functional imaging).[26] Among the functional imaging modalities, PET and SPECT are considered the most important. However, each imaging modality has its own strengths and limitations and none allows structural, functional and molecular information. For that reason, combinations of multiple imaging modalities – the so-called multimodality imaging - are currently emerging.[27]

Between the different imaging modalities mentioned above, PET and SPECT are included in the field of nuclear imaging and are clinically used for diagnosis and follow up of therapeutic strategies in several diseases, such as cancer and in the cardiology and neurology fields.[27,28]

1.4.1. Nuclear molecular imaging for diagnostic

In classical nuclear imaging, radioactive compounds named radiopharmaceuticals, are used for *in vivo* imaging. Their biodistribution is determined by their physicochemical properties, such as size, shape, charge and lipophilicity. These are called perfusion radiopharmaceuticals and usually are low MW complexes that target high-capacity systems and processes, including phagocytosis, hepatocyte clearance, glomerular filtration, and bone absorption.[29]

In nuclear molecular imaging, a radiolabelled biomolecule (BM) recognizes its target present in the target tissue, producing imaging signals by means of radioactive decay.[25] This radiolabelled BM is called a targeted radiopharmaceutical.[29] Hence, the biodistribution of these radiopharmaceuticals is determined by specific interactions between the BM and its target, which can be for example antigen, enzymatic or receptor-binding interactions. Considering the theme of this thesis, only targeted radiopharmaceuticals will be studied.

The targeted radiopharmaceutical is administered at very low concentrations (~ 10^{-6} - 10^{-10} M) and will optimally reach concentrations at the target site in the pico- to femtomolar range. For that reason, the BM should present a high affinity to its target, and also a high specificity, resulting in its selective uptake and distribution at the target tissues. Besides that, radiopharmaceuticals should not have any pharmacological effect.[29]

For diagnostic purposes, the BM can be radiolabelled with positron (β^+)-emitting isotopes for PET or gamma (γ)-emitting isotopes for SPECT. PET technique requires the use of radionuclides that decay via β^+-emission, such as the non-metallic isotopes ^{124}I ($t_{1/2}$ = 99.6 hours (h)), ^{18}F ($t_{1/2}$ = 109.7 min), ^{11}C ($t_{1/2}$ = 20.4 min), ^{13}N ($t_{1/2}$ = 9.96 min) and ^{15}O ($t_{1/2}$ = 2.03 min), or the metallic isotopes ^{64}Cu ($t_{1/2}$ = 12.7 h) and ^{68}Ga ($t_{1/2}$ = 68.1 min). These radioactive isotopes have an excess of protons in the nucleus, making them unstable, and causing the ejection of a β^+ particle from the nucleus. When this particle collides with an electron (e^-), in a process called annihilation, the combined mass of the β^+ and e^- is converted into two gamma (γ) photons of high energy (511 k electron volt (eV) each), which travel to opposite directions. A PET scanner detects the two anti-parallel γ photons and images are acquired.[27,28]

On the other hand, SPECT technique requires the use of radionuclides that decay via the emission of single γ rays with different energies, such as ^{99m}Tc ($t_{1/2}$ = 6.02 h), ^{123}I ($t_{1/2}$ = 13.20 h), ^{111}In ($t_{1/2}$ = 67.9 h) and ^{67}Ga ($t_{1/2}$ = 78.26 h). These γ rays are detected by a γ camera and images are acquired.[27,28] From these radionuclides, over 90% of all diagnostic imaging studies carried out worldwide use the ^{99m}Tc isotope, mainly due to its almost ideal physical properties and its low cost and easy availability.[29]

These nuclear imaging modalities present limitless penetration depth and allow the imaging of molecular targets/processes with high sensitivity. However, compared with other imaging modalities, they present low spatial resolution.[30,31] This problem has been overcome with instruments incorporating dual-modality imaging, for example PET-CT and SPECT-CT, which combine the high sensitivity of the nuclear techniques with the high spatial resolution of CT.[27]

1.4.2. Radiochemistry of technetium

1.4.2.1. Technetium

Technetium is a transition metal with atomic number 43, belonging to group 7 of the Periodic Table. The element was first predicted by Mendeleev and isolated, in 1937, by Segré and Perrier. Twenty-two isotopes of Tc (^{90}Tc to ^{111}Tc) have been reported, and all of them are radioactive.[32]

The ^{99m}Tc isotope is used in about 90% of all diagnostic imaging studies, mainly due to[29]:

- Low cost and easy availability, through a commercial ^{99}Mo/^{99m}Tc generator;
- Half-life of 6.02 h, which is sufficiently long to allow the synthesis of the radiopharmaceutical and the acquisition of the images, but short enough to allow administration of millicurie (mCi) amounts, minimizing the radiation dose to the patient;
- Emission of γ photons with a sufficiently high energy (140 keV) to easily penetrate in the tissues and be detected externally by a γ camera;
- Diverse coordination chemistry, allowing the formation of a wide variety of ^{99m}Tc complexes with different physico-chemical and biological properties.[32]

In 1959, the development of a ^{99}Mo/^{99m}Tc generator by the Brookhaven National Laboratory (Upton, NY, USA) contributed to the easy availability of the ^{99m}Tc isotope and, consequently, to its widespread use in the development of diagnostic radiopharmaceuticals.[33] This ^{99}Mo/^{99m}Tc generator, contains ^{99}Mo, in the form of molybdate ($[^{99}MoO_4]^{2-}$), absorbed at the top of an alumina column (**Figure 4A**). The ^{99}Mo isotope has a half-life of 66.0 h and decays

continuously via β^--emission, originating the meta stable ^{99m}Tc isotope (86%) and the ^{99}Tc isotope (14%). The ^{99m}Tc isotope can be preferentially eluted from the column, in the form of pertechnetate ($[^{99m}TcO_4]^-$), with a saline solution (0.9% NaCl). At this ionic strength, the singly charged $[^{99m}TcO_4]^-$ elutes, while $[^{99}MoO_4]^{2-}$ remains adsorbed. The ground state ^{99}Tc is a long-lived isotope ($t_{1/2}$ = 2.12x10^5 years (y)) that decays to stable ^{99}Ru via β^- emission (**Figure 4B**).[33,34]

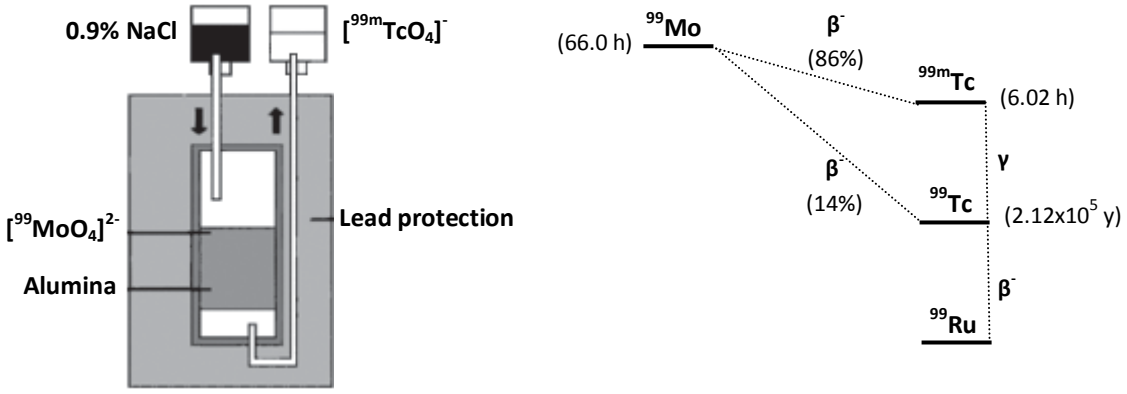

Figure 4: (**A**) Schematic representation of a ^{99}Mo/^{99m}Tc generator. (**B**) Radioactive decay of the isotopes present in a ^{99}Mo/^{99m}Tc generator.

The concentration of $[^{99m}TcO_4]^-$ in the eluate obtained from the generator is in the range of 10^{-8} to 10^{-6} M. For that reason, the synthesis of a radiopharmaceutical using the ^{99m}Tc isotope proceeds in a very dilute aqueous solution. This makes impossible the characterization of the ^{99m}Tc complexes by the usual techniques in chemistry, since only chromatographic methods with γ detection are capable of monitoring these complexes.[29,34] Therefore, due to the chemical similarities between Tc and rhenium (Re), the later has been used as a surrogate of Tc. Re also belongs to group 7 of the Periodic Table and presents an atomic radius (1.37 Å) similar to Tc (1.36 Å), i.e., they are structurally similar. If a ^{99m}Tc and a Re complex present an identical chromatographic behavior by HPLC, it is assumed that they have the same chemical structure. Hence, Re complexes can offer useful information for structural characterization of ^{99m}Tc complexes because Re complexes can be analyzed by the usual analytical and spectroscopic techniques in chemistry, for example, by nuclear magnetic resonance (NMR) or infrared spectroscopy. However, there are differences between the ^{99m}Tc and Re complexes that should be taken into account, such as the more difficulty in reducing Re complexes and their higher kinetic inertness, comparing with ^{99m}Tc complexes.[32]

1.4.2.2. Coordination chemistry of ^{99m}Tc

Regardless the strategy adopted (see below, **Section 1.4.2.4.**), the design of ^{99m}Tc-radiopharmaceuticals will depend on the understanding of the coordination chemistry of ^{99m}Tc. Factors such as stable oxidation states and core structures are crucial in the design of effective targeted ^{99m}Tc-radiopharmaceuticals.

As previously mentioned, the chemistry exhibited by Tc is rich and diverse, mainly due to the several different oxidation states that it can present (-I to +VII) and the large number of coordination geometries it can adopt.

The $[^{99m}TcO_4]^-$ anion presents the metal in the highest oxidation state possible (+VII). This ^{99m}Tc species is very stable in solution and does not bind directly to any ligand. Thus, for the synthesis of a ^{99m}Tc-radiopharmaceutical, reduction of ^{99m}Tc(VII) to a lower oxidation state in the presence of a suitable ligand is a prerequisite. When reduced in the presence of a ligand, the $[^{99m}TcO_4]^-$ usually does not release all the oxygen atoms, leading to complexes with different ^{99m}Tc cores.[32]

^{99m}Tc is usually used in the oxidation state +V as $[^{99m}TcO]^{3+}$ or $[^{99m}TcO_2]^+$ cores.[29] Since the coordination chemistry of the $[^{99m}TcO]^{3+}$ core has been explored for a long time, further advances are more likely when novel lower oxidation states are studied. One of the most promising and developed organometallic core for radiolabelling of BMs is the ^{99m}Tc(I)- and Re(I)-tricarbonyl core $[M(H_2O)_3(CO)_3]^+$ (M = ^{99m}Tc/^{188}Re), or simply the $[M(CO)_3]^+$ core. It has been adopted as an alternative strategy to the ^{99m}Tc(V) complexes for the synthesis of ^{99m}Tc-radiopharmaceuticals. Nowadays, the research is focused in the synthesis of new chelators that can coordinate strongly to the $[M(CO)_3]^+$ core.[32-35]

1.4.2.3. The $[M(CO)_3]^+$ core (M = ^{99m}Tc, Re)

Alberto *et al.* were the first to report the one-step synthesis of an organometallic ^{99m}Tc(I) aqua-ion, $[^{99m}Tc(H_2O)_3(CO)_3]^+$, useful as a precursor for the radiolabelling of BMs for diagnostic purposes.[36] The ^{99m}Tc(I)-tricarbonyl precursor was synthesized by direct reduction of the $[^{99m}TcO_4]^-$ from the oxidation state +VII to +I, using sodium boranocarbonate ($Na_2[H_3BCO_2]$) as reductant and also as an *in situ* source of carbon monoxide (CO).[37]

Nowadays, the precursor $[^{99m}Tc(H_2O)_3(CO)_3]^+$ can be obtained in quantitative yield by directly adding $[^{99m}TcO_4]^-$ in 0.9% NaCl to a lyophilized commercial kit (IsoLink® kit, Mallinckrodt-Covidien, Petten, The Netherlands), followed by incubation at 100 °C for 20

minutes. The ready availability of the precursor directly from the $[^{99m}TcO_4]^-$ constitutes one advantage of the use of this ^{99m}Tc(I)-tricarbonyl precursor (**Figure 5**).

The preparation of the Re homologue $[^{188}Re(H_2O)_3(CO)_3]^+$ was also accomplished,[38] although deviated slightly from the preparation of the ^{99m}Tc(I)-tricarbonyl precursor, since, as previously mentioned, Re is more difficult to reduce and reacts, in general, much slower.[32,39]

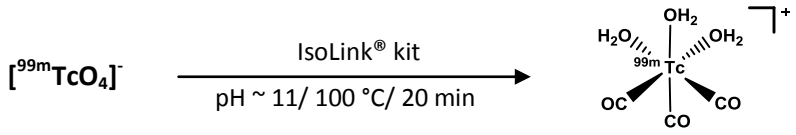

Figure 5: Synthesis of the organometallic precursor $[^{99m}Tc(H_2O)_3(CO)_3]^+$.

The $[M(CO)_3]^+$ core is stable, even at high temperature and extended reaction time.[40] Complexes of $[M(CO)_3]^+$ exhibit a d^6 low-spin electronic configuration and, for that reason, are kinetically inert. The core contains three tightly coordinated CO ligands and three water molecules, which are very labile and can be readily replaced by mono-, bi- or tridentate chelators.[41] The tridentate chelators form ^{99m}Tc(I)-tricarbonyl complexes with the highest *in vivo* stability, which is essential for medical applications.[33] The $[M(CO)_3]^+$ core is very compact, being significantly smaller than the complexes in the oxidation state (+V). This fact can be an advantage since it is thought that the smaller the complex, the higher the likelihood that the biological activity will not be altered.[33,41]

The diverse coordination chemistry of the $[M(CO)_3]^+$ core offers an opportunity for the development of new chelators. However, the ideal chelator for the $[^{99m}Tc(CO)_3]^+$ core must displace the water molecules quickly, since the reaction time is limited by the short half-life of the ^{99m}Tc isotope.

1.4.2.4. Design of targeted ^{99m}Tc-radiopharmaceuticals

The choice of the ^{99m}Tc-radiolabelling approach for the synthesis of a targeted ^{99m}Tc-radiopharmaceutical depends on the BM that constitutes the radiopharmaceutical. The BM can be an antibody (Ab), a small peptide or a nonpeptidic molecule that can act as an agonist or antagonist of a specific receptor, or substrate or inhibitor of an enzyme or channel.[29,33,35]

In the last three decades, several approaches for ^{99m}Tc-radiolabelling of BMs have been developed. These approaches include the direct and indirect method.

1.4.2.4.1. Direct method

The direct radiolabelling method relies on the binding of ^{99m}Tc to endogenous free sulfhydryl groups, generated by reduction of an Ab to provide the binding sites. This approach is easy to carry out, but the major disadvantage is that if it is used a great amount of reducing agent, too many disulfide bonds are reduced, increasing the risk for disrupting key linkages needed to maintain protein folding, integrity and immunoreactivity.[42] This method is only applied to Abs because many small BMs do not have any disulfide bonds, or in many cases the disulfide bond is too critical for maintaining their biological properties and cannot be reduced.[35]

First, the disulfide bonds present in the Ab are reduced by its incubation with a molar excess of a reducing agent, usually 2-mercaptoethanol (2-Me).[42] Due to the diverse coordination chemistry of Tc and the recent development of a new $[^{99m}Tc(CO)_3]^+$ core, the reduced Ab can be radiolabelled in two different ways. It should be noted that both radiolabelling requires the generation of sulfhydryl groups, which show high affinity binding sites for ^{99m}Tc.

Radiolabelling with ^{99m}Tc(I)[40,42]

The Ab is radiolabelled using the organometallic precursor *fac*-$[^{99m}Tc(H_2O)_3(CO)_3]^+$, readily prepared using the Isolink technology. The radiolabelling is performed under mild, physiological conditions, suitable for the radiolabelling of temperature-sensitive molecules, such as Abs. This method has been used for the radiolabelling of several monoclonal antibodies (mAb) and peptides. In general, high radiolabelling yields and high stability are obtained.[42]

Radiolabelling with ^{99m}Tc(IV) [43-45]

The Ab is radiolabelled by transchelation of ^{99m}Tc from a ^{99m}Tc-complexing agent, usually ^{99m}Tc(V) or ^{99m}Tc(IV). The complexing agent is a weak competing ligand, such as methylene diphosphonate (MDP), that serves to stabilize the reduced ^{99m}Tc for presentation to the

reduced Ab (**Figure 6**).[42,43] This radiolabelling method was introduced by Schwartz and Steinstrasser, in 1987, and later optimized by Mather and Ellison, in 1990. For example, when MDP is used, the ^{99m}Tc-MDP is produced by directly adding $[^{99m}TcO_4]^-$ in 0.9% NaCl to a MDP kit containing, between other constituents, a reducing agent, that reduces the ^{99m}Tc from the oxidation state (+VII) to (+IV). This method has also proved to be a good procedure to obtain high radiolabelling efficiency and a stable radiolabelled Ab.

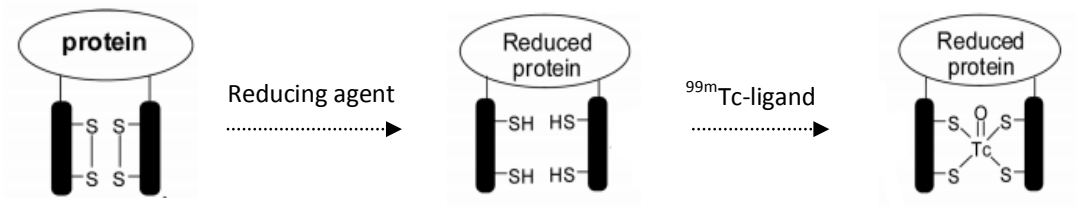

Figure 6: Radiolabelling of BMs containing endogenous sulfhydryl groups by the direct method, using a weak competing ligand.

While the ^{99m}Tc(V)/(IV) precursor has to be stabilized by multidentate ligands, which can act as competitors during the radiolabelling, only molecules of water have to be displaced in the case of the radiolabelling with the *fac*-$[^{99m}Tc(H_2O)_3(CO)_3]^+$ precursor (^{99m}Tc(I)). For that reason, much lower concentrations of the BM are required for efficient radiolabelling with ^{99m}Tc(I), since its nucleophilic groups do not have to compete with other ligands.[40]

1.4.2.4.2. Indirect method[32,35]

The growing demand for more specific ^{99m}Tc-radiopharmaceuticals has prompted the development of targeted radiopharmaceuticals mainly based on the bifunctional chelator (BFC) approach (**Figure 7**). This indirect radiolabelling method can be applied to any BM (Ab or small molecule without sulfhydryl groups) linked to a BFC.

The strategy involves a three-component system of a high affinity BM, also known as targeting BM, a BFC/spacer of different nature and the radiometal (^{99m}Tc), which together with the BFC form a chelate. The targeting capability resides in the BM covalently linked to the chelate.

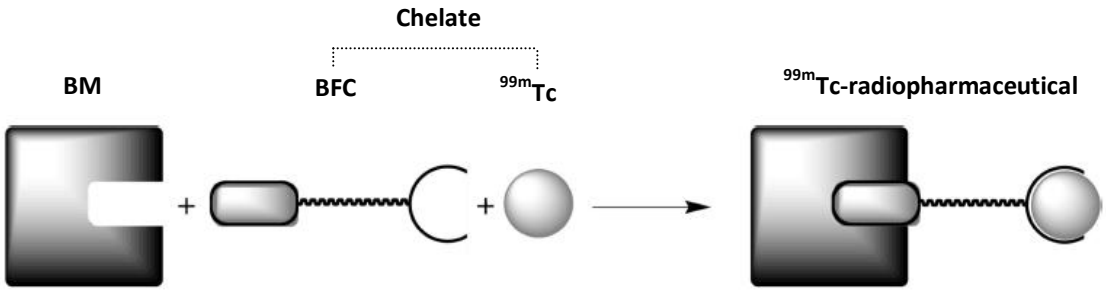

Figure 7: Schematic representation of the BFC approach (adapted from Bartholomä, 2010).[33]

The BFC is designed to bind to the radiometal, stabilizing it, while also providing a second functional group at the other terminus, used to form a strong covalent bond with the BM.[33] The choice of the BFC is determined by the nature and oxidation state of ^{99m}Tc. Whenever possible, the chelate is kept away from the target motif that recognizes the BM in order to minimize possible interferences. The site of attachment to the BM, the size, charge and lipophilicity of the chelate, and also the length of the covalent spacer, need to be optimized for maximum binding of the BM to its target.[35]

The BM can be radiolabelled using the precursor $[^{99m}Tc(H_2O)_3(CO)_3]^+$, or other ^{99m}Tc cores, depending on the BFC linked to the BM. Once the BFC-BM conjugate is prepared, radiolabelling can be accomplished with the chosen ^{99m}Tc core in the presence of a sufficient amount of the BFC-BM conjugate.

The BFC approach is the most popular strategy applied in the design of targeted radiopharmaceuticals, due to the likelihood of retaining the binding affinity of the BM to its target with a careful selection of the BFC for radiolabelling.

1.4.3. Molecular Imaging: an approach to CF

Recently, a novel CF therapy using an effective drug that targets the basic defect in CF has been approved. This therapy, and others already in clinical trials, is based on small molecules (correctors and potentiators) that partially restore the trafficking and functional defects of F508del-CFTR (and other mutants).[21-24]

However, the efficacy of the pharmacological correction of the folding/trafficking of mutant CFTR protein is assessed by the clinical outcome in terms of benefit into sweat

chloride, nasal potential difference or lung function, since there is no available methodology to detect the presence of normal or rescued mutant CFTR at the PM.

Nuclear molecular imaging can be the answer to this problem. In the field of CF, assessment of lung inflammation,[46] lung clearance[47] and aerosol delivery[48] have already been performed with PET and SPECT probes, proving the applicability of these techniques for CF patients.

Therefore, the development of a nuclear imaging probe capable of detecting CFTR at the PM in a noninvasive way would be a great advantage. This probe would allow the assessment of the efficacy of the pharmacological correction (either single or combined therapies) of mutant CFTR protein by imaging of the presence of the rescued CFTR at the epithelia of patients undergoing clinical trials. This detection would be particularly relevant in the lung, which is the most affected organ by CF. Besides that, this imaging probe could also indicate which would be the best subjects to receive a pharmacological potentiator therapy, as is the case of patients with the G551D mutation.

1.5. OBJECTIVES

The major goal of this thesis project was the development of radiolabelled imaging probes for the detection/visualization of normal and rescued F508del-CFTR at the PM of human epithelial pulmonary cells. These radiolabelled probes were based on small molecules with high affinity for CFTR, such as anti-CFTR Abs and CFTR inhibitors, labelled with the ^{99m}Tc radioisotope, due to its almost ideal physical features (see **Graphical Abstract**).

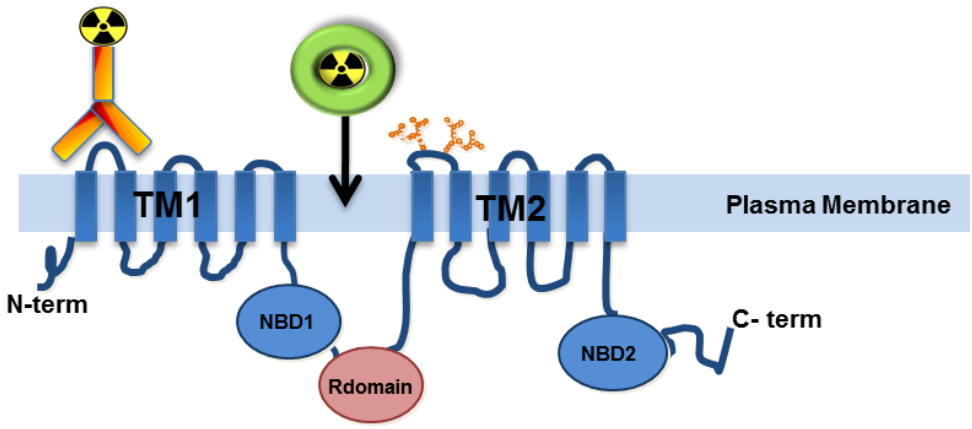

Graphical abstract of CFTR at the membrane of epithelial cells and the two types of probes to be developed

Different specific objectives were established depending on the small molecule used for the radiolabelling. Relatively to the development of radiolabelled probes using anti-CFTR Abs, the objective was the radiolabelling of two Abs against an extracellular domain of CFTR, ECL1 and MA1-935, using the direct radiolabelling method that takes advantage of the endogenous sulfhydryl groups of the Abs. The first goal was the radiolabelling of the Abs with ^{99m}Tc(I), although it was also envisaged the radiolabelling using ^{99m}Tc(IV), as alternative, in case the first radiolabelling strategy could not be successfully accomplished.

Relatively to the development of radiolabelled probes using CFTR inhibitors, the objective was the radiolabelling of two inhibitors of CFTR function, $CFTR_{inh}$-172a and GP_{inh}-5a, using the indirect radiolabelling method. For that reason, several specific objectives were established:

1. Synthesis and characterization of a BFC containing a pyrazolyl-diamine chelating unit;
2. Conjugation of both inhibitors $CFTR_{inh}$-172a and GP_{inh}-5a to the synthesized BFC and characterization of the obtained bioconjugates;
3. Radiolabelling of both bioconjugates with ^{99m}Tc(I);
4. Synthesis and characterization of the analogous Re(I) complexes for characterization of the ^{99m}Tc(I) complexes and evaluation of their inhibitory efficacy.

2. MATERIALS AND METHODS

2. 1. RADIOLABELLING OF MOLECULAR IMAGING PROBES BASED ON ANTI-CFTR ANTIBODIES

2.1.1. Anti-CFTR antibodies

Two different Abs directed against the first ECL of CFTR were used: ECL1 and MA1-935. Two other Abs, human polyclonal immunoglobulin (HIG) and IOR-carcinoembryonic antigen 1 (IOR-CEA1), were also utilized during the work with the purpose of optimizing methods/techniques.

The polyclonal antibody (pAb) ECL1, a rabbit IgG, was kindly provided by Prof. Raymond Frizzell (*Department of Cell Biology*, *University of Pittsburgh*, USA) through the CFTR Folding Consortium (CFC). Briefly, this pAb was produced by immunizing rabbits with a peptide constituted by the 15 amino acids of the first ECL of CFTR: residues 103 to 117 - GRIIASYDPDNKEER. In order to hold the peptide into a loop, two cysteines were added at the carboxy and amino termini of the peptide to form disulfide bonds. Moreover, for adequate immune response in rabbit, a third cysteine was added at the carboxy terminus of the peptide for conjugation to an immunogenic carrier protein, keyhole limpet hemocyanin.[49] The pAb was received in the form of rabbit serum.

The mAb MA1-935, a murine IgM, was purchased from Pierce (Pierce, Thermo Scientific, Rockford, IL, USA). Similarly to the pAb ECL1, MA1-935 was also produced using a synthetic peptide constituted by the 15 amino acids of the first ECL of CFTR as immunogen. The mAb was received in the form of diluted ascites, in a concentration of 7.30 mg/mL.

The HIG (Intraglobulin, Biotest Pharma GmbH, Dreieich, Hesse, Germany), a non-specific IgG, was used for comparison of its chromatographic profile with the profile of the Abs under study.

The mAb IOR-CEA1, a murine IgG directed against the CEA, was provided by the *Centro de Immunología Molecular* (Havana, Cuba), through the *International Atomic Energy Agency*. This Ab was used in the optimization of the radiolabelling by the direct method.

2.1.2. Protein quantification

Determination of protein concentration was accomplished using the *DC*™ Protein Assay kit (BioRad Laboratories, Hercules, CA, USA). Similarly to the Lowry assay, this assay is based on the Biuret reaction, wherein the peptide bonds of proteins react with copper ions (Cu^{2+}) in an alkaline medium producing Cu^{+}, and in the Folin-Ciocalteau reaction, where the Folin reagent is reduced by the copper-catalyzed oxidation of amino acids. These two steps lead to the formation of reduced species with a characteristic blue colour and maximum absorbance at 750 nm (A_{750nm}). Colour development is primarily due to the amino acids tyrosine and tryptophan, and to a lesser extent, cystine, cysteine, and histidine.

The *DC*™ Protein Assay kit is constituted by the reagent A (alkaline copper tartrate solution), reagent B (Folin reagent) and reagent S (used only with detergent-containing samples). Briefly, 5 µL of each sample were pipetted into a well of a 96-well microplate. Each well was loaded with 25 µL of reagent A and 200 µL of reagent B and the microplate was gently shaked to mix the reagents. After 15 minutes (min) of incubation at room temperature (r.t.), A_{750nm} was read using the PowerWave™ XS Microplate Reader (BioTek Instruments, Winooski, VT, USA).

Protein concentration was calculated relative to a standard curve obtained by analysis of a series of standard solutions of bovine serum albumin (BSA) (BioRad) ranging between 0.25 and 5.0 mg/mL. The BSA standards were prepared in duplicate and subjected to the same procedure as the samples. Linear regression analysis of the data gave correlation coefficients between 0.932 and 0.985.

2.1.3. Sodium dodecyl sulfate-polyacrylamide gel electrophoresis (SDS-PAGE)

SDS-PAGE was performed under reducing and non-reducing conditions to evaluate the purity of the Ab solutions. For non-reducing SDS-PAGE, an equal volume of non-reducing sample buffer (31.25 mM Tris (pH 6.8), 1.5% (w/v) SDS, 10% (v/v) glycerol, 0.001% (w/v) bromophenol blue) was added to each sample and the mixture stirred. For SDS-PAGE in reducing conditions, an equal volume of sample buffer (31.25 mM Tris (pH 6.8), 1.5% (w/v) SDS, 10% (v/v) glycerol, 0.001% (w/v) bromophenol blue, 0.5 mM dithiothreitol - DTT) was added to each sample and the mixture incubated in a boiling water bath, for 3 min. Samples were loaded at 5 or 10 µg of protein per lane and resolved in a 10% polyacrylamide gel in an

Amersham Biosciences apparatus (Amersham Biosciences, Piscataway, NJ, USA). Electrophoresis proceeded at 100 mV, 15-25 mA, for 3 h, in running buffer (0.025 M Tris, 0.192 M glycine, 0.1% (w/v) SDS). Proteins were visualized by staining gels with Bio-Safe™ Coomassie Blue G-250 stain (BioRad) and destained by washing with water for 30 min. MW standards (ColorBurst™ Electrophoresis Markers, Sigma-Aldrich, St. Louis, MO, USA) were also loaded in the gels. Finally, gels were placed between two cellophane sheets and dried in vacuum and heat.

2.1.4. Antibody purification

ECL1 Ab was purified using the Melon™ Gel IgG Spin Purification Kit (Pierce), which is constituted by a purification support, purification buffer and spin columns. This method has significant advantages such as the use of a mild purification buffer at physiological pH, suitable for storage and downstream applications, the absence of a harsh elution step, which could inactivate more labile Abs, and the fastness of the procedure, usually less than 15 min.

After equilibration of the purification support and purification buffer to r.t., the purification support was properly dispensed into a spin column placed in a microcentrifuge tube. The uncapped column/tube assembly was centrifuged for 1 min at 3000 g, the spin column removed and flow-through discarded. After washing the column twice with 300 µL of purification buffer and placing the bottom cap on the column, 500 µL of diluted serum 1:10 (approximately 4.92 mg/mL) were added, and the column incubated for 5 min, at r.t., with end-over-end mixing. Then, the bottom cap was removed and the spin column centrifuged for 1 min at 2000 g, in order to collect the purified Ab (non-bound fraction). Finally, an elution with 300 µL of purification buffer was performed, in order to increase the recovery of the purified Ab. The two eluted fractions were analyzed by SDS-PAGE and the Ab concentration determined by the microplate protein assay.

2.1.5. Size exclusion-high performance liquid chromatography (SE-HPLC)

Abs analyses were performed on a PerkinElmer Series 200 LC pump (PerkinElmer, Waltham, MA, USA) coupled to an ultraviolet/visible (UV/Vis) detector (Shimadzu SPD-10AV, Shimadzu, Kyoto, Japan) and to a γ detector (Berthold-LB 509, Berthold Technologies, Bad Wildbad, Baden-Württemberg, Germany), using a TSK G3000SW gel filtration column (10 µm,

300 x 7.5 mm) (Tosoh, Tokyo, Japan), with a flow rate of 1.0 mL/min. As mobile phase, 0.1 M Na_2SO_4 in 0.1 M phosphate buffer pH 7.0, previously filtered with 0.22 µm filters (Millipore, Billerica, MA, USA) was used. Each run was of 30 min with the detection of Abs performed at 280 nm. The column was tested with protein standards with a MW range between 13.7 and 669 kDa (Low and High Molecular Weight Markers, Pharmacia Biotech, Björkgatan, Uppsala, Sweden) (**Table 1**).

Table 1: Protein standards for testing the TSK G3000SW gel filtration column and respective MW (kDa)

Protein Standards	MW (kDa)
Ribonuclease A	13.7
BSA	67
Aldolase	158
Catalase	232
Ferritin	440
Thyroglobulin	669

2.1.6. Antibody reduction

ECL1 Ab, in purification buffer (from the Melon Purification kit), and IOR-CEA1 Ab, in phosphate buffer saline (PBS) pH 7.4 without Ca^{2+} and Mg^{2+} (Invitrogen, Life Tecnhologies, Carlsbad, CA, USA), were reduced in order to generate free sulfhydryl groups. Briefly, the Ab reacted with a 1000-fold molar excess of 2-ME (Sigma), at r.t. for 30 min.[45] In the cases where the volume of 2-Me needed for the reduction was very small, a 1:10 dilution in PBS pH 7.4 was performed. The reduced Ab was then purified on a previously equilibrated PD-10 desalting column (1.45 x 5.0 cm) (GE Healthcare, Björkgatan, Uppsala, Sweden) using as eluent PBS pH 7.4 degassed with helium, purged with nitrogen and kept at 4 °C. Fractions of approximately 250 µL were collected and the Ab concentration determined by reading of absorbance at 280 nm (A_{280nm}) on a Nanodrop 2000 (Thermo Scientific) or a DMS 80 spectrophotometer (Varian Techtron, Mulgrave, VIC, Australia). The Ab concentration was calculated knowing that a 1 mg/mL solution of an IgG gives an A_{280nm} of 1.35 against the appropriate reference solution. The fractions containing Ab were pooled and the final concentration of the reduced Ab determined. When needed, the Ab solution was concentrated using a Microcon centrifugal filter fitted with an Ultracel YM-10 membrane (Millipore) and the final concentration determined.

2.1.7. Determination of sulfhydryl groups

The number of sulfhydryl groups was determined spectrophotometrically in the presence of Ellman's reagent[50] (5-5'-dithiol bis-(2-nitrobenzoic acid) (Sigma). Typically, 25 µL of sample were added to a solution containing 25 µL of freshly prepared Ellman's reagent (1 mg/mL) and 450 µL of 50 mM phosphate buffer pH 7.5 (Sigma). The mixture was incubated for 15 min at r.t. and absorbance at 412 nm (A_{412nm}) was read using the DMS 80 spectrophotometer, or in some cases, using the Nanodrop 2000. Sulfhydryl groups were calculated relative to a standard curve obtained by analysis of a series of L-cysteine solutions. Linear regression analysis of data gave the correlation coefficients between 0.985 and 0.999.

2.1.8. Radiolabelling methods

2.1.8.1. Manipulation of radioactive compounds

Manipulation of radioactive compounds was performed according to the guidelines for protection against ionizing radiation and for the safety of radiation sources, in the presence of devices that detect radiation, and in laboratories with appropriated ventilation systems and with negative pressure relatively to the exterior. All the vials containing radioactive solutions were kept in lead containers of appropriate thickness. The radiation dose absorbed during the experiments was measured periodically by the reading of radiation in individual detectors of chest and extremities.

2.1.8.2. Reading of radioactivity of radioactive solutions

The radioactivity of the radioactive solutions was read using an ionization chamber (Curiemeter IGC-3, Aloka, Tokyo, Japan).

2.1.8.3. Preparation of the *fac*-$[^{99m}Tc(H_2O)_3(CO)_3]^+$ precursor

$[^{99m}TcO_4]^-$ was eluted from a $^{99}Mo/^{99m}Tc$ generator (ELUMATIC® III, Iba Molecular, Ottignies-Louvain-la-Neuve, Belgium) with a solution of 0.9% (w/v) NaCl. From that eluate, 2.0

mL (~ 1.25 mCi) were added to a commercial kit (IsoLink® kit, Mallinckrodt-Covidien, Petten, The Netherlands), containing the following lyophilized formulation: sodium tartrate dihydrate (8.50 mg), sodium tetraborate decahydrate (2.85 mg), sodium carbonate (7.15 mg) and sodium boranocarbonate (4.50 mg). The reaction vial was incubated at 100 °C for 30 min. After cooling the vial to r.t., the solution was neutralized with 1 M HCl (140.0 – 160.0 µL) to decompose any residual boranocarbonate. The formation of the precursor was controlled by reversed phase (RP)-HPLC (see **Materials and Methods**, **Section 2.2.2. , RP-HPLC**, method 1 for more details).

2.1.8.4. Radiolabelling with ^{99m}Tc

Based on previous reports in literature, ECL1 Ab was radiolabelled with ^{99m}Tc(I)[51] and ^{99m}Tc(IV)[44,45] using the direct method, as described in **Section 1.4.2.4.1.** (**Introduction**). IOR-CEA1 was only radiolabelled with ^{99m}Tc(IV).

Radiolabelling with ^{99m}Tc(I):

In a capped nitrogen purged glass vial, 20 µL of reduced Ab in PBS pH 7.4 were added to 20 µL of a solution of *fac*-$[^{99m}Tc(H_2O)_3(CO)_3]^+$ in 0.9% (w/v) NaCl (1:1 proportion). Typically, the mixture was incubated at 37 °C for 30 min but other incubation times were also assessed. To assess the effect of the relative proportions of Ab and tricarbonyl precursor, radiolabelling was also performed with 10 µL of Ab in 5 µL of *fac*-$[^{99m}Tc(H_2O)_3(CO)_3]^+$ (2:1 proportion) and 15 µL of Ab in 5 µL of *fac*-$[^{99m}Tc(H_2O)_3(CO)_3]^+$ (3:1 proportion).

Radiolabelling with ^{99m}Tc(IV):

First, a MDP kit (GE Healthcare), containing sodium medronate (0.25 mg), stannous fluoride (0.34 mg) and sodium p-aminobenzoate (2.0 mg) as a freeze-dried mixture, was reconstituted with 5.0 mL of 0.9% (w/v) NaCl.

After the reconstitution and for the Ab radiolabelling, different variables such as the volume of Ab, MDP solution and $[^{99m}TcO_4]^-$ and reaction time were studied. As a starting condition, 50 µL of $[^{99m}TcO_4]^-$ were added to a reaction vial containing a mixture of 5 µL of the reduced Ab and 5 µL of the MDP solution previously prepared. The reaction vial was incubated at 15 min at r.t. and the radiolabelling efficiency evaluated.

2.1.8.5. Instant thin-layer chromatography-silica gel (ITLC-SG)

The radiolabelling efficiency and radiochemical purity of the Abs at different incubation times were evaluated by ITLC, using 6.5 x 1.0 cm ITLC-SG strips (Agilent Technologies, Palo Alto, CA, USA) and a radio-thin layer scanner Dunnschicht-scanner II LB 2723 (Berthold Technologies).

In the Ab radiolabelling with ^{99m}Tc(I), the mixture 6 M HCl/MeOH (5/95) was used as mobile phase. With this eluent, radiolabelled Ab and colloidal ^{99m}Tc stay at the origin (retention factor (R_f) = 0), while *fac*-$[^{99m}Tc(H_2O)_3(CO)_3]^+$ and $[^{99m}TcO_4]^-$ migrate with the solvent front (R_f = 0.8 - 1.0).[52]

In the Ab radiolabelling with ^{99m}Tc(IV), two chromatographic systems were used: methyl ethyl ketone (MEK) and 1.0 M sodium acetate (**Table 2**). The first ITLC method (MEK) allows the detection of the $[^{99m}TcO_4]^-$ impurity and gives rise to two peaks - ^{99m}Tc-Ab, ^{99m}Tc-MDP and colloidal ^{99m}Tc at the origin and free $[^{99m}TcO_4]^-$ at the solvent front[53] (**Table 2**). With the second ITLC method (1.0 M sodium acetate), ^{99m}Tc-Ab and colloidal ^{99m}Tc remain at the origin while ^{99m}Tc-MDP and free $[^{99m}TcO_4]^-$ migrate with the solvent front[54] (**Table 2**).

Table 2: ITLC-SG mobile phases used to identify ^{99m}Tc species according to their R_f

Mobile phase	**R_f**			
	^{99m}Tc-Ab	^{99m}Tc-MDP	^{99m}Tc-colloids	$[^{99m}TcO_4]^-$
MEK	0	0	0	0.8-1.0
1.0 M sodium acetate	0	0.8-1.0	0	0.8-1.0

2.2. RADIOLABELLING OF MOLECULAR IMAGING PROBES BASED ON CFTR INHIBITORS

2.2.1. Solvents and reagents

All chemicals and solvents were of reagent grade and were used without purification, unless otherwise stated. Dry solvents were used for reactions in inert atmosphere and were dried according to published procedures.[55]

The CFTR inhibitors **$CFTR_{inh}$-172a** and **GP_{inh}-5a** were kindly provided through the *Chemical Compound Distribution Program*, sponsored by *Cystic Fibrosis Foundation Therapeutics* (CFFT) and administered by Professor Robert Bridges' laboratory at the *Rosalind Franklin University of Science and Medicine* (Chicago, IL, USA). **$CFTR_{inh}$-172a** is a potent and rapid voltage-independent inhibitor of CFTR in human airway cells. It is shown to interact specifically with CFTR at the region of the channel pore, not inhibiting other Cl^- channels, or a series of other transporters.[56] **GP_{inh}-5a** is a potent, water-soluble, nontoxic inhibitor of CFTR. It has been described as the most potent inhibitor of CFTR channels with picomolar affinity in wt- and F508del-CFTR cells.[57,58]

The compound *tert*-butyl 2-aminoethylcarbamate and the organometallic precursor *fac*-$[Re(CO)_3(H_2O)_3]Br$ were prepared in the *Radiopharmaceutical Sciences Group* of IST/CTN (RSG-IST/CTN) according to published methods.[59,39]

2.2.2. Characterization and purification techniques

RP-HPLC

RP-HPLC analyses of compounds were performed on a PerkinElmer Series 200 LC pump (PerkinElmer) coupled to an UV/VIS detector (PerkinElmer LC 290 or Shimadzu SPD-10AV) and to a γ detector (Berthold-LB 509), using a Macherey-Nagel C18 reversed phase column (Nucleosil 10 µm, 250 x 4 mm, Macherey Nagel, Düren, Germany), with a flow rate of 1.0 mL/min. The eluents were of HPLC grade and the water bidistilled from a quartz distillation unit. The solvents were filtered with 0.22 µm filters (Millipore) and purged with helium. Two different elution methods (method 1 and 2) were used, according to the characteristics of the analyzed compounds.

METHOD 1:

This method was used for the analysis of **CFTR$_{inh}$-172a**, **L1**, **B1**, **Re1** and **Tc1** (λ = 220 and 254 nm). Eluents: **A** - 0.1% (v/v) trifluoroacetic acid (TFA) in H_2O; **B** - 0.1% (v/v) TFA in acetonitrile (ACN).

Table 3: HPLC method 1

Time (min)	% A	% B
0-5	80	20
5-20	80→0	20→100
20-28	0	100
28-29	0→80	100→20
29-30	80	20

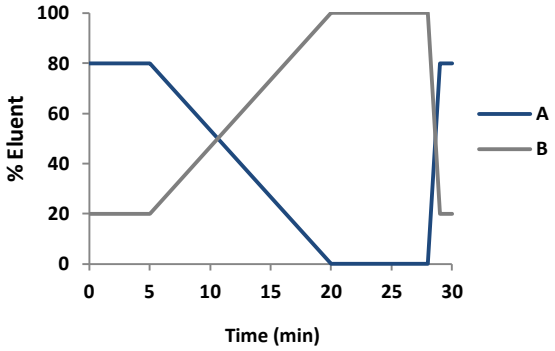

Figure 8: HPLC profile for method 1.

METHOD 2:

This method was used for the analysis of **GP$_{inh}$-5a** (λ = 220 nm). Eluents: A - 0.1% (v/v) TFA in H_2O; B - methanol (MeOH).

Table 4: HPLC method 2

Time (min)	% A	% B
0-5	80	20
5-30	80→0	20→100
30-34	0	100
34-35	0→80	100→20
35-40	80	20

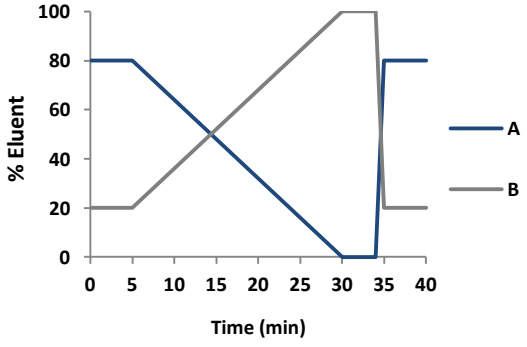

Figure 9: HPLC profile for method 2.

Thin-layer chromatography (TLC)

All chemical reactions were monitored by TLC, carried out on ALUGRAM® Xtra silica-gel aluminium sheets (Macherey-Nagel) with 0.20 mm of thickness. Compounds were detected with UV radiation (λ = 254 nm) or revealed with iodine vapor.

Column chromatography

Some of the synthesized compounds were purified by column chromatography using silica-gel 60 with 70-230 mesh granulometry (Merck, Darmstadt, Germany) and glass columns of appropriated dimensions to the amount of compound to purify. Eluent was also chosen according to the compound to purify. The presence of the desired compound in the elution fractions was monitored by TLC and in some cases by ^{1}H-NMR spectroscopy (see below).

Sep-Pak C18 Chromatography

Compound **B2** was purified using a Sep-Pak C18 cartridge (0.85 cc/360mg, Waters Co, Milford, MA, USA), preconditioned with MeOH (2.0 mL) and water (5.0 mL). Elution of the compound started with water, followed by a gradient of MeOH (10→100%) in water. The presence of the desired compound in the collected fractions was monitored by TLC and in some cases by ^{1}H-NMR spectroscopy.

Mass spectrometry (MS)

Mass spectra were obtained using an electrospray ionization/quadrupole ion trap (ESI/QIT) mass spectrometer (Bruker HCT, Bruker, Billerica, MA, USA) and were performed by Dr. Joaquim Marçalo from the *Unidade de Ciências Químicas e Radiofarmacêuticas* of IST/CTN. The mass spectrum of **Re1** was obtained using a matrix-assisted laser desorption/ionization-time of flight (MALDI-TOF) mass spectrometer (Voyager-DE™ PRO Biospectrometry Workstation, Applied Biosystems, Life Technologies) and 2,5-dihydroxybenzoic acid (DHB) as

matrix. The analysis was performed by the *Laboratório de Análises/Requimte* of the *Departamento de Química da Universidade Nova de Lisboa*.

NMR spectroscopy

^{1}H-, ^{13}C- and ^{19}F-NMR spectra were recorded, at r.t., on a Varian Unity Inova-300 spectrometer (Varian, Agilent Technologies), with a radiofrequency of 300, 75.5 and 281.98 MHz, respectively. The spectra were obtained in $CDCl_3$, CD_3OD, D_2O or dimethyl sulfoxide (DMSO)-d_6. ^{1}H and ^{13}C chemical shifts (δ) are reported in parts per million (ppm) and were referenced with the residual solvent resonances relative to tetramethylsilane (TMS). ^{13}C chemical shifts for spectra in D_2O were referenced with the residual solvent resonance relative to 1,4-dioxane. ^{19}F chemical shift is also reported in ppm and was referenced with the residual solvent resonance relative to α,α,α-trifluorotoluene (0.05% (v/v) in C_6D_6). Signal multiplicity is described using the following abbreviations: s (singlet), d (doublet), t (triplet), q (quartet), quint (quintuplet), sep (septuplet), m (multiplet) and bs (broad singlet).

Table 5: ^{1}H- and ^{13}C-NMR chemical shifts (ppm) for the residual solvents present in the deuterated solvents $CDCl_3$, CD_3OD, D_2O and DMSO-d_6

Deuterated solvent	**Solvent**	**δ (ppm)**	
		^{1}H	**^{13}C**
$CDCl_3$	$CHCl_3$	7.26 (s)	77.00 (t)
CD_3OD	CH_3OH	3.31 (quint)	49.05 (sep)
	H_2O	4.87 (s)	
D_2O	H_2O	4.79 (s)	-
DMSO-d_6	DMSO	2.50 (quint)	39.43 (sep)

2.2.3. Synthesis and characterization of compounds

2.2.3.1. $CFTR_{inh}$-172a and GP_{inh}-5a

2.2.3.1.1. (Z)-4-((4-oxo-2-thioxo-3-(3-(trifluoromethyl)phenyl)thiazolidin-5-ylidene)methyl) benzoic acid ($CFTR_{inh}$-172a)

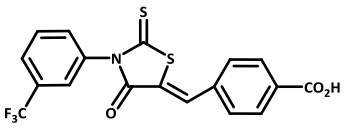

MW = 409.01 g/mol

The synthesis and characterization of **$CFTR_{inh}$-172a** (^{1}H-NMR spectroscopy in DMSO-d_6) has been reported in literature.[60,61] Within the framework of this thesis, **$CFTR_{inh}$-172a** was characterized by ^{1}H- and ^{13}C-NMR spectroscopy using also CD_3OD as solvent.

^{1}H-NMR (CD_3OD): δ_H (ppm) 8.14 (2H, d, carboxyphenyl), 7.86-7.65 (7H, m, trifluoromethylphenyl, exocyclic =CH and carboxyphenyl).

^{1}H-NMR (CD_3OD and DMSO-d_6): δ_H (ppm) 8.21 (2H, d, carboxyphenyl), 7.96-7.77 (7H, m, trifluoromethylphenyl, exocyclic =CH and carboxyphenyl).

^{13}C-NMR (CD_3OD and DMSO-d_6): δ_C (ppm) 195.3 (C=S), 168.6 (C=O), 168.5 (C=O), 138.5, 137.4, 134.4, 134.2, 132.8, 131.8, 131.6, 127.7 (q, CF_3, $^{3}J_{CF}$ = 4.18 Hz), 127.4 (q, CF_3, $^{3}J_{CF}$ = 3.85 Hz), 127.1.

^{19}F-NMR (CD_3OD): δ_C (ppm) -64.62

HPLC (Retention time - R_t): 20.3 min (method 1, λ = 220nm).

2.2.3.1.2. (7R,9S)-7,8-dihydroxy-3-(4-hydroxy-5-(hydroxymethyl)tetrahydrofuran-2-yl)-7,9-dimethyl 3,7,8,9-tetrahydropyrimido[1,2-i]purine-9-carboxylic acid (GP_{inh}-5a)

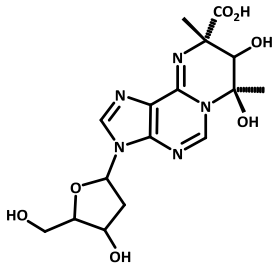

MW = 395.37 g/mol

The synthesis and characterization of **GP_{inh}-5a** (^{1}H-NMR spectroscopy in D_2O and ESI-MS) has been reported in literature.[62] Within the framework of this thesis, **GP_{inh}-5a** was characterized by ^{1}H- and ^{13}C-NMR spectroscopy using also CD_3OD as solvent.

^{1}H-NMR (CD_3OD): δ_H (ppm) 8.35 (1H, s, Ar-CH), 8.14 (1H, d, Ar-CH), 6.41 (1H, t, *N*-CH), 4.59-4.48 (2H, broad m, CH), 4.05 (1H, broad m, CH), 3.79 (2H, q, DO-CH_2), 2.81-2.71 (1H, broad m, CH_2), 2.50-2.40 (1H, broad m, CH_2), 1.72 (6H, s, CH_3).

^{13}C-NMR (D_2O) δ_C (ppm) 174.1 (C=O), 86.7, 82.3, 68.3, 68.1, 68.0, 60.8, 58.8, 36.5, 23.1 (CH_3), 19.5 (CH_3).

HPLC (R_t): 2.6 min (method 2, λ = 220nm).

2.2.3.2. Bifunctional chelator L1

This compound was synthesized by multistep synthetic procedures as previously reported by the RSG-IST/CTN.[63,64]

2.2.3.2.1. 1-(2-bromoethyl)-3,5-dimethyl-1*H*-pyrazole (1)

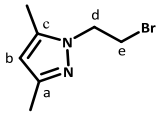

To a solution of 3,5-dimethyl-1*H*-pyrazole (5.00 g, 52.00 mmol) in 1,2-dibromoethane (45.0 mL, 522.20 mmol) was added a solution of 40% NaOH (15.6 mL, 556.40 mmol) and tetrabutylammonium bromide (TBAB) (0.43 g, 1.33 mmol). After overnight reflux, the solution

was cooled down to r.t. and extracted with $CHCl_3$. The organic phase was dried over $MgSO_4$, filtered and the solvent evaporated. The resulting product was purified by silica gel column chromatography, using ethyl acetate (EtOAc) as eluent. After evaporation of the solvent from the collected fractions, **1** was obtained as a pale yellow oil.

Yield (η): 53% (5.37 g, 27.78 mmol).

^{1}H-NMR ($CDCl_3$): δ_H (ppm) 5.80 (1H, s, CH^b), 4.32 (2H, t, CH_2^d), 3.69 (2H, t, CH_2^e), 2.27 (3H, s, CH_3, pyrazole - pz), 2.21 (3H, s, CH_3, pz).

2.2.3.2.2. *Tert*-butyl 2-(2-(3,5-dimethyl-1*H*-pyrazol-1-yl)ethylamino)ethylcarbamate (2)

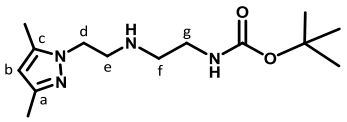

To a solution of **1** (2.78 g, 13.69 mmol) in dry ACN (30.0 mL) were added *tert*-butyl 2-aminoethylcarbamate (1.10 g, 6.85 mmol), K_2CO_3 (1.89 g, 13.70 mmol) and KI (227.32 mg, 1.37 mmol). After overnight reflux, the suspension was cooled down to r.t. and the solvent evaporated. The resulting product was purified by silica gel column chromatography, using $CHCl_3$/MeOH (95/5) as eluent. After evaporation of the solvent from the collected fractions, **2** was obtained as an orange oil.

Yield: 58% (1.12 g, 3.96 mmol).

^{1}H-NMR ($CDCl_3$): δ_H (ppm) 5.75 (1H, s, CH^b), 5.27 (1H, bs, NH-*tert*-butoxycarbonyl – NHBoc), 3.89 (2H, t, CH_2^d), 3.08 (2H, m, CH_2^g), 2.87 (2H, t, CH_2^e), 2.58 (2H, t, CH_2^f), 2.19 (3H, s, CH_3, pz), 2.17 (3H, s, CH_3, pz), 1.43 (9H, s, $(CH_3)_3$, Boc).

2.2.3.2.3. *Tert*-butyl 2-((2-(3,5-dimethyl-1H-pyrazol-1-yl)ethyl)(3-(1,3-dioxoisoindolin-2-yl)propyl)amino ethylcarbamate (3)

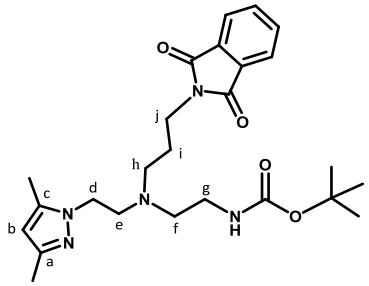

To a solution of **2** (0.97 g, 3.44 mmol) in dry ACN (30.0 mL) were added 3-bromopropylphthalimide (1.85 g, 6.88 mmol), K_2CO_3 (0.95 g, 6.88 mmol) and KI (114.24 mg, 0.69 mmol). After overnight reflux, the solution was filtered and the solvent evaporated. The resulting product was purified by silica gel column chromatography, using a gradient of EtOAc (30→100%) in hexane followed by a gradient of MeOH (20→50%) in EtOAc. After evaporation of the solvent from the collected fractions, compound **3** was obtained as a yellow oil.

Yield: 59% (0.95 g, 2.03 mmol).

^{1}H-NMR ($CDCl_3$): δ_H (ppm) 7.83 (2H, m, phtalimide), 7. 71 (2H, m, phtalimide), 5.72 (1H, s, CH^b), 5.16 (1H, bs, NHBoc), 3.98 (2H, t, CH_2^d), 3.62 (2H, t, CH_2^j), 3.09 (2H, m, CH_2^g), 2.81 (2H, t, CH_2^e), 2.52 (4H, m, $CH_2^{f/h}$), 2.23 (3H, s, CH_3, pz), 2.17 (3H, s, CH_3, pz), 1.74 (2H, quint, CH_2^i), 1.42 (9H, s, $(CH_3)_3$, Boc).

2.2.3.2.4. *Tert*-butyl2-((3-aminopropyl)(2-(3,5-dimethyl-1*H*-pyrazol-1-yl)ethyl)amino) ethylcarbamate (L1)

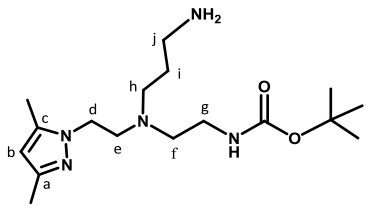

To a solution of **3** (0.95 g, 2.04 mmol) in MeOH (15.0 mL) was added hydrazine monohydrate (1.58 mL, 32.59 mmol). After refluxing for 6 h, the solution was carefully

acidified with 4 M HCl to pH ~ 6 and neutralized with 2.5 M NaOH, forming a white precipitate that was removed by filtration. After removal of the solvent, the obtained solution was extracted with cold $CHCl_3$ and the resulting organic phase dried over Na_2SO_4. The resulting product was purified by silica gel column chromatography using a gradient of MeOH (0→40%) in CH_2Cl_2, followed by a gradient of NH_4OH (1→10%) in MeOH. After evaporation of the solvents from the collected fractions, **L1** was obtained as a yellow oil.

Yield: 65% (0.45 g, 1.32 mmol).

^{1}H-NMR ($CDCl_3$): δ_H (ppm) 5.75 (1H, s, CH^b), 5.39 (1H, bs, N<u>H</u>Boc), 3.99 (2H, t, CH_2^d), 3.73 (2H, bs, NH_2), 3.06 (2H, m, CH_2^g), 2.75 (4H, t, $CH_2^{e/j}$), 2.51 (4H, m, $CH_2^{f/h}$), 2.21 (3H, s, CH_3, pz), 2.18 (3H, s, CH_3, pz), 1.61 (2H, m, CH_2^i), 1.41 (9H, s, $(CH_3)_3$, Boc).

^{1}H-NMR (CD_3OD): 5.85 (1H, s, CH^b), 4.06 (2H, t, CH_2^d), 3.04 (2H, t, CH_2^g), 2.92 (2H, t, CH_2^e), 2.79 (2H, t, CH_2^j), 2.61 (2H, t, CH_2^f), 2.54 (2H, t, CH_2^h), 2.28 (3H, s, CH_3, pz), 2.18 (3H, s, CH_3, pz), 1.76 (2H, quint, CH_2^i), 1.43 (9H, s, $(CH_3)_3$, Boc).

^{13}C-NMR ($CDCl_3$): δ_C (ppm) 156.1 (C=O, Boc), 147.4 (C^c), 138.9 (C^a), 105.4 (C^b), 79.1 (<u>C</u>$(CH_3)_3$, Boc), 53.7 (C^e), 52.6 (C^h), 51.8 (C^f), 46.5 (C^d), 38.3 (C^g), 38.0 (C^j), 28.3 ($(CH_3)_3$, Boc), 24.0 (C^i), 13.2 (CH_3, pz), 11.0 (CH_3, pz).

HPLC (R_t): 11.3 min (method 1, λ = 220 nm).

2.2.3.3. Bioconjugates B1 and B2

2.2.3.3.1. (Z)-tert-butyl 2-((2-(3,5-dimethyl-1H-pyrazol-1-yl)ethyl)(3-(4-((4-oxo-2-thioxo-3-(3-(trifluoromethyl)phenyl)thiazolidin-5-ylidene)methyl)benzamido)propyl)amino)ethyl carbamate (B1-Boc)

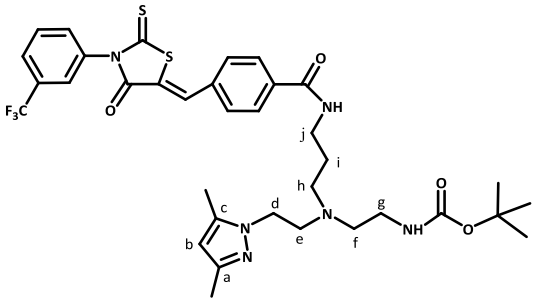

To a solution of **L1** (28.00 mg, 82.48 µmol) in dry *N,N*-dimethylformamide (DMF) (2.0 mL) were added **$CFTR_{inh}$-172a** (19.00 mg, 46.41 µmol), *O*-(benzotriazol-1-yl)-*N,N,N',N'*tetramethyl uranium hexafluorophosphate (HBTU) (22.00 mg, 58.01 µmol) and *N*,*N*-diisopropylethylamine (DIPEA) (43.4 µL, 249.00 µmol). The reaction mixture was stirred at r.t., under nitrogen atmosphere, for 4 d. The solvent was removed under vacuum and the resulting product purified by silica gel column chromatography using a gradient of MeOH (4→20 %) in $CHCl_3$. After evaporation of the solvents from the collected fractions, **B1-Boc** was obtained as a yellow solid.

Yield: 77% (26.00 mg, 35.57 µmol).

^{1}H-NMR ($CDCl_3$): δ_H (ppm) 8.15 (2H, d, carboxyphenyl), 7.77 (2H, m), 7.70 (1H, m), 7.59-7.49 (4H, m), 5.87 (1H, s, CH^b), 4.96 (1H, bs, NHBoc), 4.16 (2H, bs, CH_2^d), 3.48 (2H, bs, CH_2^j), 3.12 (2H, bs, CH_2^g), 2.92 (2H, bs, CH_2^e), 2.75 (2H, bs, CH_2^f), 2.64 (2H, bs, CH_2^h), 2.27 (3H, s, CH_3, pz), 2.19 (3H, s, CH_3, pz), 1.89 (2H, bs, CH_2^i), 1.41 (9H, s, $(CH_3)_3$, Boc).

^{13}C-NMR ($CDCl_3$): δ_C (ppm) 192.5 (C=S), 167.1 (C=O), 166.0 (C=O), 156.0 (C=O, Boc), 147.1 (C^c), 138.6 (C^a), 136.3, 135.3, 135.1, 132.8, 131.9, 130.6, 130.1, 128.3, 126.9 (q, CF_3, $^1J_{CF}$ = 271.70 Hz), 126.6, 125.7, 124.2, 105.6 (C^b), 79.3 ($\underline{C}(CH_3)_3$, Boc), 53.3 (C^e), 52.1 (C^h), 37.8 (C^f), 36.2 (C^d), 31.2 (C^g), 29.7 (C^j), 28.4 ($(CH_3)_3$, Boc), 25.1 (C^i), 13.1 (CH_3, pz), 11.1 (CH_3, pz).

ESI-MS (+) (mass/charge-m/z): 731.4 $[M + H]^+$, 753.4 $[M + Na]^+$, calculated for $C_{35}H_{41}F_3N_6O_4S_2$ = 730.9.

2.2.3.3.2. (Z)-N-(3-((2-aminoethyl)(2-(3,5-dimethyl-1H-pyrazol-1-yl)ethyl)amino)propyl)-4-((4-oxo-2-thioxo-3-(3-(trifluoromethyl)phenyl)thiazolidin-5-ylidene)methyl)benzamide (B1)

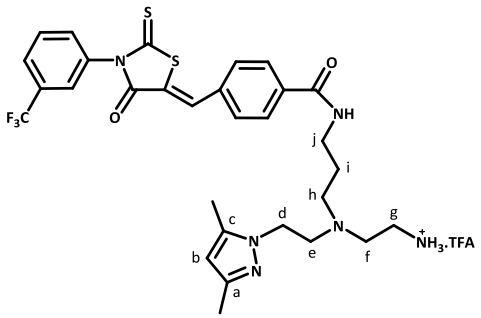

To a solution of **B1-Boc** (26.00 mg, 35.57 µmol) in CH_2Cl_2 (2.0 mL) was added TFA (1 mL, 13.06 mmol)**.** The reaction mixture was stirred at r.t. for 2 h. The solvent was removed under vacuum and the resulting product purified by silica gel column chromatography using a gradient of MeOH (10→20 %) in $CHCl_3$. After evaporation of the solvents from the collected fractions, **B1** was obtained as a yellow solid.

Yield: 68% (18.00 mg, 24.14 µmol).

^{1}H-NMR (CD_3OD): δ_H (ppm) 7.98 (2H, d, carboxyphenyl), 7.86-7.64 (7H, m, trifluoromethylphenyl, exocyclic =CH and carboxyphenyl), 5.85 (1H, s, CH^b), 4.09 (2H, t, $CH_2{}^d$), 3.25 (2H, t, $CH_2{}^j$), 3.01 (2H, t, $CH_2{}^g$), 2.86-2.75 (4H, m, $CH_2{}^{e/f}$), 2.54 (2H, t, $CH_2{}^h$), 2.27 (3H, s, CH_3, pz), 2.18 (3H, s, CH_3, pz), 1.62 (2H, quint, $CH_2{}^i$).

^{13}C-NMR (CD_3OD): δ_C (ppm) 194.9 (C=S), 169.0 (C=O), 168.6 (C=O), 148.5 (C^c), 141.1 (C^a), 137.6, 137.3, 137.2, 133.9, 132.9 (q, $^2J_{CF}$ = 33.04 Hz), 132.7, 131.7, 131.5, 129.3, 127.5 (q, CF_3, $^3J_{CF}$ = 3.60 Hz), 127.2 (q, CF_3, $^3J_{CF}$ = 3.80 Hz), 125.1 (q, CF_3, $^1J_{CF}$ = 272.03 Hz), 126.7, 106.4 (C^b), 54.4 (C^e), 52.6 (C^h), 52.4 (C^f), 47.5 (C^d), 39.0 (C^g), 38.5 (C^j), 28.3 (C^i), 13.3 (CH_3, pz), 11.0 (CH_3, pz).

ESI-MS (+) (m/z): 631.4 $[M + H]^+$, calculated for $C_{30}H_{33}F_3N_6O_2S_2$ = 630.2.

HPLC (R_t): 17.6 min (λ = 220 nm, method 1).

2.2.3.3.3. *Tert*-butyl 2-((3-((7S,9S)-7,8-dihydroxy-3-(4-hydroxy-5(hydroxymethyl) tetrahydrofuran-2-yl)-7,9-dimethyl-3,7,8,9-tetrahydropyrimido[1,2-i]purine-9-carboxamido) propyl)(2-(3,5-dimethyl-1H-pyrazol-1-yl)ethyl)amino)ethylcarbamate (B2-Boc)

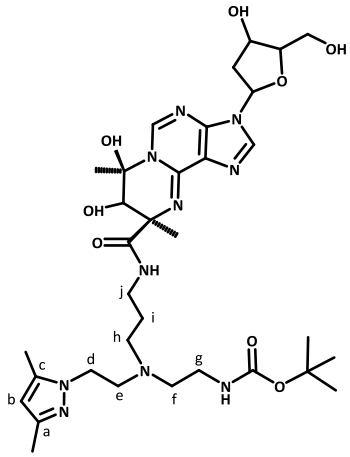

To a solution of **L1** (25.00 mg, 73.64 µmol) in dry DMF (2.0 mL) were added **GP_{inh}-5a** (17.00 mg, 42.99 µmol), HBTU (20.0 mg, 52.74 µmol) and DIPEA (38.7 µL, 222 µmol). The reaction mixture was stirred at r.t., under nitrogen atmosphere, for one week. The solvent was removed under vacuum and the resulting product purified by silica gel column chromatography using a gradient of MeOH (0→100%) in $CHCl_3$. After evaporation of the solvents from the collected fractions, **B2-Boc** was obtained as a brownish oil.

Yield: 49% (15.00 mg, 20.93 µmol).

^{1}H-NMR (CD_3OD): δ_H (ppm) 8.36 (1H, s, Ar-CH), 8.17 (1H, s, Ar-CH), 6.44 (1H, t, *N*-CH), 5.84 (1H, s, CH^b), 4.58 (2H, m, CH), 4.06 (3H, t, $CH_2{}^d$ and CH), 3.79 (2H, q, DO-CH_2), 3.17-3.07 (4H, m, $CH_2{}^{j/g}$), 2.89 (2H, t, $CH_2{}^e$), 2.80 (1H, broad m, CH_2), 2.62 (4H, m, $CH_2{}^{f/h}$), 2.43 (1H, broad m, CH_2), 2.28 (3H, s, CH_3, pz), 2.17 (3H, s, CH_3, pz), 1.73 (2H, t, $CH_2{}^i$), 1.67 (6H, s, $(CH_3)_2$), 1.43 (9H, s, $(CH_3)_3$, Boc).

^{13}C-NMR (CD_3OD): δ_C (ppm) 163.1, 158.5, 148.7 (C^c), 141.9, 141.5 (C^a), 106.1 (C^b), 89.9, 87.0, 80.2, 73.0, 63.6, 54.9 (C^e), 54.7 (C^h), 52.5 (C^f), 47.4 (C^d), 44.3, 41.6 (C^g), 40.3, 39.2 (C^j), 28.8 ($(CH_3)_3$, Boc), 27.6 (CH_3), 21.7 (CH_3), 13.4 (CH_3, pz), 11.2 (CH_3, pz).

2.2.3.3.4. (7R,9R)-N-(3-((2-aminoethyl)(2-(3,5-dimethyl-1H-pyrazol-1-yl)ethyl)amino) propyl)-7,8-dihydroxy-3-(4-hydroxy-5-(hydroxymethyl)tetrahydrofuran-2-yl)-7,9-dimethyl-3,7,8,9-tetrahydropyrimido [1,2-i]purine-9-carboxamide (B2)

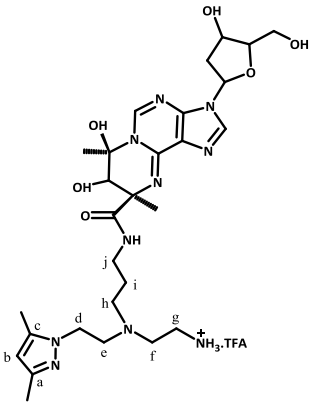

To a solution of **B2-Boc** (15.00 mg, 20.93 µmol) in CH_2Cl_2 (2.0 mL) was added TFA (1.0 mL, 13.06 mmol)**.** The reaction mixture was stirred at r.t. for 2 h. The solvent was removed under vacuum and the resulting product purified by Sep-Pak C18 chromatography. After application of an aqueous solution of the compound in the column, elution started with water, followed by a gradient of MeOH (10→100 %) in water. After analysis of the elution fractions by TLC and ^{1}H-NMR spectroscopy, it was not possible to obtain **B2** in a pure form.

2.2.3.4. Rhenium complex - *fac*-[Re(CO)$_3$(κ^3-B1)]$^+$ (Re1)

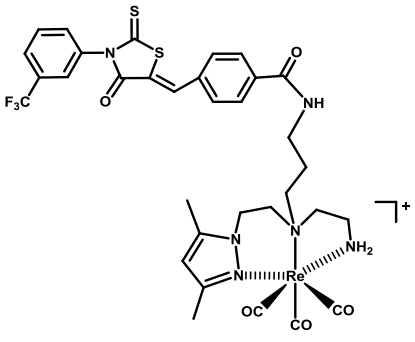

To a solution of **B1** (20.00 mg, 26.84 µmol) in water (5.0 mL) was added the *fac*-[Re(CO)$_3$(H$_2$O)$_3$]Br precursor (12.50 mg, 30.93 µmol). The solution was neutralized with 2.5 M NaOH and refluxed for 18 h. The yellow precipitate obtained corresponding to **Re1** was isolated by decantation and washed several times with water, hexane and dichloromethane.

Yield: 55% (13.30 mg, 14.76 µmol).

^{1}H-NMR (CD_3OD): δ_H (ppm) 8.00 (2H, d, carboxyphenyl), 7.86-7.65 (7H, m, trifluoromethylphenyl, exocyclic =CH and carboxyphenyl), 6.20 (1H, s, CH^b), 5.54 (1H, bs, NH), 4.51 (dd, 1H, CH^d), 4.24 (m, 1H, $CH^{d'}$), 4.09 (1H, bs, NH), 3.78 (m, 1H), 3.54 (2H, t), 3.17 (2H, m), 2.85 (2H, m), 2.72 (2H,m), 2.55 (1H,m), 2.44 (3H, s, CH_3, pz), 2.35 (3H, s, CH_3, pz), 2.29-2.16 (2H, m, $C^{i/i'}$).

^{13}C-NMR (CD_3OD): δ_C (ppm) 198.2 (C≡O), 195.3 (C≡O), 194.9 (C=S), 193.8 (C≡O), 169.4 (C=O), 168.6 (C=O), 155.2 (C^c), 145.4 (C^a), 137.7, 137.4, 137.0, 134.0, 132.6, 131.7, 129.7, 129.3, 127.5, 127.2, 126.8, 109.3 (C^b), 66.3 (C^h), 63.0 (C^f), 54.3 (C^e), 43.8 (C^d), 38.7 (C^g), 30.8 (C^j), 25.9 (C^i), 16.1 (CH_3, pz), 11.6 (CH_3, pz).

MALDI-MS (+) (m/z): 901.1 $[M]^+$, calculated for $C_{33}H_{33}F_3N_6O_5ReS_2$ = 901.2.

HPLC (R_t): 19.9 min (method 1, λ = 254 nm).

2.2.4. Radiolabelling of B1 with the *fac*-$[^{99m}Tc(CO)_3]^+$ core

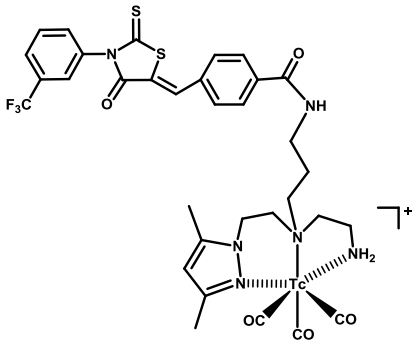

A solution of *fac*-$[^{99m}Tc(H_2O)_3(CO)_3]^+$ (160.0 µL) in 0.9% (w/v) NaCl, prepared as described in **Section 2.1.8.3.**, was added to a capped nitrogen purged glass vial containing a solution of **B1** 10^{-3} M (20.0 µL) and 20.0 µL of an aqueous solution of polyethylene glycol (PEG) 10x (v/v). The final concentration of the bioconjugate **B1** was 10^{-4} M. The reaction vial was incubated at 100 °C for 30 min and the product analyzed by RP-HPLC, using the same method of the rhenium surrogate (method 1, γ detection).

3. RESULTS AND DISCUSSION

The main goal of this thesis was the development of radiolabelled probes for imaging of CFTR at the PM. These probes were based on anti-CFTR Abs and CFTR inhibitors and, for that reason, the work was divided in two parts: radiolabelling of anti-CFTR Abs (**Section 3.1.**) and radiolabelling of CFTR inhibitors (**Section 3.2.**).

3.1. RADIOLABELLING OF MOLECULAR IMAGING PROBES BASED ON ANTI-CFTR ANTIBODIES

In the first part of the thesis, the goal was the radiolabelling of two anti-CFTR Abs, ECL1 and MA1-935, using the direct method (**Scheme 1**). These two Abs were selected because they recognize an epitope on the first ECL of CFTR: residues 103 to 117. Therefore, if successfully achieved, these radiolabelled probes will allow the detection of PM CFTR (in opposition to intracellular CFTR).

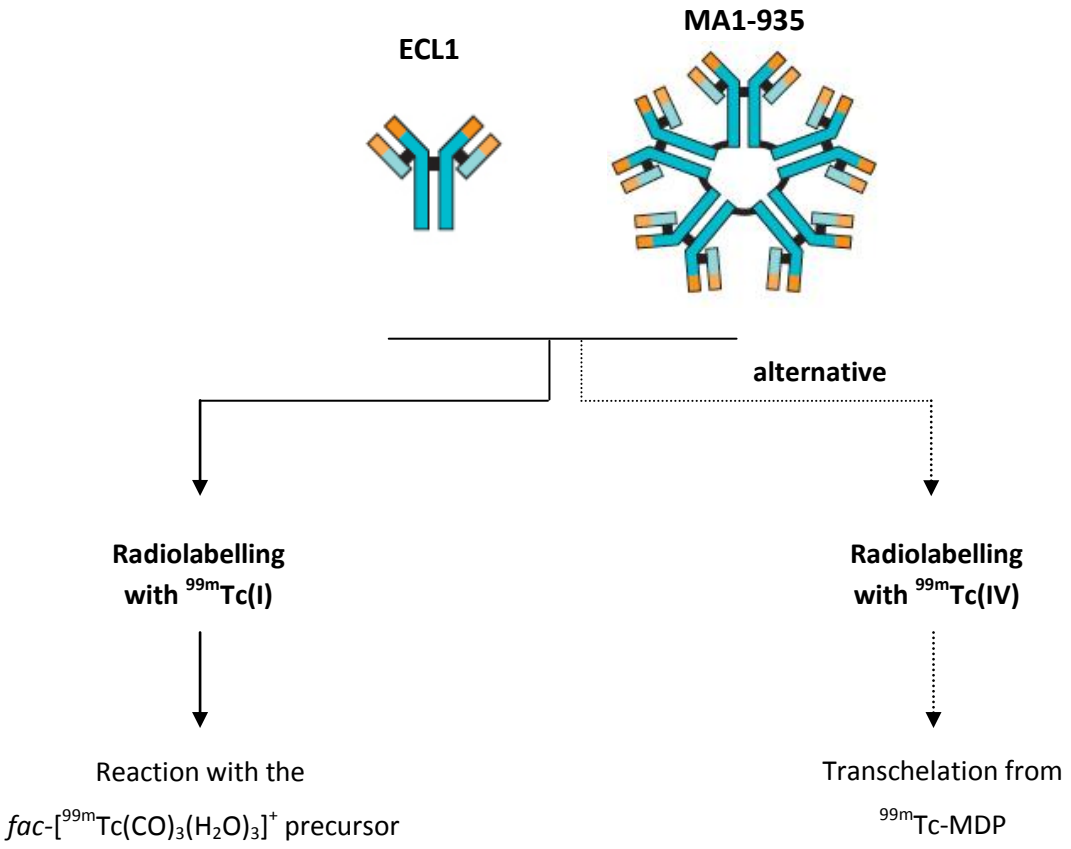

Scheme 1: Radiolabelling of anti-CFTR Abs with ^{99m}Tc(I) or ^{99m}Tc(IV).

First, it was intended to radiolabel the Abs with ^{99m}Tc(I), using the organometallic precursor *fac*-[^{99m}Tc$(H_2O)_3(CO)_3]^+$, that strongly binds to sulfhydryl groups generated by reduction of the Abs.[42]

In case the first radiolabelling strategy would not be successfully accomplished, the radiolabelling with ^{99m}Tc(IV) was envisaged as an alternative. For that, MDP would be used as a weak competing ligand, and the radiolabelling would occur due to the transchelation of ^{99m}Tc from ^{99m}Tc-MDP.

In this chapter is described the characterization and purification of Abs (**Section 3.1.1.**), the Ab analysis by SE-HPLC (**Section 3.1.2.**) and the radiolabelling of Abs by the direct method (**Section 3.1.3.**), using ^{99m}Tc(I) (**Section 3.1.3.2.**) or ^{99m}Tc(IV) (**Section 3.1.3.3.**).

3.1.1. Characterization and purification of antibodies

Characterization of ECL1 serum

The pAb ECL1, a rabbit IgG, was produced by immunizing rabbits with a conformationally constrained ECL1 peptide as antigen,[49] as described in **Section 2.1.1.** (**Materials and Methods**), and was received for this work in the form of rabbit serum. The serum of the immunized rabbits is theoretically constituted by the IgG raised against this peptide, but also by many other proteins often preset in serum, such as albumin, transferrin, α- and β-globulins, among others.[65] Therefore, to fully characterize this sample, the determination of its total protein concentration and protein composition was performed.

First, the protein concentration present in the complete rabbit serum was determined using the *DC*™ Protein Assay kit, as described in **Section 2.1.2.** (**Materials and Methods**). A standard curve describing the relation between BSA concentration and A_{750nm} (see **Annexes, Figure 33**) enabled the determination of the protein concentration in the complete rabbit serum, which was approximately 49.2 mg/mL.

After determining the total protein concentration of the serum sample, and knowing that rabbit serum is constituted by different proteins, the rabbit serum was analyzed in order to understand which proteins were in fact present. For that, an SDS-PAGE under reducing and non-reducing conditions was performed as described in **Section 2.1.3.** (**Materials and Methods**). Rabbit serum was analyzed (**Figure 10**, lanes 2 and 4) in comparison with a sample

of ultra-pure BSA (**Figure 10**, lanes 1 and 3), since albumin is the most abundant protein present in serum.[65]

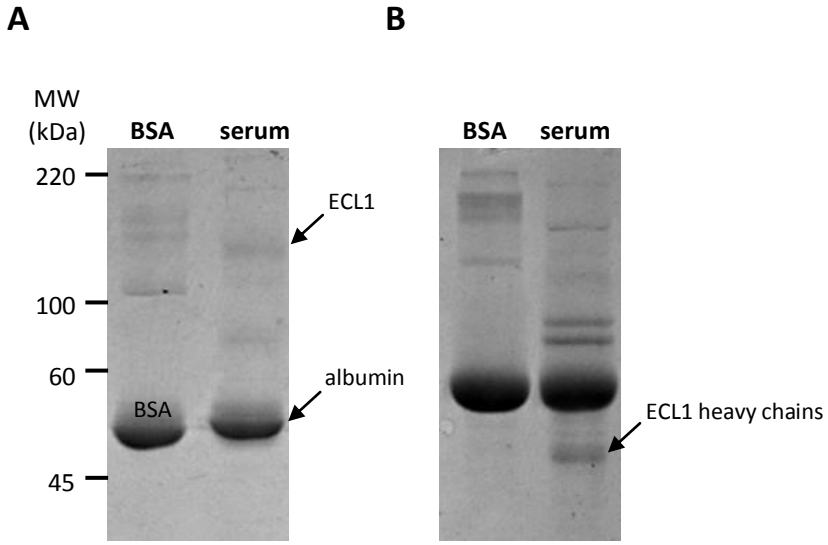

Figure 10: SDS-PAGE analysis of rabbit serum. Samples were loaded at 10 µg of protein per lane. Proteins were resolved in a 10% polyacrylamide gel under non-reducing (**A**) and reducing (**B**) conditions, followed by staining with Bio-Safe Coomassie Blue G-250 stain. MWs of Molecular Weight Markers loaded in an adjacent lane are indicated.

Under non-reducing conditions, an intense band of ~ 50-55 kDa is seen in rabbit serum sample (**Figure 10A**, lane 2). Taking into account that BSA presents a similar migration (**Figure 10A**, lane 1), it can be concluded that the major band seen in rabbit serum sample corresponds to albumin. A band of ~ 160-170 kDa is also observed in rabbit serum sample and this band might correspond to the IgG in its native form, which has a MW of approximately 150 kDa. Later on, the identity of this band was confirmed, since the migration of this protein was similar to the pAb ECL1 obtained after purification (see **Figure 11**, lanes 2 and 3).

Under reducing conditions, when DTT was used in sample buffer, the main difference observed in the rabbit serum sample is a band of ~ 45-50 kDa (**Figure 10B**, lane 4), which is not present under non-reducing conditions. It is well known that the reductive dissociation of an IgG molecule splits the inter-chain disulfide bonds, resulting in the formation of two identical heavy chains (50 kDa each) and to identical light chains (25 kDa each). This dissociation can be caused by the presence of a reducing agent, such as DTT. Hence, the observed band of ~ 45-50 kDa probably corresponds to the heavy chains of the ECL1, which appear due to dissociation of ECL1. However, it was not possible to observe the bands corresponding to the ECL1 light chains.

Purification of polyclonal Ab ECL1

The results of the SDS-PAGE analysis showed that the rabbit serum was constituted by various proteins, mainly albumin but also the IgG of interest. For that reason, the next task consisted in purifying the pAb ECL1 in order to remove the non-desired proteins present in serum. The purification was performed using the Melon^{TM} Gel IgG Spin Purification Kit, a system that purifies Abs, mostly from serum, by retaining the non-Ab serum proteins (often in high abundance), such as albumin and transferrin, while allowing the Ab to flow through in the non-bound fraction.

After following the purification protocol described in **Section 2.1.4.** (**Materials and Methods**), the non-bound fraction (1st fr.) was collected and the protein concentration determined as approximately 0.62 mg/mL. To increase the recovery of the purified Ab, an elution with purification buffer was performed, and a second non-bound fraction obtained (2nd fr.) with a concentration of approximately 0.08 mg/mL.

Finally, the two fractions obtained in the purification were analyzed by SDS-PAGE, under non-reducing and reducing conditions (**Figure 11**).

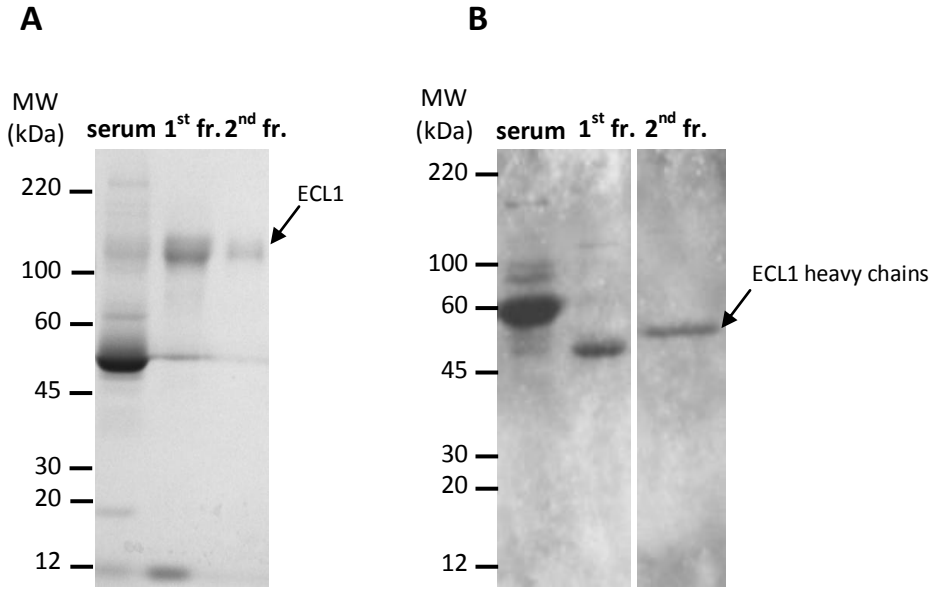

Figure 11: SDS-PAGE analysis of non-bound fractions. Samples were loaded at 10 µg of protein per lane. Proteins were resolved in a 10% polyacrylamide gel under non-reducing (**A**) and reducing (**B**) conditions, followed by staining with Bio-Safe Coomassie Blue G-250 stain. MWs of Molecular Weight Markers loaded in an adjacent lane are indicated.

The majority of serum proteins present in rabbit serum sample before purification (**Figure 11A**, lane 1) are not seen in samples of the fractions obtained after the purification (**Figure 11A**, lanes 2 and 3), specially albumin, which was the most abundant protein present in serum. The efficiency of the system used in the purification is confirmed by the appearance of a band of ~ 150-160 kDa in samples of the collected fractions under non reducing conditions, which corresponds to the Ab in its native form. Similarly to the assay with the complete serum sample, in the presence of DTT (**Figure 11B**), a band of ~ 45-50 kDa appears in samples of both fractions (lanes 5 and 6), corresponding to the heavy chains of the pAb ECL1.

Altogether, the data obtained by the SDS-PAGE analysis showed that the purified sample was indeed enriched in the ECL1 Ab. Hence, it was concluded that all non-relevant proteins had been removed and that the Ab solution was pure and could be utilized for the radiolabelling with ^{99m}Tc.

Characterization of MA1-935 mouse ascites

The mAb MA1-935 was acquired in the form of diluted ascites with a protein concentration of 7.30 mg/mL. This solution of ascites is constituted by the Ab produced by the hybridoma cells (MA1-935), as well as many other proteins, including background Abs produced by the immunized animal, and albumin. Taking that into account, to analyze the composition of the ascites solution, the protein content was assessed by SDS–PAGE, under non-reducing and reducing conditions (**Figure 12**).

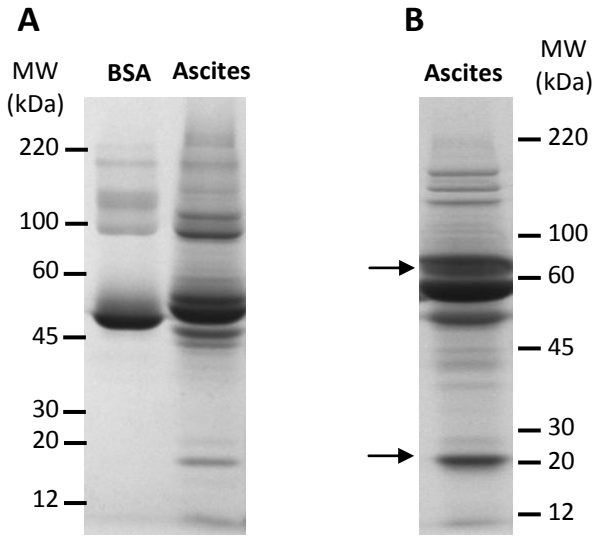

Figure 12: SDS-PAGE analysis of mouse ascites. Samples were loaded at 5 µg of protein per lane. Proteins were resolved in a 10% polyacrylamide gel under non-reducing (**A**) and reducing (**B**) conditions, followed by staining with Bio-Safe Coomassie Blue G-250 stain. MWs of Molecular Weight Markers loaded in an adjacent lane are indicated.

The MA1-935 Ab is a mouse IgM, which is a pentameric immunoglobulin, with each of the five monomers composed by two identical heavy chains and two identical light chains. Under non-reducing conditions (**Figure 12A**), it was not possible to identify the band corresponding to native MA1-935, which presents a MW of about 900 kDa and, consequently, did not migrate easily along the gel.

From the analysis of **Figure 12A** and **B**, it is clear that this mouse ascites solution contains mostly albumin, but also other proteins with different MWs.

Under reducing conditions, there are two bands whose intensity increased (**Figure 12B**, see arrows). The MW of these two bands is consistent with MW of the heavy and light chains of IgM (75 and 25 kDa, respectively). This was predicted, since the treatment of the pentameric IgM with reducing agents cleaves the inter- and intra-chains disulfide bonds of the five monomers.

The analyses by SDS-PAGE of the rabbit serum and the mouse ascites revealed that both samples contained proteins other than the pretended Abs, with a predominance of albumin. Considering the facts that: a) radiolabelling of Abs should be performed with purified Abs; b) the ECL1 Ab was easily and efficiently purified from serum; c) IgMs are more difficult to isolate from mouse ascites; and d) there is more information reported in literature about radiolabelling of IgGs than of IgMs, it was decided to continue the radiolabelling work with the ECL1 Ab.

3.1.2. Antibody analysis by SE-HPLC

Denaturation or aggregation of Abs can be a significant problem in the radiolabelling procedures. Besides that, after radiolabelling, it is necessary to evaluate the radiochemical purity and stability of the radiolabelled Abs. Therefore, SE-HPLC was the chosen technique to analyze the Abs ECL1 and MA1-935. The column used was the TSK G3000SW gel filtration column, which allows the discrimination of molecules from 10 to 500 kDa. First, the column was tested using protein standards with a MW between 13.7 and 669 kDa (**Table 6**). The chromatograms obtained for each of the protein standards are presented in **Figure 34** (**Annexes**).

Table 6: Protein standards for testing the TSK G3000SW gel filtration column and respective MW (kDa) and R_t (min)

Protein Standards	MW (kDa)	R_t (min)
Ribonuclease A	13.7	11.6
BSA	67	9.2
Aldolase	158	8.6
Catalase	232	8.6
Ferritin	440	7.4
Thyroglobulin	669	6.0

Next, the purified ECL1 Ab was analyzed by SE-HPLC (**Figure 13**). The HIG Ab was also analyzed by SE-HPLC (**Figure 13**, **inset**) in order to determine the detection limit in terms of concentration that could be detected at 280 nm. The choice of this Ab was related to the fact that both the Abs are IgGs, so they present similar R_t.

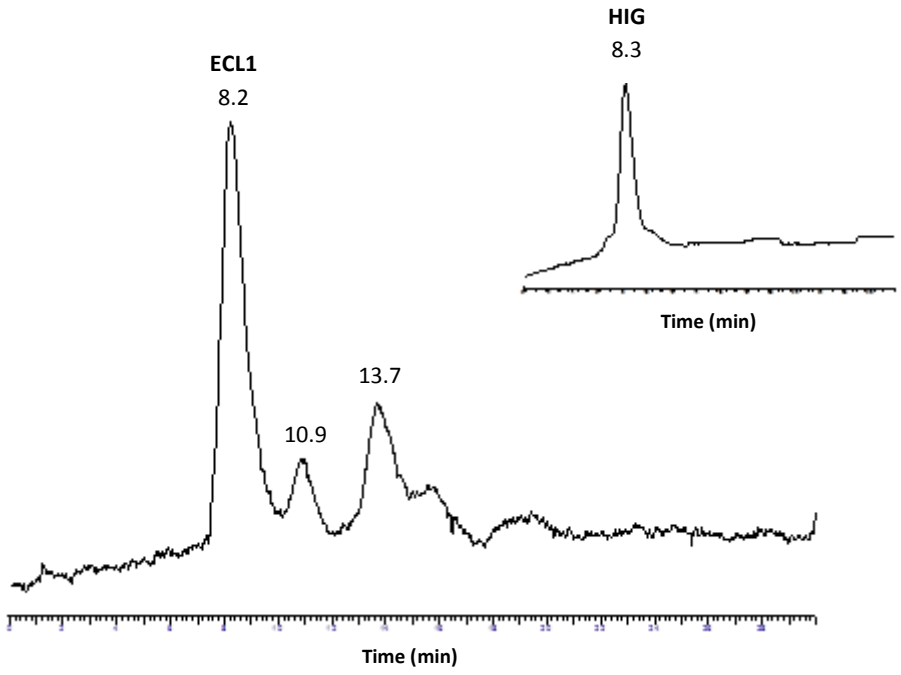

Figure 13: SE-HPLC profile of the purified ECL1, using a TSK G3000SW gel filtration column, with a flow rate of 1.0 mL/min and detection at 280 nm. 0.1 M Na_2SO_4 in 0.1 M phosphate buffer pH 7.0 was used as mobile phase. 20 µL of ECL1 (1:2 dilution - 0.40 mg/mL) were injected. **Inset:** 40 µL of HIG (1:80 dilution - 0.11 mg/mL) were injected and analyzed under the same conditions as ECL1.

The chromatogram of ECL1 in **Figure 13** presents a major peak at 8.2 min corresponding to a native IgG, in agreement to the R_t obtained for the IgG HIG (R_t = 8.3 min), and other two

minor peaks at 10.9 and 13.7 min. Importantly, the HIG Ab was detected at a concentration of approximately 0.11 mg/mL (**Figure 13**, **inset**), which means that, in future analyses, a concentration similar to this value will allow a good detection of ECL1.

The mouse ascites solution of MA1-935 was also analyzed by SE-HPLC, and the separation of the Ab from the other present proteins is shown in **Figure 14**.

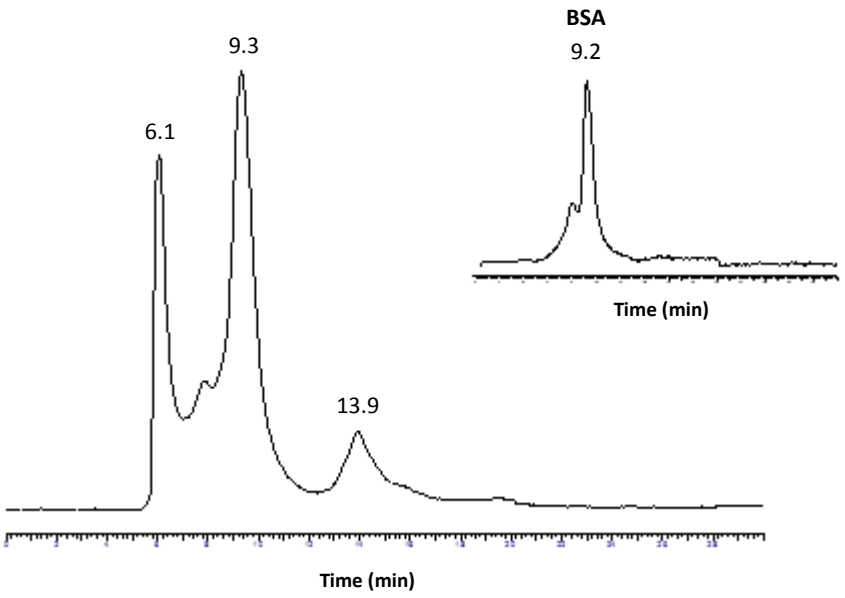

Figure 14: SE-HPLC profile of the mouse ascites, using a TSK G3000SW gel filtration column, with a flow rate of 1.0 mL/min and detection at 280 nm. 0.1 M Na_2SO_4 in 0.1 M phosphate buffer pH 7.0 was used as mobile phase. 10 µL of ascites (1:10 dilution - 0.73 mg/mL) were injected. **Inset:** 40 µL of BSA (0.2 mg/mL) were injected and analyzed under the same conditions as mouse ascites.

As previously mentioned, MA1-935 has a MW of approximately 900 kDa. Considering that the exclusion limit of the column, i.e., the upper limit of MW beyond which molecules will elute at the same R_t, is 500 kDa, the Ab will not be separated of other proteins with a MW superior to 500 kDa. The chromatogram in **Figure 14** presents a peak with a R_t of 6.1 min which, as expected, coincides with the R_t of thyroglobulin (R_t = 6.0 min), a protein with a MW of 669 kDa. Hence, this peak probably corresponds to MA1-935, but also eventually to other proteins with a MW superior to 500 kDa, in case they are present in the ascites.

Regardless of this, the analysis of the mouse ascites by SE-HPLC corroborates the previous data obtained by SDS-PAGE (**Figure 12**). It was concluded by SDS-PAGE that albumin was the most abundant protein present in ascites due to its intense band in the gel. By SE-

HPLC, it is possible to observe a major peak at 9.3 min (**Figure 14**), which according to the R_t of BSA (R_t = 9.2 min) (**Figure 14**, **inset**), corresponds to albumin.

Taken together, these results demonstrate once again that the MA1-935 Ab should be purified before radiolabelling with ^{99m}Tc in order to remove all the contaminant proteins that can impair the radiolabelling.

3.1.3. Radiolabelling with ^{99m}Tc by the direct method

3.1.3.1. Antibody reduction

The Ab radiolabelling by the direct method relies on the binding of ^{99m}Tc to endogenous sulfhydryl groups, generated by reduction of disulfide bonds present in Abs. Therefore, the first step towards the radiolabelling of the purified ECL1 Ab was the reduction of portion of its inter- or intrachain disulfide bonds to free sulfhydryl groups by treatment with an excess of 2-Me, a reducing agent.

The two fractions resulting from the purification of ECL1 with the Melon^{TM} Gel IgG Spin Purification Kit (see **Section 3.1.1.**) were pooled and the A_{280nm} read in a Nanodrop spectrophotometer, giving a final concentration of 0.18 mg/mL. Due to the limitations in the amount of Ab available, the Nanodrop spectrophotometer was chosen for this procedure, as it allows the use of small volumes of Ab for the quantification.

Next, ECL1 Ab was reduced with 2-ME in a molar relation of 1:1000, which has been described as the reducing ratio required to obtain high radiolabelling efficiency.[44,45] After purification of the mixture with a gel filtration PD-10 desalting column to remove the excess of 2-ME, the A_{280nm} of each fraction was read, in order to understand which fractions contained the Ab (**Figure 15**).

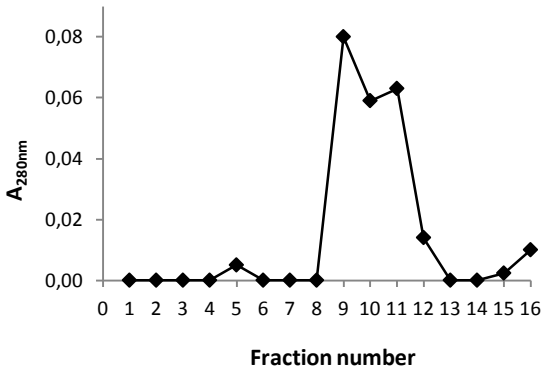

Figure 15: A_{280nm} for each fraction obtained in the purification of the reduced ECL1 with a PD-10 desalting column. Absorbance was read using Nanodrop 2000 spectrophotometer.

Fractions 9 to 11 presented the highest values of A_{280nm} (**Figure 15**), so they were pooled and the Ab solution concentrated to a final concentration of approximately 0.12 mg/mL.

The number of sulfhydryl groups of the reduced ECL1 was assayed using the Ellman's reagent (**Section 2.1.7.**, **Materials and Methods**) and calculated relative to a standard curve obtained by analysis of a series of L-cysteine solutions ranging between 0.01 to 10 mM (**Figure 35A**, **Annexes**). The final number of sulfhydryl groups consists in the ratio between the number of moles of L-cysteine/SH groups present in the Ab and the number of moles of Ab.

The number of sulfhydryl groups determined for the reduced ECL1 was 500 -SH groups per molecule of Ab, a value theoretically too high for an IgG molecule. For example, a murine IgG contains only 6 inter-chain and 12 intra-chain disulfide bonds, giving a maximum of 36 -SH groups per molecule of Ab.[44]

However, it is important to mention that during the course of the work, the A_{412nm} of cysteine solutions was read using two different spectrophotometers: the Nanodrop 2000 and the Varian DMS 80 (see **Section 3.1.3.3.1.**). Comparing the results obtained using the two spectrophotometers, it is possible to observe that for the same concentration of cysteine, the A_{412nm} values are lower when the Nanodrop was used, revealing a lower sensitivity (**Table 8**, **Annexes**). Another problem with the Nanodrop was the low reproducibility between the readings of absorbance for the same sample. Moreover, the concentration of the first non-bound fraction of ECL1 obtained by the protein assay was not in agreement with the calculated in the Nanodrop.

Therefore, one explanation for this high value of sulfhydryl groups might be the fact that the concentration of cysteine/SH groups present in ECL1 was not determined accurately, similarly to the concentration of the final pools of ECL1.

3.1.3.2. Radiolabelling with ^{99m}Tc(I)

Due to the recent development of a new $[^{99m}Tc(CO)_3]^+$ core,[40] and its application in the radiolabelling of several Abs,[42] it was decided to start the radiolabelling of the ECL1 Ab with this core.

Even though the number of sulfhydryl groups determined for the reduced ECL1 was apparently too high for a typical IgG molecule, the radiolabelling of ECL1 was performed. The precursor *fac*-$[^{99m}Tc(CO)_3(H_2O)_3]^+$ was prepared, as described in **Section 2.1.8.3.** (**Materials and Methods**) and 20 µL of a solution of this precursor were added to 20 µL of reduced ECL1 in PBS pH 7.4. The mixture was incubated at 37 °C and the radiolabelling efficiency determined by ITLC-SG at different incubation times (**Figure 16**), to assess the influence of the time of

incubation in the radiolabelling yield. A mixture of 6 M HCl/MeOH (5/95) was used as mobile phase, allowing to separate the radiolabelled Ab and colloidal species (R_f = 0) from the precursor $[^{99m}Tc(H_2O)_3(CO)_3]^+$ and $[^{99m}TcO_4]^-$ (R_f = 0.8 – 1.0). In **Figure 16** are shown the chromatograms of the radiolabelling products obtained by ITLC-SG.

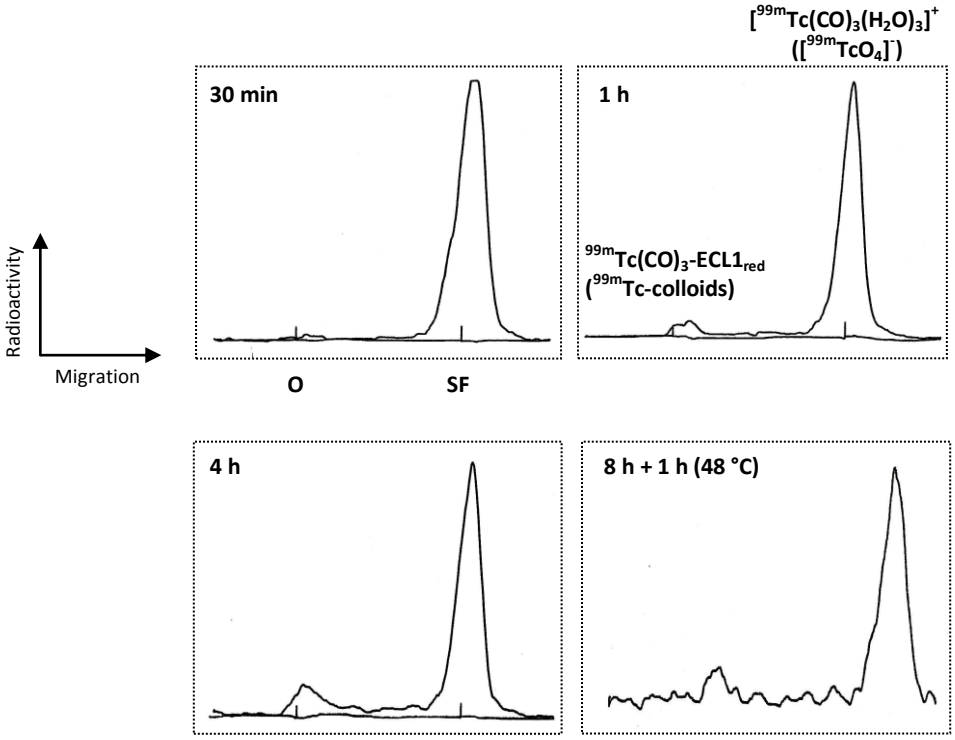

Figure 16: Analysis of the radiolabelling of ECL1 with ^{99m}Tc(I) by ITLC-SG at different incubation times, using ITLC-SG strips as stationary phase and 6 M HCl/MeOH (5/95) as mobile phase. The initial concentration of ECL1 was approximately 0.12 mg/mL. **O** - origin, **SF** - solvent front.

In all chromatograms is observed a major peak corresponding to species that migrated with the solvent front, which can be assigned to $[^{99m}TcO_4]^-$ or to the ^{99m}Tc(I)-tricarbonyl precursor. Since the synthesis of the ^{99m}Tc(I)-tricarbonyl precursor using $[^{99m}TcO_4]^-$ is an well established and optimized procedure with high yield (see **Figure 30 – Section 3.2.4.**), it is expected that the peak observed corresponds mainly to the ^{99m}Tc(I)-tricarbonyl precursor that did not react with ECL1. This can be translated into a low radiolabelling yield of the Ab, although the measured radioactivity at the origin had increased with time (η = 11.0% at 4 h of incubation). The species that remained at the origin can correspond to the radiolabelled Ab or to ^{99m}Tc-colloids. However, ^{99m}Tc-colloids do not occur frequently at low oxidation states of ^{99m}Tc, so this species probably corresponds to the ^{99m}Tc-ECL1.[34]

After 8 h of incubation at 37 °C, the temperature was increased to 48 °C to assess if a higher temperature could promote a higher radiolabelling yield of ECL1. Again, the majority of

the radioactivity was present as ^{99m}Tc(I)-tricarbonyl precursor, revealing that, in this case, the increase of temperature did not contribute to a higher radiolabelling efficiency.

These radiolabelling experiments were performed in a relative proportion of 1:1 of ECL1 and ^{99m}Tc(I)-tricarbonyl precursor. Considering the low radiolabelling yield obtained in these experiments, the relative proportions of ECL1:$[^{99m}Tc(H_2O)_3(CO)_3]^+$ were altered to 2:1 and 3:1 and the radiolabelling efficiency was determined by ITLC-SG at different incubation times. The chromatograms are shown in **Figures 36** and **37** (**Annexes**). Once again, the majority of the radioactivity was present in the form of ^{99m}Tc(I)-tricarbonyl precursor, resulting in a low radiolabelling yield at all the incubation times.

Possible causes for this unsuccessful outcome could be the low concentration of the antibody solution or the incorrect estimation of the SH group in the reduced Ab.

3.1.3.3. Radiolabelling with ^{99m}Tc(IV)

Due to the unsuccessful radiolabelling of ECL1 with ^{99m}Tc(I), an alternative approach was performed, using the weak competing ligand MDP, which allows the stabilization of the reduced ^{99m}Tc (from the oxidation state +VII to +V) and the radiolabelling of ECL1 by transchelation from ^{99m}Tc-MDP.

3.1.3.3.1. Radiolabelling optimization

Attending to the limitations in the amount of ECL1 available for the radiolabelling experiments, the radiolabelling protocol of the IgG with ^{99m}Tc(IV) was first optimized with the IOR-CEA1 Ab. It was necessary to test different radiolabelling conditions and achieve the maximal radiolabelling efficiency, in order to apply those conditions in the radiolabelling of ECL1.

Similarly to ECL1, the IOR-CEA1 Ab solution was also quantified, reduced and purified. First, the A_{280nm} of IOR-CEA1 was read in the Varian DMS 80 spectrophotometer, giving a concentration of approximately 1.32 mg/mL. Based on previous reports in literature in which the Ab was reduced at a concentration of 10 mg/mL,[44,45] IOR-CEA1 was concentrated to 10 mg/mL and reduced with 2-ME, in a molar relation of 1000:1 (2-ME:IOR-CEA1). After purification with a PD-10 desalting column, the fractions containing Ab were pooled, and the final concentration calculated as 0.33 mg/mL.

The number of sulfhydryl groups was determined with Ellman's assay in the Varian DMS 80 spectrophotometer, giving 53 -SH groups per molecule of Ab. The standard curve describing the relation between the concentration of a series of L-cysteine solutions ranging between 0.01 and 2 mM and A_{412nm} is shown in **Figure 35B** (**Annexes**). Again, this value is considered somewhat high for what would be expected for an IgG molecule (36 -SH groups), although much lower than the one calculated for the ECL1.

After the reduction of the IOR-CEA1 mAb and before its radiolabelling by transchelation, the radiolabelling of MDP alone was performed under different conditions, in order to understand which were the best conditions for the formation of ^{99m}Tc-MDP.

In **Figure 17** are shown three chromatograms obtained by ITLC-SG, wherein the amount of MDP was varied and the amount of $[^{99m}TcO_4]^-$ maintained (50 µL). MEK was used as mobile phase, allowing to detect ^{99m}Tc-MDP and ^{99m}Tc-colloids at the origin and free $[^{99m}TcO_4]^-$ at the solvent front.

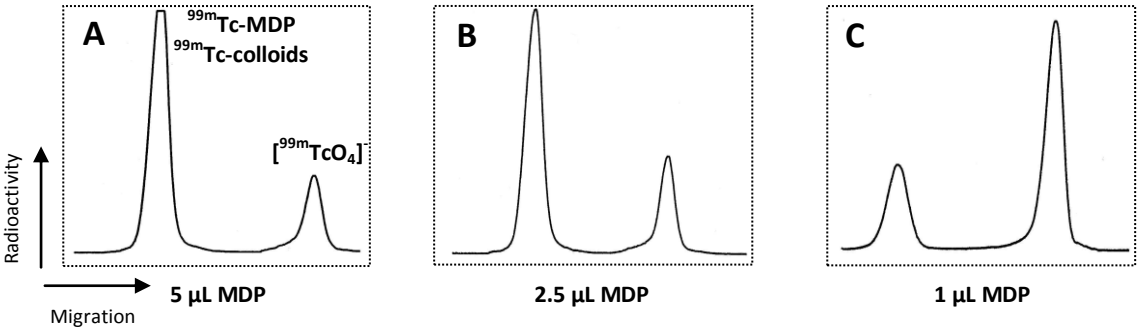

Figure 17: Analysis of the radiolabelling of MDP with ^{99m}Tc(IV) by ITLC-SG, using ITLC-SG strips as stationary phase and MEK as mobile phase. 50 µL of $[^{99m}TcO_4]^-$ were added to 5 µL (**A**), 2.5 µL (**B**) and 1 µL (**C**) of MDP and the reaction vial incubated at r.t. for 15 min.

As can be observed in **Figure 17**, the radiolabelling efficiency, as expected, is dependent of the amount of MDP. The formation of ^{99m}Tc-MDP was achieved with 79% of yield for (**A**), 77% for (**B**) and 32% for (**C**).

One of the goals of these experiments was to understand what was the minimum amount of MDP and $[^{99m}TcO_4]^-$ that could be used without impairing the radiolabelling efficiency, in order to dilute the Ab the least possible in the next experiments. However, in the conditions used in **C** (1 µL of MDP to 50 µL $[^{99m}TcO_4]^-$), the worst radiolabelling yield was obtained, possibly due to the small amount of MDP that was available to react with $[^{99m}TcO_4]^-$

or due to the low amount of reducing agent necessary to reduce ^{99m}Tc from the oxidation state (VII) to (V). This reducing agent is present in the MDP kit that is reconstituted with a solution of 0.9% (w/v) NaCl.

Other radiolabelling conditions with different amounts of MDP and $[^{99m}TcO_4]^-$ were tested (e.g., 2.5 µL of MDP in 25 µL of $[^{99m}TcO_4]^-$), but the radiolabelling conditions used in **A** and **B** presented the highest yields.

Next, the IOR-CEA1 mAb was radiolabelled with ^{99m}Tc(IV) by transchelation of ^{99m}Tc from ^{99m}Tc-MDP, using the above described conditions in **A** and **B**. In **Figure 18** are shown the chromatograms obtained by ITLC-SG with the radiolabelling with 5 µL of IOR-CEA1, 2.5 µL of MDP and 50 µL of $[^{99m}TcO_4]^-$ for 15 min at r.t.. Besides the use of MEK as mobile phase (**Figure 18A**), 1.0 M sodium acetate was also used (**Figure 18B**), to differentiate ^{99m}Tc-IOR-CEA1 and ^{99m}Tc-colloids from ^{99m}Tc-MDP, which migrate with the solvent front.

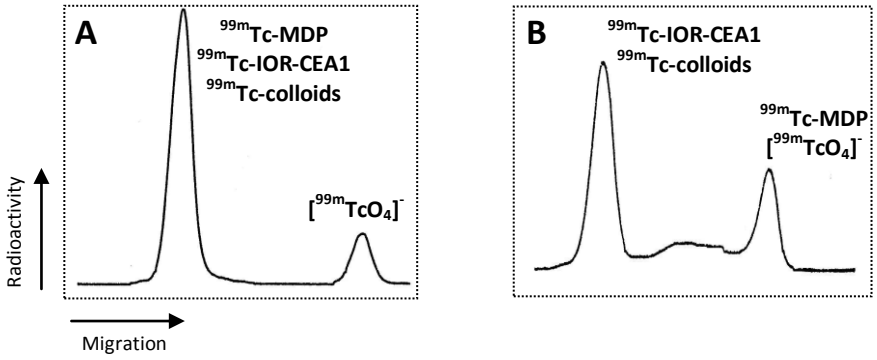

Figure 18: Analysis of radiolabelling of IOR-CEA1 with ^{99m}Tc(IV) by ITLC-SG, using ITLC-SG strips as stationary phase and MEK (**A**) and 1.0 M sodium acetate (**B**) as mobile phases. 5 µL of IOR-CEA1 were added to a solution of 2.5 µL of MDP and 50 µL of $[^{99m}TcO_4]^-$ and the reaction vial incubated at r.t. for 15 min. The initial concentration of IOR-CEA1 was approximately 0.33 mg/mL.

As shown in **Figure 18A**, the majority of radioactivity remained at the origin present as ^{99m}Tc-IOR-CEA1, ^{99m}Tc-MDP (or ^{99m}Tc-colloids). The separation of ^{99m}Tc-IOR-CEA1/^{99m}Tc-colloids from ^{99m}Tc-MDP was achieved with 1.0 M sodium acetate, the eluent used in the chromatogram in **Figure 18B**. Thus, it was obtained a 72% yield for the radiolabelling of IOR-CEA1.

The above radiolabelling was achieved with IOR-CEA1 at a concentration of approximately 0.33 mg/mL. Considering that the concentration of ECL1 was approximately 0.12 mg/mL, the radiolabelling of IOR-CEA1 at 0.23 and 0.13 mg/mL was also tested (**Table 7**).

Table 7: Percentage of ^{99m}Tc species formed in the radiolabelling of IOR-CEA1 at different concentrations, using 5 µL of Ab, 2.5 µL of MDP and 50 µL of $[^{99m}TcO_4]^-$. The different species were separated using MEK and 1.0 M sodium acetate as mobile phases

^{99m}Tc species	[IOR-CEA1] (mg/mL)		
	0.33	**0.23**	**0.13**
$[^{99m}TcO_4]^-$	17%	30%	38%
^{99m}Tc-MDP	11%	38%	47%
^{99m}Tc-IOR-CEA1 + ^{99m}Tc-colloids	72%	32%	15%

The percentage of free $[^{99m}TcO_4]^-$ and ^{99m}Tc-MDP increased as the concentration of Ab decreased (**Table 7**). Hence, it can be concluded that the radiolabelling with ^{99m}Tc(IV) is dependent of the Ab concentration, obtaining higher radiolabelling yields when the Ab is more concentrated.

3.1.3.3.2. Radiolabelling of ECL1

Taking into account that radiolabelling of ECL1 with ^{99m}Tc(I) was not possible at high yields (**Section 3.1.3.2.**), the Ab was then radiolabelled with ^{99m}Tc(IV). Considering that higher radiolabelling yields were obtained when IOR-CEA1 was more concentrated (~ 0.33 mg/mL, η = 72%), it was decided to concentrate ECL1 to a final concentration of approximately 0.30 mg/mL. ECL1 was radiolabelled with ^{99m}Tc(IV) under the same conditions as IOR-CEA1 (**Figure 18**), i.e., 5 µL of ECL1, 2.5 µL of MDP and 50 µL of $[^{99m}TcO_4]^-$, for 15 min at r.t. and the radiolabelling efficiency was evaluated by ITLC-SG, using MEK and 1.0 M sodium acetate as mobile phases (**Figure 19A** and **B**, respectively).

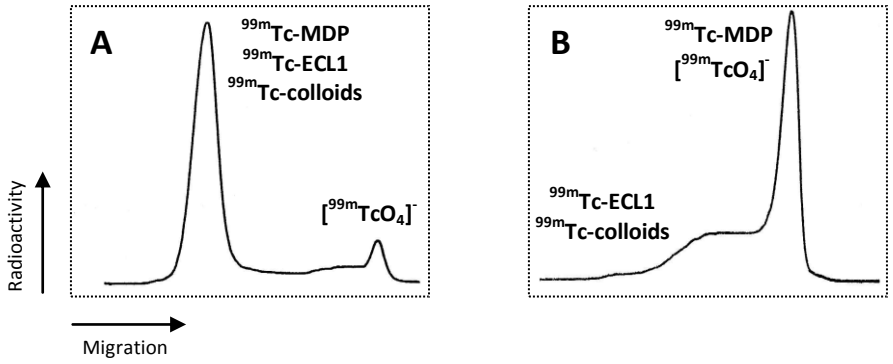

Figure 19: Analysis of radiolabelling of ECL1 with ^{99m}Tc(IV) by ITLC-SG, using ITLC-SG strips as stationary phase and MEK (**A**) and 1.0 M sodium acetate (**B**) as mobile phases. 5 µL of ECL1 were added to 2.5 µL of MDP and 50 µL of $[^{99m}TcO_4]^-$ and the reaction vial incubated at r.t. for 15 min. The initial concentration of ECL1 was ~0.30 mg/mL.

A very small amount of free $[^{99m}TcO_4]^-$ (approximately 7%) was observed in the chromatogram obtained with MEK as mobile phase (**Figure 19A**). However, there were not observed radioactive species at the origin when 1.0 M sodium acetate was used as mobile phase (**Figure 19B**), meaning that the radioactivity observed at the origin in **Figure 19A** corresponded to ^{99m}Tc-MDP, which migrates with the solvent front when 1.0 sodium acetate is used.

Due to the failure in the radiolabelling of ECL1 with the above conditions, the amount of ECL1 used in the radiolabelling was increased (15 µL of ECL1, 2.5 µL of MDP and 50 µL of $[^{99m}TcO_4]^-$) and the radiolabelling efficiency evaluated by ITLC-SG at different incubation times (1h15 min, 3h), using MEK and 1.0 M sodium acetate as mobile phases. Once again, it was not observed radiolabelled ECL1 by ITLC-SG using 1.0 M sodium acetate as mobile phase.

Although the radiolabelling of ECL1 had been performed under the same conditions as the radiolabelling of IOR-CEA1, ^{99m}Tc-ECL1 was not detected. A possible cause can be the fact that the Ab was reduced and stored for a few weeks until it was radiolabelled with ^{99m}Tc(IV). This storage was done at 4 °C under a nitrogen atmosphere, in order to prevent the oxidation of the sulfhydryl groups, necessary to the radiolabelling. However, it cannot be completely excluded the possibility that oxidation of these groups may have occurred, originating disulfide bonds, which prevent the radiolabelling by the direct method.

3.2. RADIOLABELLING OF MOLECULAR IMAGING PROBES BASED ON CFTR INHIBITORS

In addition to the radiolabelling of anti-CFTR Abs, the aim of this thesis was also the radiolabelling of the small molecules **$CFTR_{inh}$-172a** and **GP_{inh}-5a**, known to inhibit the function of CFTR, with the *fac*-$[^{99m}Tc(CO)_3]^+$ core, using the BCF approach (**Scheme 2**). These two small organic molecules were chosen because they interact with CFTR at the channel pore and therefore, if successfully achieved, these radiolabelled probes will allow the detection of CFTR present at the PM.

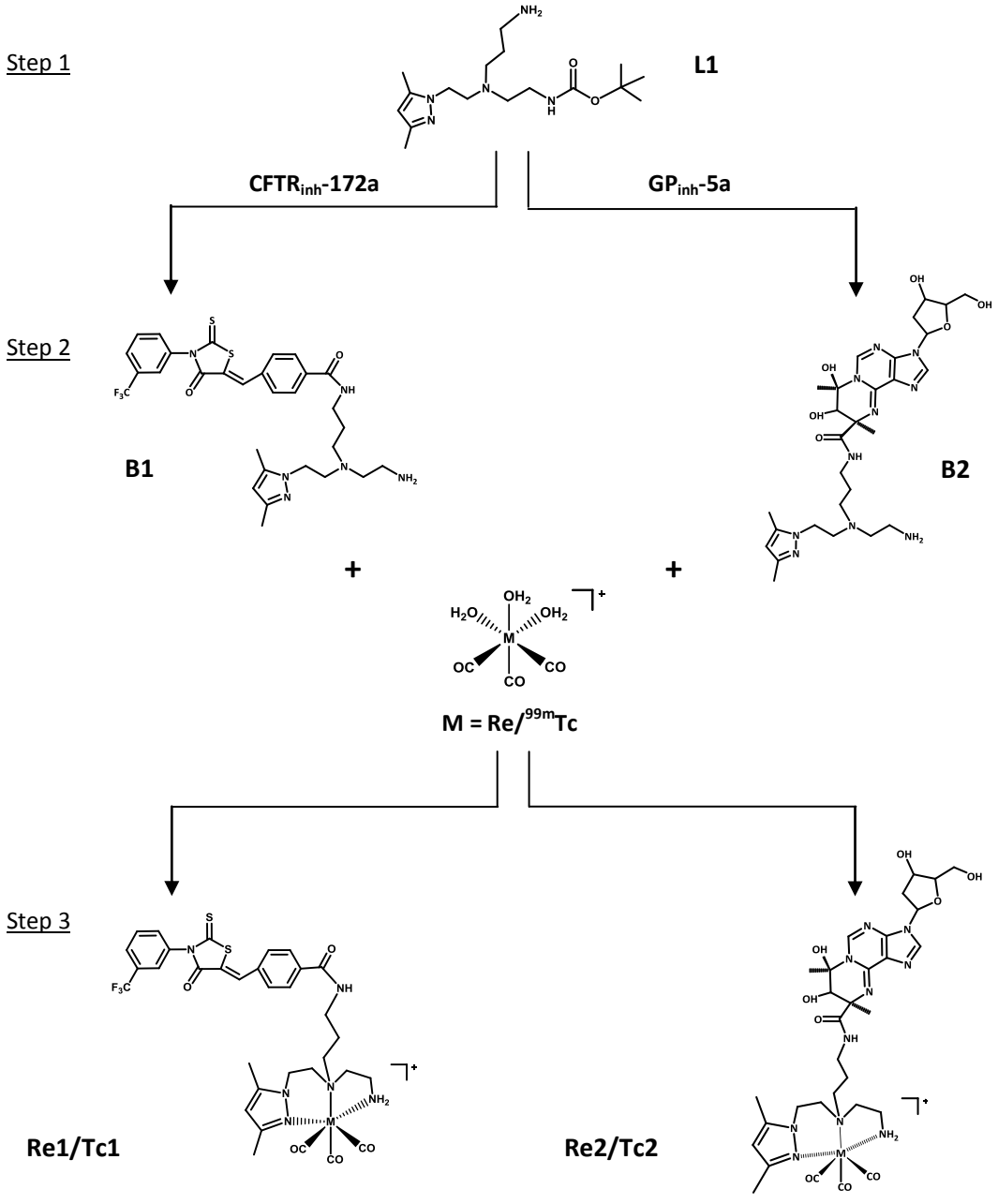

Scheme 2: Radiolabelling of the CFTR inhibitors $CFTR_{inh}$-172a and GP_{inh}-5a with the *fac*-$[^{99m}Tc(CO)_3]^+$ core.

In this strategy, the first step aimed at the synthesis of the BFC (**L1**) containing a pyrazolyl-diamine unit (with a *N*,*N*,*N* donor atom set), a spacer of three carbons and a terminal functional group (-NH_2) for conjugation to biomolecules. This BFC was chosen since it is known that tridentate BFCs are better at stabilizing the *fac*-[^{99m}Tc(CO)$_3$]$^+$ core. Monodentate and bidentate BFCs form ^{99m}Tc(I)-tricarbonyl complexes that still have one or two water molecules, respectively, that can be easily substituted by other ligands.[29,33] After conjugation of both inhibitors to the BFC (step 2), step 3 was the reaction of both bioconjugates (**B1** and **B2**) with the *fac*-[M(CO)$_3$(H_2O)$_3$]$^+$ precursor (M = Re/^{99m}Tc), in order to obtain the final compounds, the Re(I) and ^{99m}Tc(I) complexes (**Re1/Re2** and **Tc1/Tc2**, respectively).

In this chapter is described the synthesis and characterization of the BFC **L1** (**Section 3.2.1.**) and bioconjugates **B1** and **B2** (**Section 3.2.2.**), and their reaction with the organometallic precursors *fac*-[Re(CO)$_3$(H_2O)$_3$]$^+$ (**Section 3.2.3.**) and *fac*-[^{99m}Tc(CO)$_3$(H_2O)$_3$]$^+$ (**Section 3.2.4.**).

3.2.1. Synthesis and characterization of the bifunctional chelator L1

The asymmetric and BFC **L1** was synthesized via a multistep synthetic procedure previously reported by the RSG-IST/CTN (**Scheme 3**).[63,64]

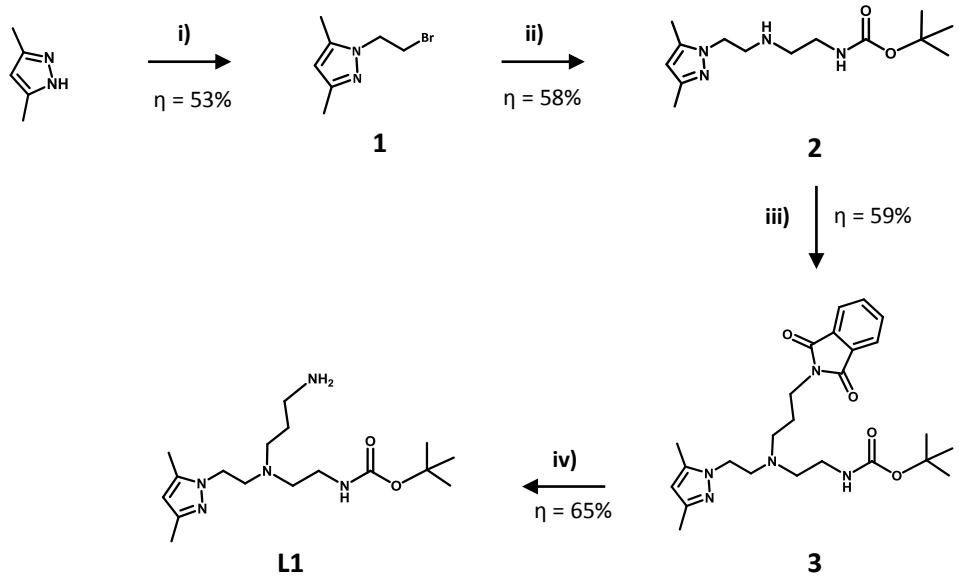

Scheme 3: Synthesis of L1. **i)** 1,2-dibromoethane, NaOH 40%, TBAB, reflux, overnight; **ii)** *tert*-butyl 2-aminoethylcarbamate, K_2CO_3, KI, dry ACN, reflux, overnight; **iii)** 3-bromopropylphthalimide, K_2CO_3, KI, dry ACN, reflux, overnight; **iv)** hydrazine monohydrate, MeOH, reflux, 6 h.

The first synthetic step involved the *N*-alkylation of 3,5-dimethyl-pyrazole in the presence of an excess of 1,2-dibromoethane, under the conditions depicted in **Scheme 3**, to yield intermediate **1**. TBAB was used as a phase transfer catalyst in order to allow the migration of 3,5-dimethylpyrazole from the aqueous to the organic phase. Intermediate **1** reacted with *tert*-butyl-2-aminoethylcarbamate in dry ACN to give intermediate **2**. Alkylation of the central amine in **2** with 3-bromopropylphthalimide gave intermediate **3**, which upon treatment with hydrazine monohydrate in refluxing MeOH resulted in **L1**. All intermediates (**1**, **2** and **3**) were characterized by ^{1}H-NMR spectroscopy (**Figures 43-45**, **Annexes**).

The final compound **L1** was characterized by NMR spectroscopy (^{1}H and ^{13}C) and RP-HPLC. The use of bidimensional-NMR experiments (^{1}H-^{1}H gradient correlation spectroscopy (gCOSY) and ^{1}H-^{13}C gradient heteronuclear single quantum coherence (gHSQC)) was essential for peak assignment in the ^{1}H and ^{13}C spectra.

The ^{1}H-NMR spectrum of **L1** in $CDCl_3$ with peak assignment is shown in **Figure 20**. Briefly**,** the spectrum presents a singlet peak (δ 5.80) corresponding to proton 4 of the pyrazole ring (CH^{b}) and two singlet peaks (δ 2.27 and 2.21), integrating each one to three protons, corresponding to the methyl protons of the heteroaromatic ring. The presence of the Boc group is confirmed by an intense singlet (δ 1.41) integrating for nine protons. The protons of the amide (δ 5.39) and the free amine (δ 3.73) appear as broad peaks. Resonances for all methylenic protons were also found and fully assigned (δ 3.99, CH_2^{d}; 3.06, CH_2^{g}; 2.75, $CH_2^{e/j}$; 2.51, $CH_2^{f/h}$; 1.61, CH_2^{i}).

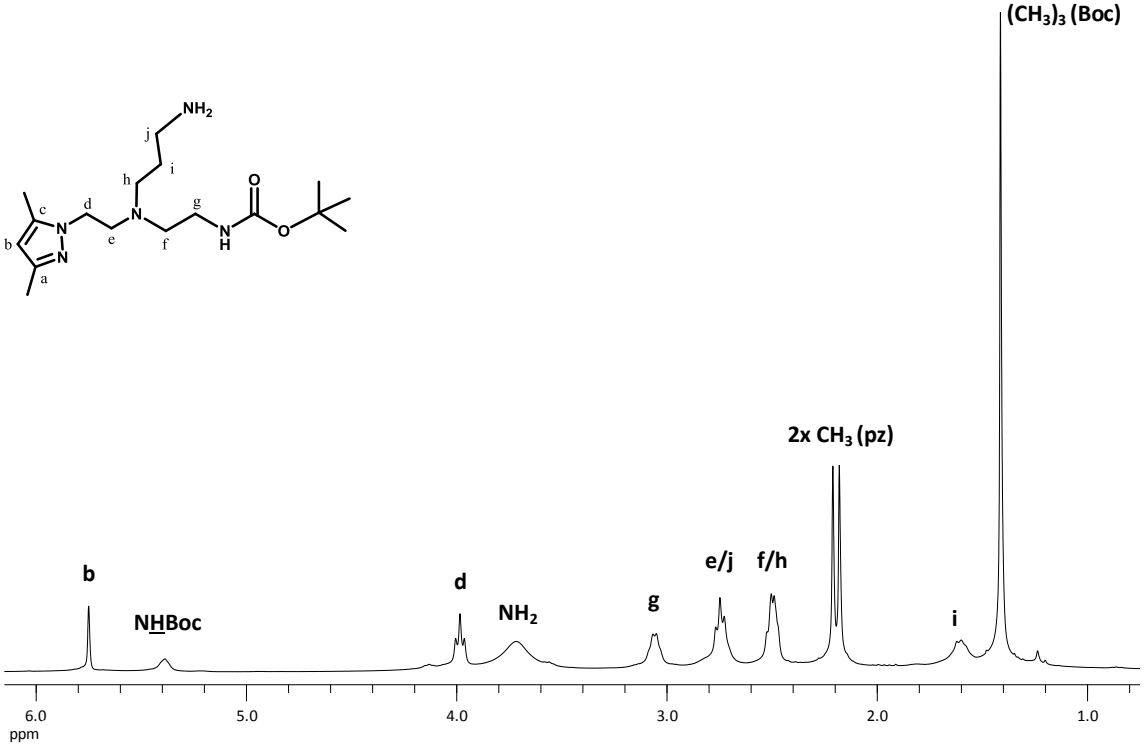

Figure 20: ^{1}H-NMR spectrum of **L1** in $CDCl_3$.

The ^{1}H-NMR spectrum of **L1** was also obtained in CD_3OD (**Figure 46**, **Annexes**). The chemical shifts as well as the multiplicities observed in this spectrum are very similar with those found in the ^{1}H-NMR spectrum of **L1** in $CDCl_3$.

The ^{13}C-NMR spectrum of **L1** in $CDCl_3$ with peak assignment is shown in **Figure 21**. The spectrum presents signals corresponding to all the expected carbon nuclei of **L1**. Relatively to the Boc group, the three different carbon atoms resonate at different chemical shifts and the assignment was based on previous characterization of organic compounds with a Boc group.[66] The most deshielded peak in the spectrum (δ 156.1) corresponds to the C=O group. The quaternary carbon of Boc resonates at δ 79.1, and this type of carbons (without an attached proton) is characterized by peaks of distinctly low intensities. Finally, the three Boc methyl groups appear as an intense singlet at δ 28.3. The signals corresponding to the pyrazolyl ring carbons appear at low field (δ 147.4, C^c; 138.9, C^a; 105.4, C^b) and at high field in the case of the two methyl goups (δ 13.2 and 11.0). Resonances for all methylenic carbons were also found and fully assigned (δ 53.7, C^e; 52.6, C^h; 51.8, C^f; 46.5, C^d; 38.3, C^g; 38.0, C^j; 24.0, C^i).

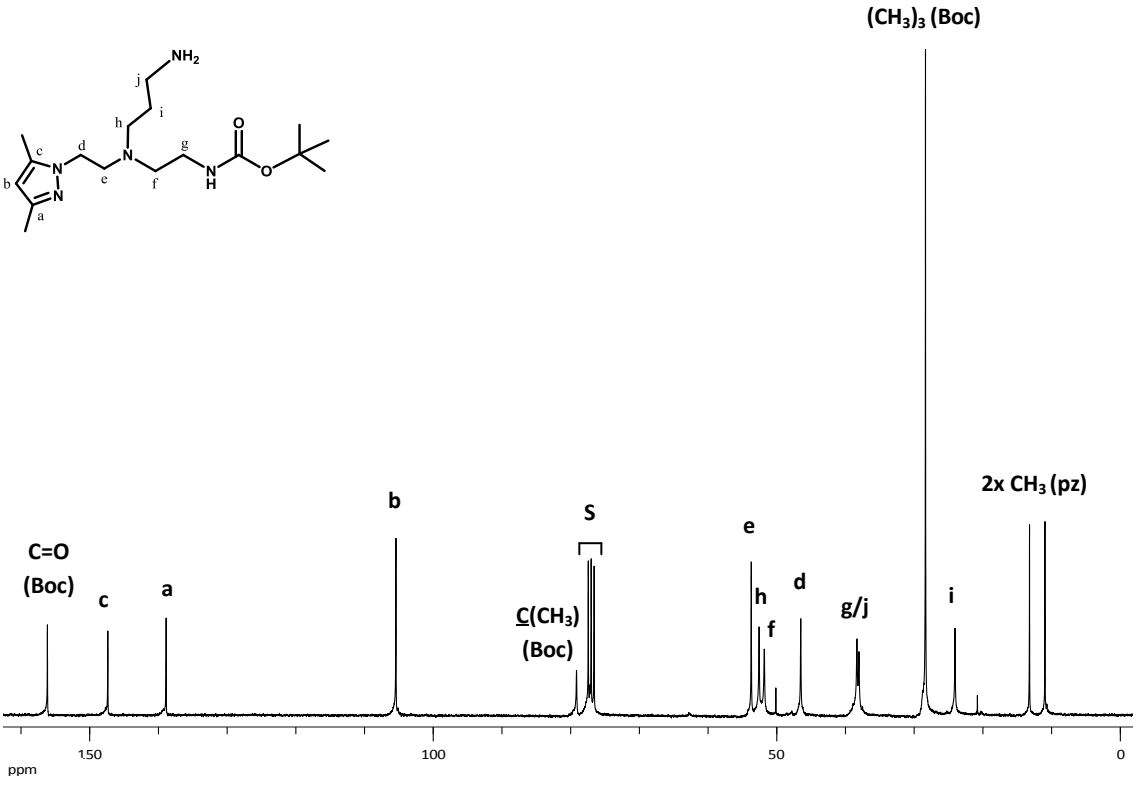

Figure 21: ^{13}C-NMR spectrum of **L1** in $CDCl_3$. S = chloroform.

The bifunctional chelator **L1** was also characterized by RP-HPLC, with a R_t of 11.2 min.

3.2.2. Synthesis and characterization of bioconjugates

3.2.2.1. Synthesis and characterization of B1

To obtain the bioconjugate **B1**, the small molecule inhibitor **$CFTR_{inh}$-172a** was conjugated to **L1**, the BFC previously synthesized (**Section 3.2.1.**), via a two-step synthetic pathway, as depicted in **Scheme 4**.

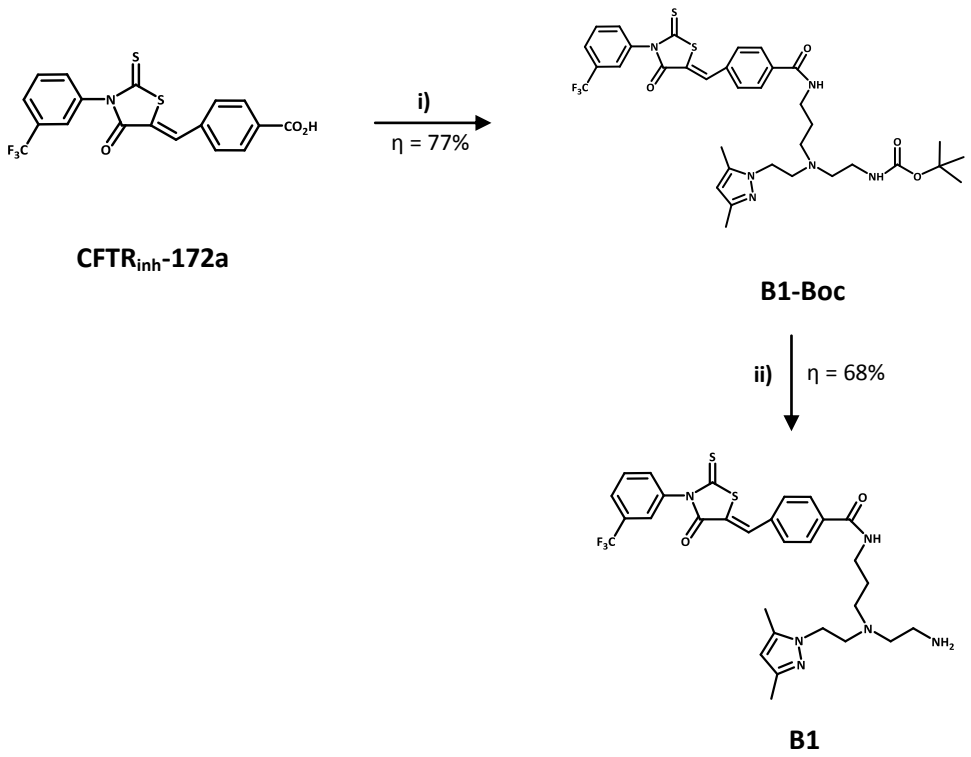

$CFTR_{inh}$-172a

B1-Boc

B1

Scheme 4: Synthesis of B1. **i) L1**, HBTU, DIPEA, dry DMF, r.t., 4 d; **ii)** TFA:CH_2Cl_2 (1:2), r.t., 2 h.

Direct conjugation of **$CFTR_{inh}$-172a** to **L1** using HBTU as a coupling reagent and DIPEA, in dry DMF, yielded **B1-Boc** (η = 77%). The protective Boc group of **B1-Boc** was removed with a mixture of TFA:CH_2Cl_2 (1:2) giving bioconjugate **B1** with 68% yield, after purification by silica gel column chromatography.

Intermediate **B1-Boc** was characterized by ^{1}H- and ^{13}C-NMR spectroscopy (**Figures 47** and **48**, **Annexes**) and the final compound **B1** was characterized by NMR spectroscopy (^{1}H and ^{13}C), ESI-MS and RP-HPLC. The peak assignment in the NMR spectra was based on two-dimensional-NMR experiments (^{1}H-^{1}H gCOSY and ^{1}H-^{13}C gHSQC).

In order to help with the characterization of **B1**, the free inhibitor **$CFTR_{inh}$-172a** was also studied by NMR spectroscopy (^{1}H and ^{13}C), (**Figures 38-40**, **Annexes**). Due to the partial

solubility of **CFTR$_{inh}$-172a** in MeOH, two ^{1}H-NMR spectra of **CFTR$_{inh}$-172a** were acquired: in CD_3OD and in a mixture of CD_3OD and DMSO-d_6. Although the inhibitor is totally soluble only with the use of CD_3OD and DMSO-d_6, the chemical shifts, as well as, the multiplicities were very similar in both spectra. Therefore the ^{1}H-NMR spectrum in CD_3OD was chosen for a more accurate comparison with the spectrum of the bioconjugate **B1**.

The ^{1}H-NMR spectrum of **B1** in CD_3OD with peak assignment is shown in **Figure 22**. The chemical shifts as well as the multiplicities present similarities to those found both for free **L1** and **CFTR$_{inh}$-172a**. The spectrum presents the signals relative to all protons of the **CFTR$_{inh}$-172a** moiety, namely a doublet at δ 7.98, integrating for two protons and corresponding to two protons of the carboxyphenyl group, and a multiplet (δ 7.86 - 7.64) integrating for seven protons, four of the trifluoromethylphenyl group, two of the carboxyphenyl group and one exocyclic proton. The signals relative to all protons of the **L1** moiety were also found and assigned. The spectrum presents the typical singlet peaks for proton 4 (CH^b, δ 5.85) and methyl groups (δ 2.27 and 2.18) of pyrazolyl ring and also resonances for all the methylenic protons (δ 4.09, CH_2^d; 3.25, CH_2^j; 3.01, CH_2^g; 2.86-2.75, $CH_2^{e/f}$; 2.54, CH_2^h; 1.62, CH_2^i).

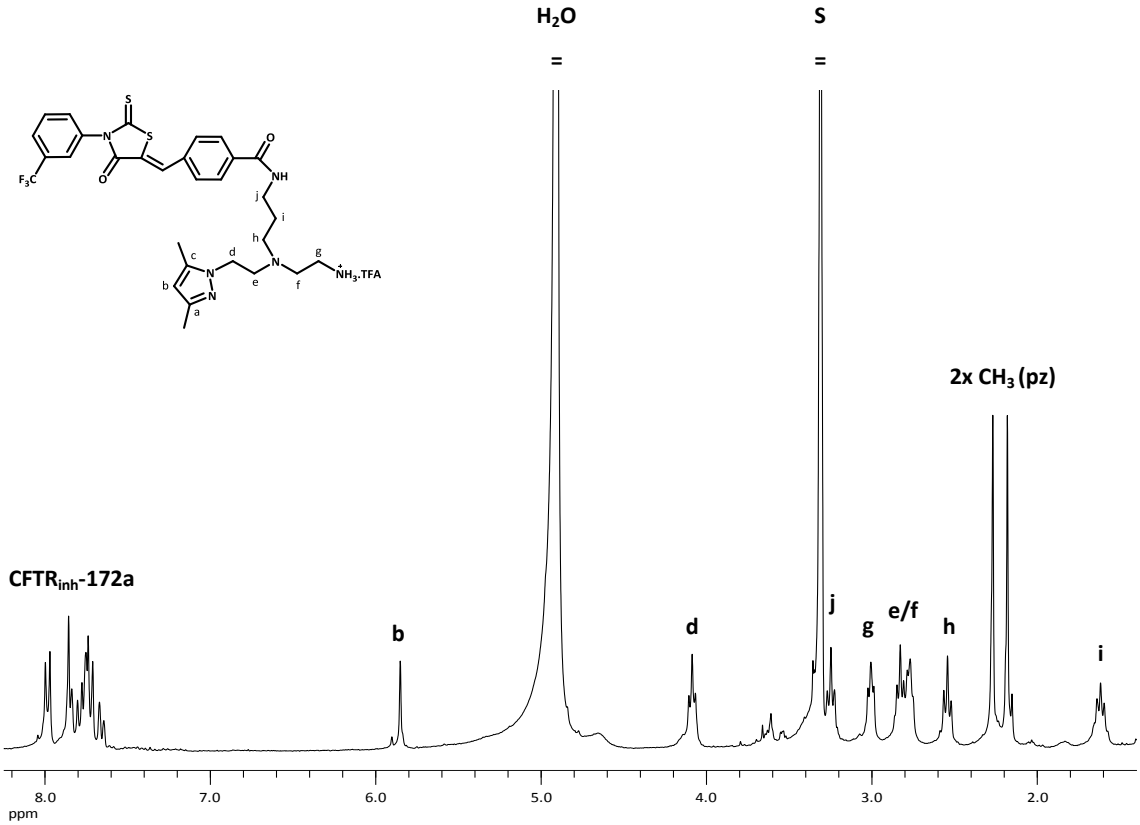

Figure 22: ^{1}H-NMR spectrum of **B1** in CD_3OD. S = residual MeOH.

However, there are differences in the chemical shifts of some protons that evidence conjugation of the inhibitor to **L1**. Two aromatic protons of the carboxyphenyl group of **CFTR$_{inh}$-172a** (δ 8.14) are shifted upfield (δ 7.98, Δ = 0.16 ppm) in the spectrum of **B1**. Additionally, the protons *j* of **L1** (δ 2.79) are shifted downfield (δ 3.25, Δ = 0.46 ppm) in the spectrum of **B1**.

The ^{13}C spectrum of **B1** in CD_3OD (**Figure 23**) presents also the signals relative to all the carbons of the **L1** and **CFTR$_{inh}$-172a** moieties. The most deshielded peaks correspond to the carbon atoms of the double bonds C=S (δ 194.9) and C=O (δ 169.0 and 168.6) in **CFTR$_{inh}$-172a**, and the chemical shifts are similar to those observed in ^{13}C spectrum of the free **CFTR$_{inh}$-172a** (**Figure 40**, **Annexes**).

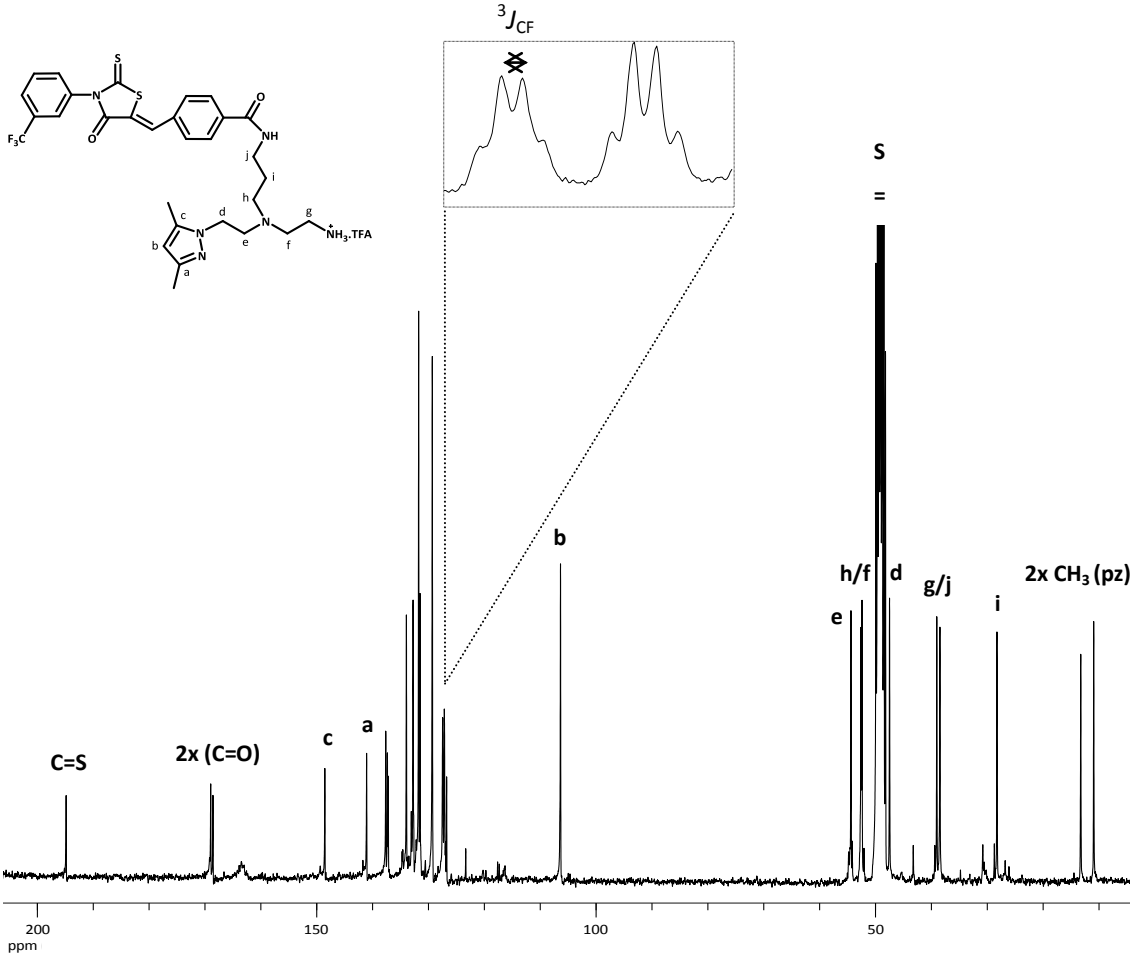

Figure 23: ^{13}C-NMR spectrum of **B1** in CD_3OD. **Inset:** Quartets resulting from the ^{13}C - ^{19}F coupling at three bonds distance. S = residual MeOH.

An important characteristic of **CFTR$_{inh}$-172a** (and **B1**) relates with the presence of the CF_3 group. This group, located on an aromatic system, is advantageous because of an easy assignment of carbon atoms due to the coupling with the fluorine nucleus. Plus, the coupling

constants (J_{CF}) and respective chemical shifts are well described in literature.[67,68] This coupling is observed in the ^{13}C spectrum of **B1** as quartets, with coupling constants of 272.03 Hz ($^{1}J_{CF}$, δ 125.1) at one bond distance, 33.04 Hz ($^{2}J_{CF}$, δ 132.9) at two bonds distance, and 3.60 Hz ($^{3}J_{CF}$, δ 127.5) and 3.80 Hz ($^{3}J_{CF}$, δ 127.2) at three bonds distance (**Figure 23**, **inset**). The chemical shifts of the peaks observed for each C-F coupling are presented in **Table 9** in **Annexes** (see also **Figure 49, Annexes**).

The carbon atoms of the **L1** moiety were fully assigned with the help of ^{1}H-^{13}C gHSQC experiment. However, it was not possible to fully assign the remaining carbons corresponding to the **CFTR$_{inh}$-172a** pharmacophore.

The bioconjugate **B1** was also characterized by ESI-MS. The positive mode spectrum (**Figure 24**) presents a major peak, corresponding to the molecular ion, with a m/z value of 631.4, which is in agreement with the expected value for **B1** ($[M + H]^+$ = 631.2).

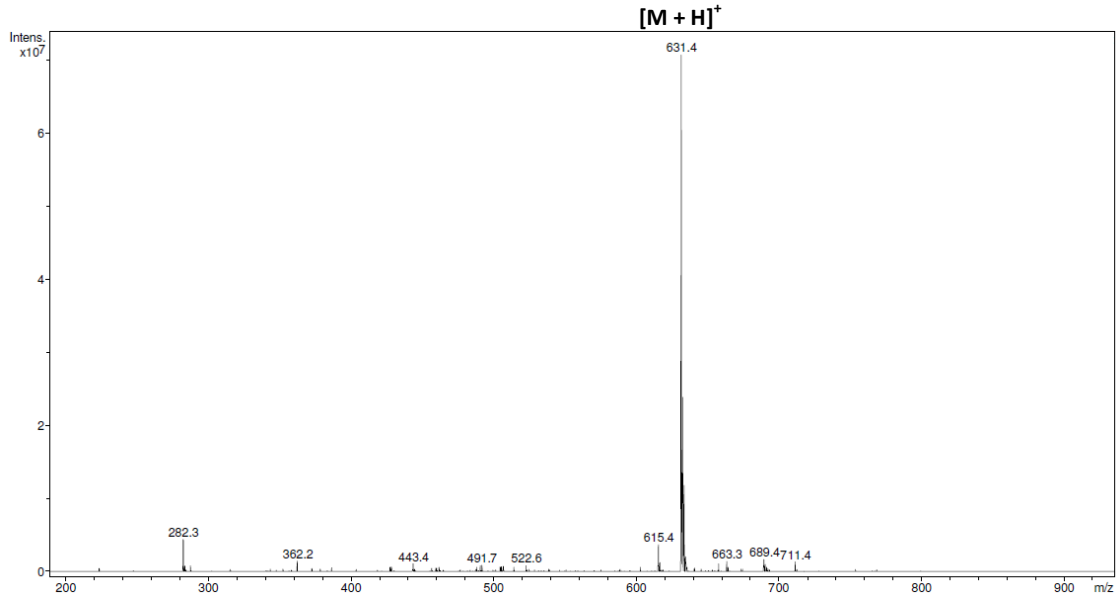

Figure 24: Mass spectrum of **B1** in the positive mode, obtained by ESI (631.4 $[M + H]^+$, calculated for $C_{30}H_{33}F_3N_6O_2S_2$ = 630.2).

Finally, the bioconjugate **B1** was analyzed by RP-HPLC (method 1, λ = 220 nm) and the R_t of 17.6 min obtained was different from the R_t of the free inhibitor (20.3 min) and from the R_t of free ligand **L1** (R_t = 11.3 min).

Taken together, the results obtained by different characterization techniques (^{1}H-NMR, ^{13}C-NMR, ESI-MS and RP-HPLC) allowed the full structural characterization of **B1**.

3.2.2.2. Synthesis and characterization of B2

Similarly to **B1**, bioconjugate **B2** was obtained by the conjugation of the small molecule inhibitor **GP_{inh}-5a** to the BFC **L1**, as depicted in **Scheme 5**.

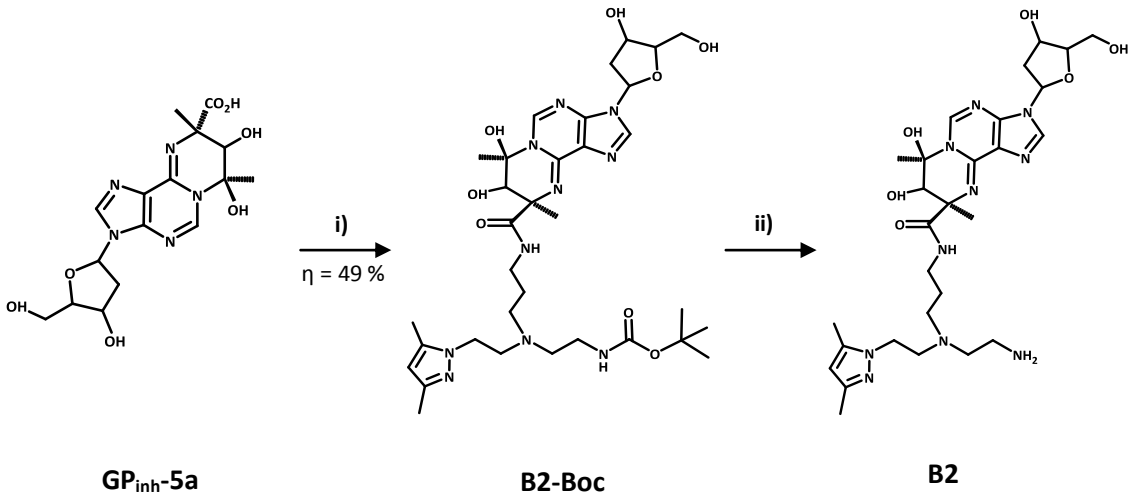

Scheme 5: Synthesis of B2. **i) L1**, HBTU, DIPEA, dry DMF, r.t., 7 d; **ii)** TFA:CH_2Cl_2 (1:2), r.t., 2 h.

Direct conjugation of **GP_{inh}-5a** to **L1** gave **B2-Boc** in 49% yield. Treatment of **B2-Boc** with a TFA:CH_2Cl_2 (1:2) mixture, yielded bioconjugate **B2**. Unfortunately, after several attempts of purification of **B2** by Sep-Pak C18 chromatography and silica-gel column chromatography, and analysis of the elution fractions by TLC and ^{1}H-NMR spectroscopy, it was not possible to obtain pure fractions of **B2**.

Therefore, only the characterization of **B2-Boc** by NMR spectroscopy (^{1}H and ^{13}C) is presented next. Once again, to help with the characterization of **B2-Boc** (and **B2**), the free inhibitor **GP_{inh}-5a** was also studied by NMR spectroscopy (^{1}H and ^{13}C), (**Figures 41** and **42**, **Annexes**).

The ^{1}H-NMR spectrum of **B2-Boc** in CD_3OD with peak assignment is shown in **Figure 25.** Signals relative to all the protons of the **GP_{inh}-5a** and **L1** moieties are present and the chemical shifts, as well as the multiplicities, are very similar to those found for free **GP_{inh}-5a** and **L1**. Relatively to the protons of the **GP_{inh}-5a** moiety, resonances corresponding to the aromatic C-H protons (Ar-CH) are seen at low field (δ 8.36 and 8.17), as expected. Further upfield, a quartet, integrating to two protons, is seen (δ 3.79), due to the –CH_2 protons adjacent to the –OH group (DO-CH_2). Another characteristic signal of the **GP_{inh}-5a** pharmacophore is the intense peak (δ 1.67), integrating to six protons, corresponding to the methyl protons. The signals relative to the protons of the **L1** moiety were also found and assigned. **B2-Boc** spectrum

presents the typical singlet peaks for proton 4 (CH^b, δ 5.84) and the methyl groups (δ 2.27 and 2.18) of pyrazolyl ring and Boc group (δ 1.43). Resonances for all the methylenic protons were also found and assigned (δ 4.06, CH_2^d; 3.17-3.07, $CH_2^{j/g}$; 2.89, CH_2^e; 2.62, $CH_2^{f/h}$; 1.73, CH_2^i).

As with the previous bioconjugate **B1**, the peak corresponding to protons *j* of **L1** (δ 2.79) is shifted downfield (δ 3.17-3.07, Δ = 0.32-0.42 ppm) in **B2-Boc** spectrum, which constitutes an evidence of conjugation of **GP_{inh}-5a** to **L1**.

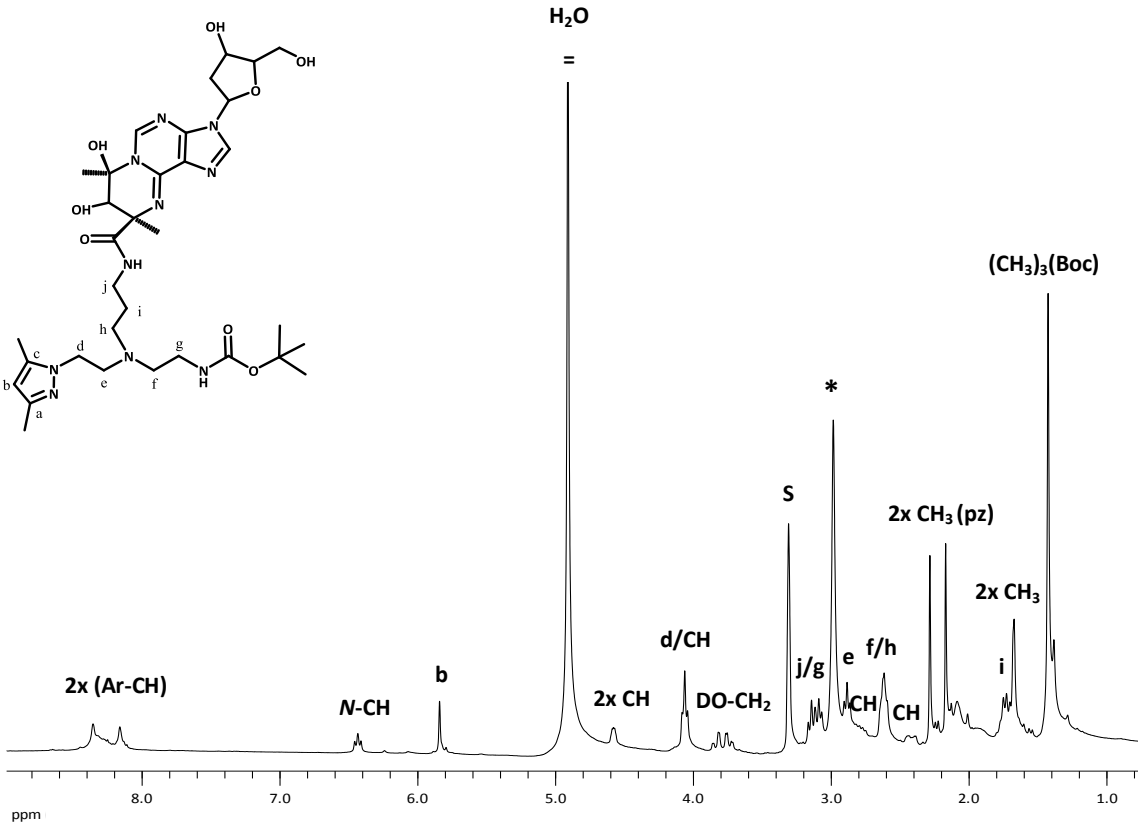

Figure 25: ^{1}H-NMR spectrum of **B2-Boc** in CD_3OD. S = residual MeOH. *Impurity.

In the ^{13}C-NMR spectrum of **B2-Boc** in CD_3OD (**Figure 26**) all the expected resonances for the carbons of the **L1** moiety are present, in particular the resonances for the methyl groups of Boc group (δ 28.8) and for the methyl groups (δ 13.4 and 11.2) and other carbon atoms (δ 148.7, C^c; 141.5, C^a; 106.1, C^b) of the pyrazolyl ring. Resonances for all the methylenic carbons were also found and assigned (δ 54.9, C^e; 54.7, C^h; 52.5, C^f; 47.4, C^d; 41.6, C^g; 39.2, C^j). The carbons corresponding to the **GP_{inh}-5a** moiety were also found, namely the methyl groups (δ 27.6 and 21.7).

The analysis of the ^{1}H- and ^{13}C-NMR spectra confirmed the presence of the intermediate bioconjugate **B2-Boc**, resulting from the conjugation of **GP$_{inh}$-5a** to **L1**.

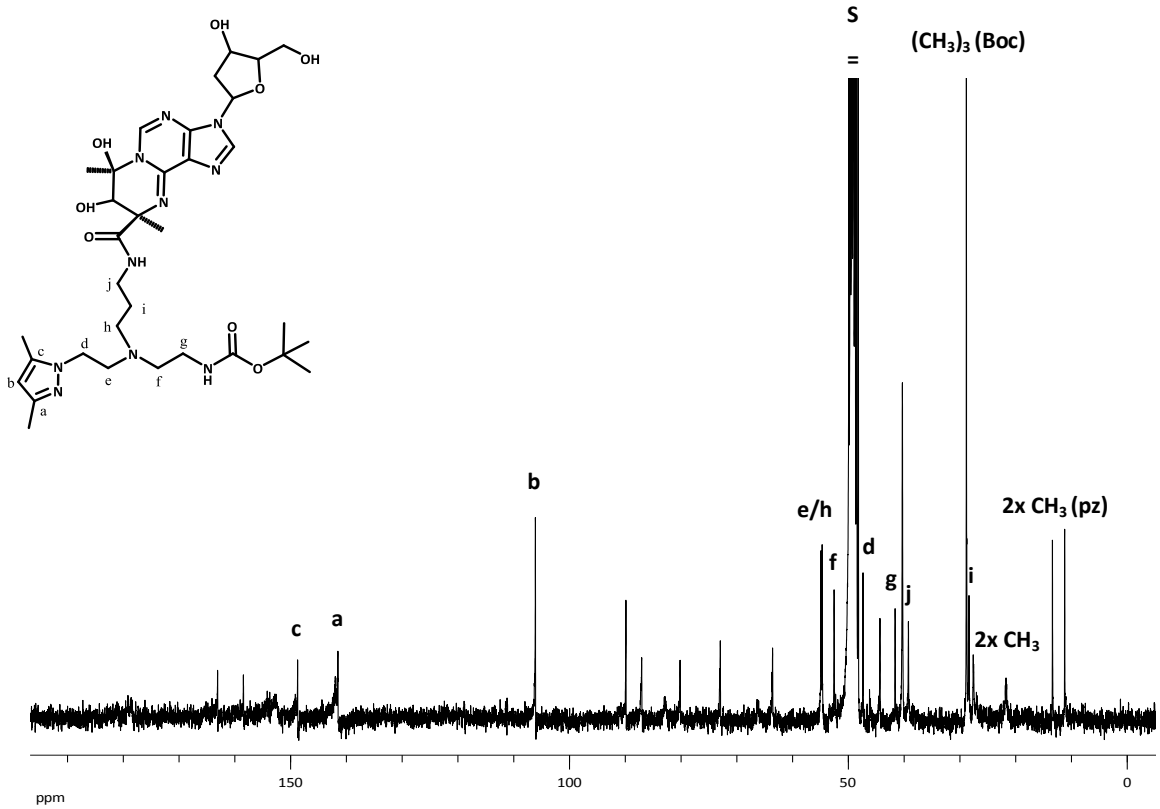

Figure 26: ^{13}C-NMR spectrum of **B2-Boc** in CD_3OD. S = residual MeOH.

3.2.3. Synthesis and characterization of the complex *fac*-[Re(CO)$_3$(κ^3-B1)]$^+$ Re1

From the two initially envisaged bioconjugates, only **B1**, based on the **CFTR$_{inh}$-172a** inhibitor, was obtained in pure conditions. Therefore, only the synthesis of the Re(I) complex **Re1** is presented next. The complex *fac*-[Re(CO)$_3$(κ^3-**B1**)]$^+$ (**Re1**) was obtained by reacting **B1** with the precursor *fac*-[Re(CO)$_3$(H$_2$O)$_3$]Br in refluxing water for 18 h (**Scheme 6**).

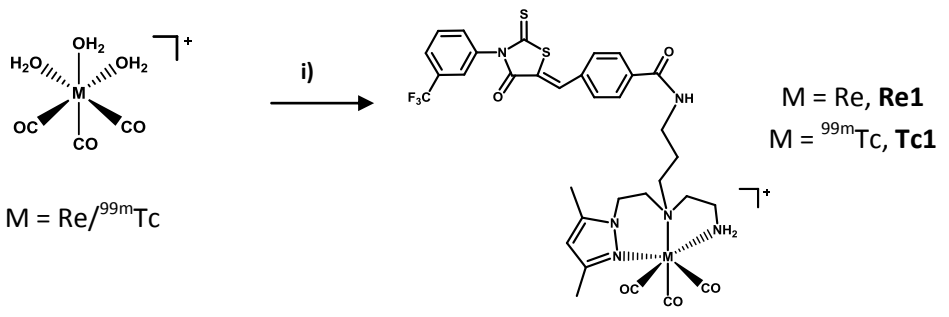

Scheme 6: Synthesis of Re1/Tc1. **i)** M = Re: **B1**, H_2O, reflux, 18 h, η = 55 %; M = ^{99m}Tc: **B1**, PEG 10x, 100 °C, 30 min.

Complex **Re1** was characterized by the usual analytical techniques in chemistry, namely NMR spectroscopy (^{1}H and ^{13}C), MALDI-TOF MS and RP-HPLC.

The ^{1}H- and ^{13}C NMR spectra of **Re1** are comparable to spectra of similar complexes previously synthesized and characterized by the RSG-IST/CTN.[69-71] The ^{1}H-NMR spectrum of **Re1** in CD_3OD (**Figure 27**) presents the typical singlet peaks assigned to proton 4 (CH^{b}, δ 6.20) and methyl groups (δ 2.44 and 2.35) of the pyrazolyl ring. These protons are shifted downfield (CH^{b}, Δ = 0.35 ppm; CH_3(pz), Δ = 0.17 ppm) relatively to the corresponding resonances in the spectrum of the free bioconjugate **B1** (δ 5.85, CH^{b}; 2.27, CH_3(pz); 2.18, CH_3(pz)), indicating coordination to the metal center.

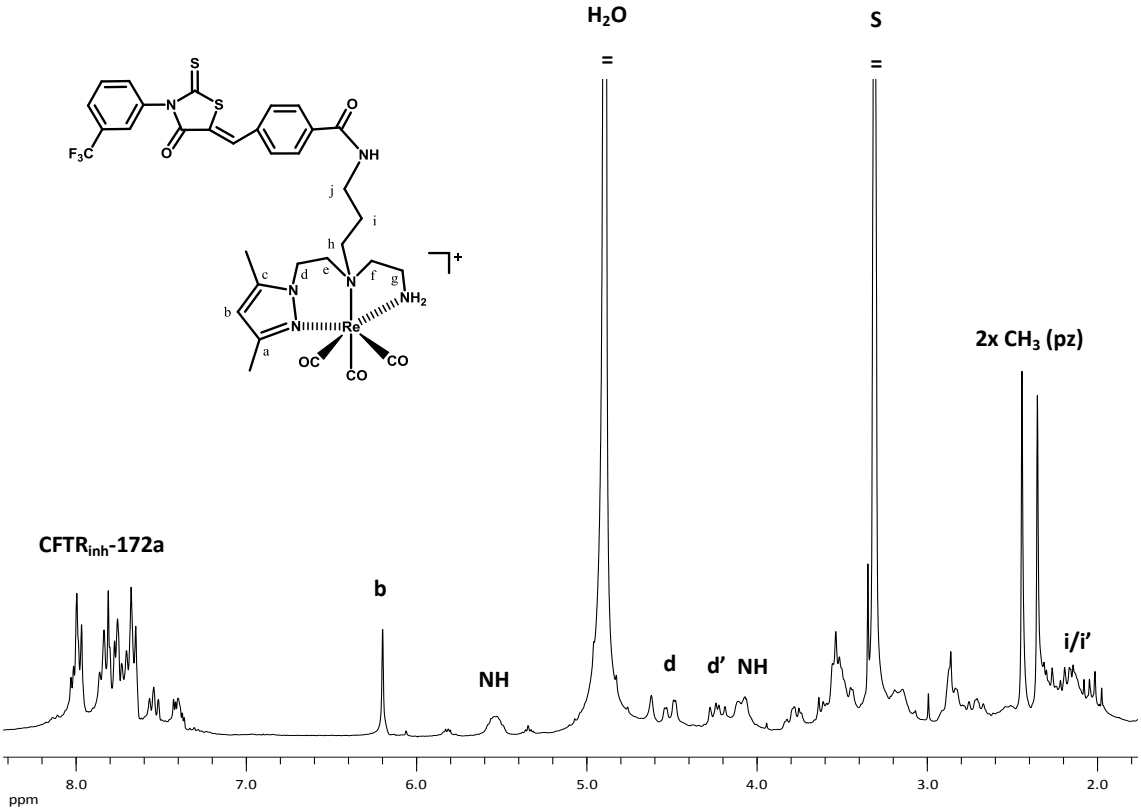

Figure 27: ^{1}H-NMR spectrum of **Re1** in CD_3OD. S = residual MeOH.

The tridentate coordination mode of **B1** to the metal is confirmed by two broad resonances assigned to the NH_2 protons (δ 5.54 and 4.09). After coordination of the amine group to the rhenium center, the NH_2 protons become non-equivalent magnetically, originating a diastereotopic pattern. In addition, the presence of a series of multiplet signals due to methylenic protons is also consistent with the tridentate coordination mode for **B1**. Although the assignment was only possible for protons *d* and *i*, for each of these protons, two resonances, integrating for one proton each, are found, due to the diastereotopic character of the methylenic protons after coordination to the metal center (e.g. δ 4.51, CH^{d}; 4.24, $CH^{d'}$).

This behavior, considered an evidence of ligand coordination to the metal, has already been observed in other rhenium tricarbonyl complexes stabilized by the same type of ligands.[69-71] The signals corresponding to the protons of the **CFTR$_{inh}$-172** moiety are also present in the spectrum of **Re1**. It is possible to observe a doublet at δ 8.00 integrating to two protons, which corresponds to two protons of the carboxyphenyl, and a multiplet at δ 7.86-7.65 integrating to the seven remaining protons.

The ^{13}C-NMR spectrum of **Re1** in CD_3OD with peak assignment is shown in **Figure 28**. The spectrum presents all the expected signals for **Re1**. An important feature in the ^{13}C spectrum is the presence of three resonances (δ 198.2, 195.3 and 193.8) due to the C≡O ligands coordinated to the metal. Resonances for all the methylenic carbons were also found and assigned (δ 66.3, C^h; 63.0, C^f; 54.3, C^e; 43.8, C^d; 38.7, C^g; 30.8, C^j; 25.9, C^i), based on published ^{13}C-NMR characterization of a similar rhenium complex.[69]

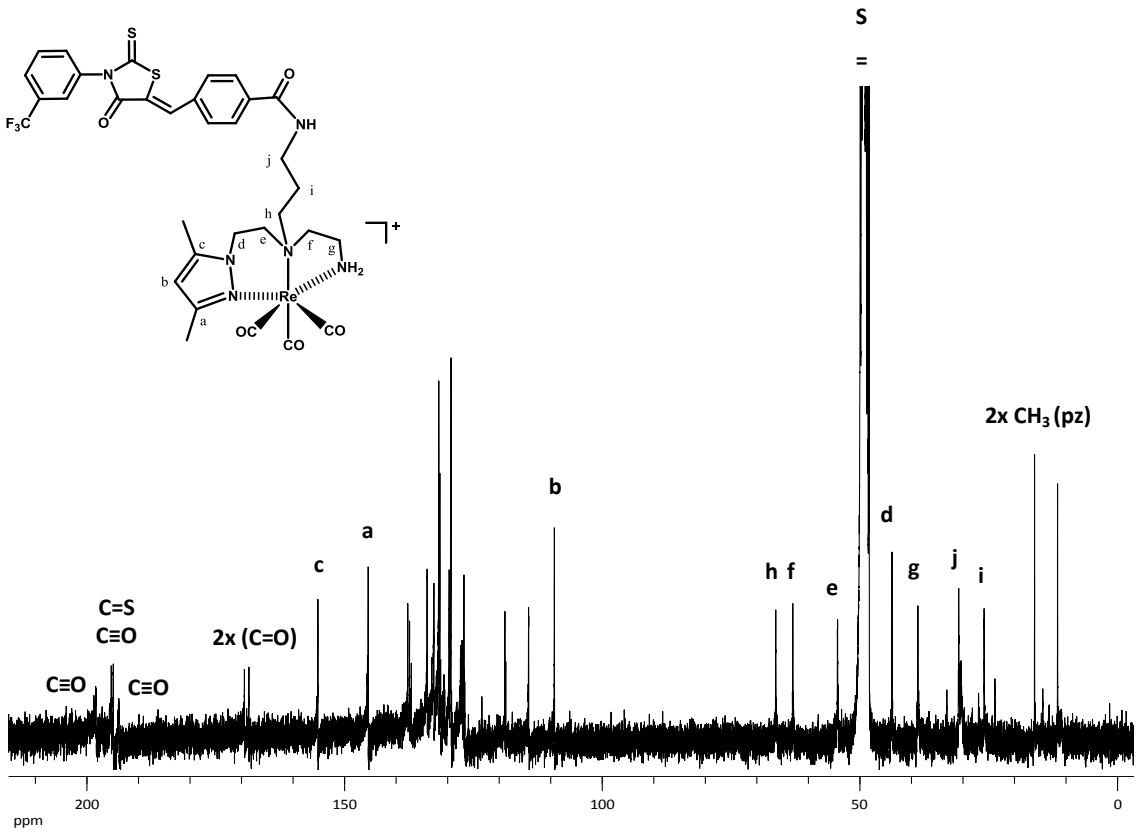

Figure 28: ^{13}C-NMR spectrum of **Re1** in CD_3OD. S = residual MeOH.

Complex **Re1** was also characterized by MALDI-TOF MS. The positive mode spectrum of **Re1** (**Figure 29**), recorded with DHB as matrix, presents the molecular ion peak, with a m/z value of approximately 901.1, which is in agreement with the expected value for **Re1** ($[M]^+$ = 901.2). The isotopic pattern observed in the experimental data matches the isotopic model

expected for **Re1** (**Figure 29**, **inset**). The peaks at m/z 698.2 and 730.2 possibly result from the fragmentation of **Re1**, most likely of the **CFTR$_{inh}$-172a** moiety, during the ionization process of the sample.

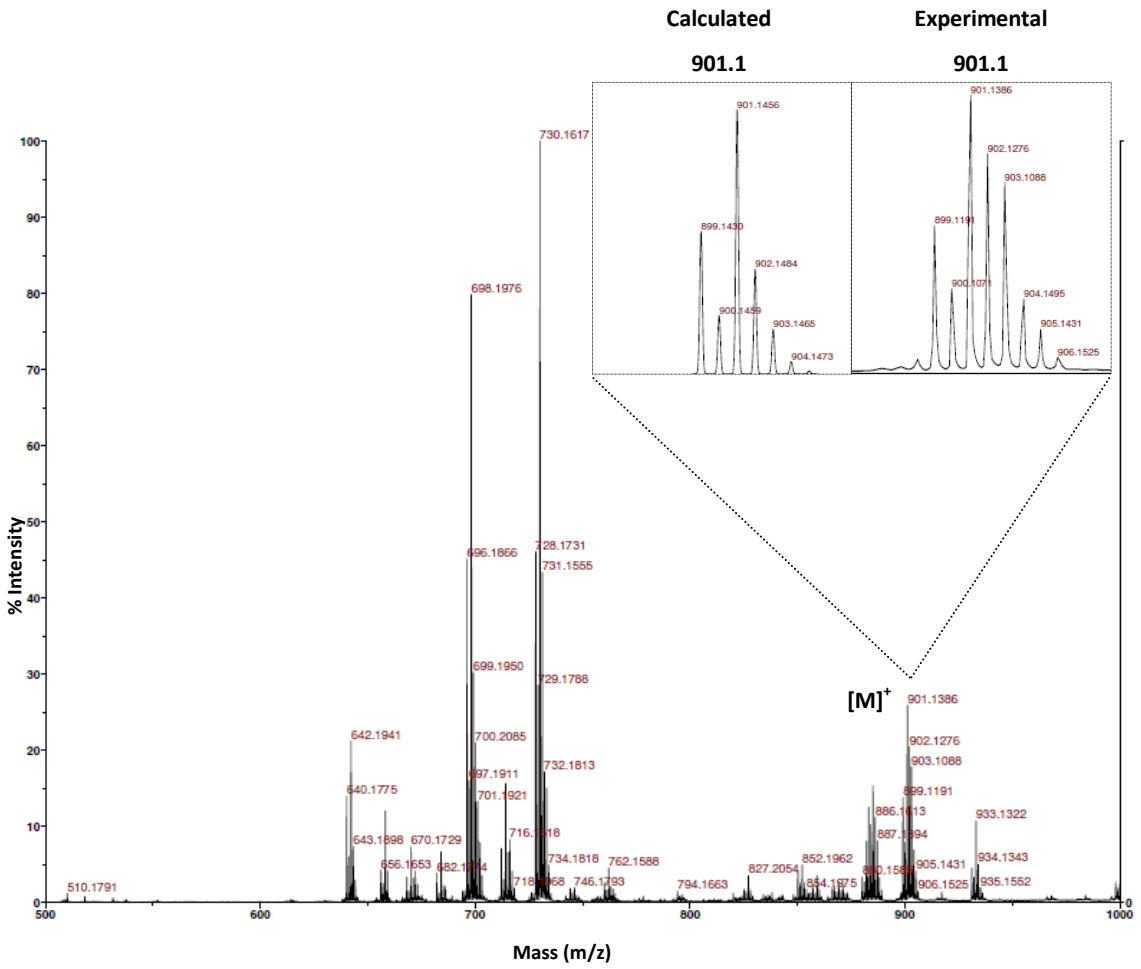

Figure 29: Mass spectrum of **Re1** in the positive mode, obtained by MALDI-TOF, with DHB as matrix (901.14 $[M]^+$, calculated for $C_{33}H_{33}F_3N_6O_5ReS_2$ = 901.15). **Inset**: Isotopic model for **Re1** ($[M]^+$)) and isotopic pattern obtained.

Finally, **Re1** was also analyzed by RP-HPLC (method 1, λ = 254 nm), presenting a R_t of 19.9 min. This R_t was different from the R_t of the bioconjugate **B1** (17.6 min), R_t of free ligand **L1** (R_t = 11.3 min) and R_t of free inhibitor (R_t = 20.3 min). Brought together, the results of the different analytic techniques allowed the full structural characterization of **Re1**.

3.2.4. Radiolabelling with ^{99m}Tc by the indirect method

The radiolabelling of novel probes based on the small molecule CFTR inhibitors performed via the indirect method has its final step in the labelling of the bioconjugates with ^{99m}Tc(I). Similarly to the Re(I) complex, only the synthesis and characterization of the radioactive complex based on **CFTR$_{inh}$-172a**, **Tc1**, is described below. First, the precursor *fac*-$[^{99m}Tc(CO)_3(H_2O)_3]^+$ was prepared in high yield by adding a $Na[^{99m}TcO_4]$ solution, eluted from a ^{99}Mo/^{99m}Tc generator, to an IsoLink® kit (**Section 2.1.8.3.**, **Materials and Methods**). After incubation at 100 °C for 30 min, the solution was neutralized with 1 M HCl in order to decompose any residual boranocarbonate. The formation of the precursor was controlled by RP-HPLC (method 1, γ-detection) (**Figure 30**).

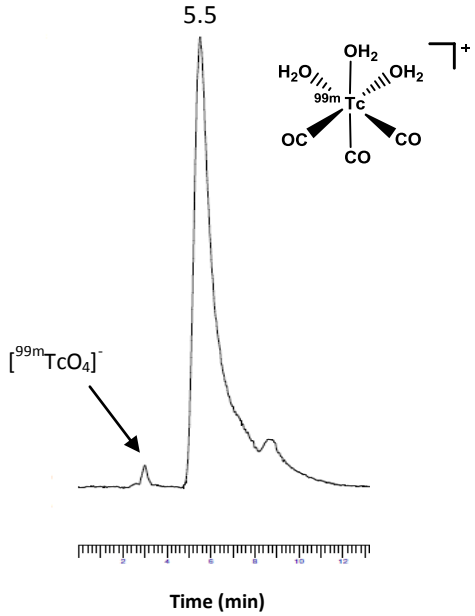

Figure 30: RP-HPLC analysis of the synthesis of the *fac*-$[^{99m}Tc(CO)_3(H_2O)_3]^+$ precursor. The analysis was performed using method 1 and the compounds detected by γ-detection.

Then, the radioactive complex *fac*-$[^{99m}Tc(CO)_3(\kappa^3$-**B1**$)]$, **Tc1,** was obtained by addition of the *fac*-$[^{99m}Tc(CO)_3(H_2O)_3]^+$ precursor to an aqueous solution of **B1** ([**B1**] = 10^{-3} M]) and PEG 10x (v/v), followed by incubation at 100 °C for 30 min (**Scheme 3,** M = ^{99m}Tc). PEG was added in order to prevent adsorption of the radiolabelled compound onto the glass surface. The reaction was monitored by RP-HPLC (**Figure 31**).

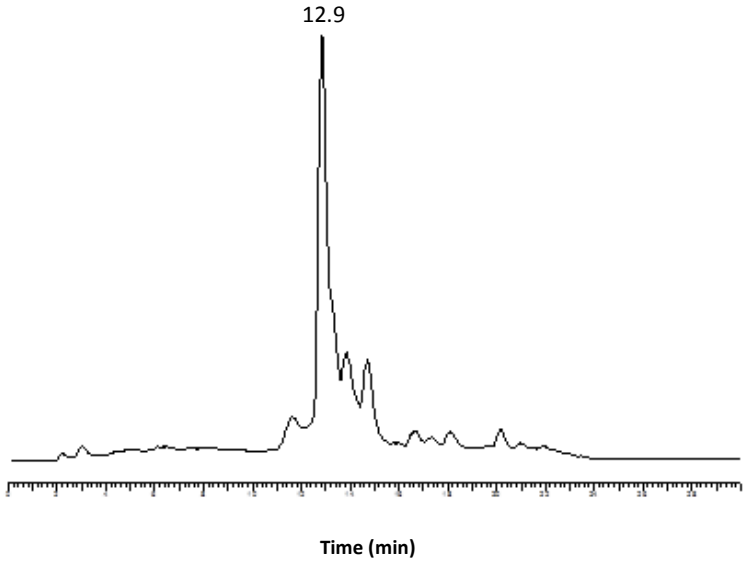

Figure 31: RP-HPLC analysis of *fac*-[^{99m}Tc(CO)$_3$(κ^3-B1)], Tc1. The analysis was performed using method 1 and the compounds detected by γ-detection.

Bearing in mind that rhenium complexes are usually used as non-radioactive surrogates of the analogous ^{99m}Tc(I) complexes, their retention time should be similar under the same conditions (with only a slight difference due to the use of two different detectors, UV/Vis and γ, connected in line). The major peak observed in **Figure 31** presents a R_t of 12.9 min (method 1, γ-detection). However, the R_t obtained for **Re1** was 19.9 min (method 1, λ = 254 nm). This considerable difference suggests that the radiolabelled compound that presents a R_t of 12.9 min does not correspond to **Tc1**.

This result can be due to the possible degradation of **B1** in solution, either before the radiolabelling or during the harsh radiolabelling procedures (100 °C for 30 min). In the former case, that degradation could have arisen from the fact that the **B1** solution (kept at 4 °C) was prepared a few weeks before the radiolabelling, and possibly **B1** could present some instability in solution.

Therefore to address the question of the stability of **B1** in solution and during the radiolabelling, this bioconjugate should have been analyzed by RP-HPLC, before and after incubation at 100 °C. Unfortunately, at the time, all of the **B1** compound synthesized had been used in other analyses/reactions. Taking in consideration that **B1** results from the conjugation of **CFTR$_{inh}$-172a** to **L1** and that **L1** is known to be stable at 100 °C,[64] it was decided, as an alternative, to analyze the stability of **CFTR$_{inh}$-172a**.

Stability of $CFTR_{inh}$-172a

To assess the stability of the inhibitor **$CFTR_{inh}$-172a** at 100 °C, a solution of 0.5 mM in MeOH was prepared and incubated at 100 °C for 30 and 60 min. Samples with the same volume (10 µL) of solutions, from before and after incubation at 100 °C, were analysed by RP-HPLC (**Figure 32**).

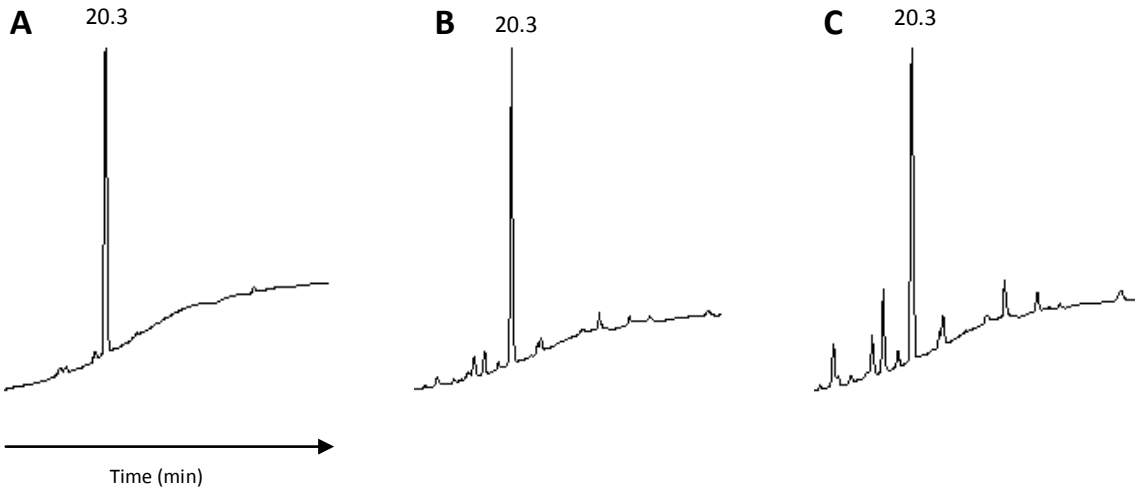

Figure 32: RP-HPLC analysis of $CFTR_{inh}$-172a at different experimental condition. A solution of 0.5 mM **$CFTR_{inh}$-172a** in MeOH was incubated at 100 °C and analyzed by RP-HPLC (method 1, λ = 220 nm). Chromatograms were obtained before incubation (**A**), at 30 min (**B**) and at 60 min (**C**).

The major peak observed before incubation at 100 °C (**Figure 32A**) corresponds to **$CFTR_{inh}$-172a** (R_t = 20.3 min). After incubation at 30 and 60 min (**Figures 32B** and **32C**), this major peak is also observed. However, other minor peaks are seen, whose intensity increases with the incubation time. These peaks possibly correspond to fragments of **$CFTR_{inh}$-172a** caused by degradation of the inhibitor at high temperature.

These results are indicative of the instability of **$CFTR_{inh}$-172a** under high temperature, mainly after 60 min of incubation. Therefore, the temperature and time of radiolabelling of **B1** with ^{99m}Tc(I) should be optimized in the future, in order to obtain high radiolabelling yields with high radiochemical purity.

CONCLUDING REMARKS

The main goal of this thesis was the development of radiolabelled imaging probes for the detection/visualization of normal and rescued F508del-CFTR at the PM of human epithelial pulmonary cells. These radiolabelled probes would be based on anti-CFTR antibodies and CFTR inhibitors, radiolabelled with the ^{99m}Tc isotope using different radiolabelling methods.

The thesis was divided in two main parts according to the biomolecules studied: anti-CFTR antibodies and CFTR inhibitors.

In the first part of the work two anti-CFTR antibodies were studied: the polyclonal ECL1 (IgG) and the monoclonal MA1-935 (IgM), received in the form of rabbit serum and mouse ascites, respectively. Radiolabelling procedures must be performed with biomolecules with high purity, since other proteins can also be radiolabelled, impairing the radiolabelling efficiency. For that reason, the solutions containing the antibodies were first characterized to assess if a purification step would be necessary.

Starting with the polyclonal ECL1 antibody, it was observed by SDS-PAGE that the rabbit serum solution contained the antibody of interest but mainly albumin, as expected. The antibody was purified using a purification kit suitable for IgGs, which was very efficient in removing the non-relevant proteins, allowing to obtain the ECL1 antibody with high purity. Through the analysis by SE-HPLC, it was possible to identify the antibody in its native form, by comparison with the chromatographic profile obtained for a control IgG. However, peaks other than the one corresponding to ECL1, were observed. A possible cause for one (or both) peak(s) might be the fact that the antibody sample used in this SE-HPLC analysis was exposed to room temperature for a few days, which may have contributed to its partial degradation.

In parallel, the monoclonal MA1-935 was also analyzed by SDS-PAGE and SE-HPLC, and altogether, the data showed that the mouse ascites contained the MA1-935 antibody and other proteins, mainly albumin. Interestingly, the chromatogram obtained by SE-HPLC for MA1-935 showed a peak with a retention time similar to one of the “extra” peaks present in the chromatogram of ECL1. This peak might correspond to a protein present on both solutions that in the case of ECL1 was not possible to separate from the antibody with the purification procedure.

After the characterization studies, we decided to continue the work with the ECL1 antibody, mainly due to the fact that MA1-935 was not purified yet, and that there is more information reported in literature about radiolabelling of IgGs than of IgMs.

The radiolabelling of ECL1 was performed using the direct method, which relies upon endogenous sulfhydryl groups generated by reduction of the antibody, to provide the binding sites for ^{99m}Tc. After reduction of ECL1, we obtained an estimated value of 500 sulfhydryl groups per molecule of antibody, which is in principle a value too high for a typical IgG. In the literature is reported that no more than 16% of the 36 sulfhydryl groups of an IgG are reduced, i.e., around 5 to 6 sulfhydryl groups per molecule of IgG.[43]

One of the possible causes for the high number of sulfhydryl groups determined might be the fact that the estimation of the sulfhydryl groups was done in a Nanodrop 2000 spectrophotomether (due to limitation in the amount of antibody available), which revealed a lower sensitivity and also low reproducibility when compared with the other spectrophotometer used during the course of this work. Therefore, the concentration of cysteine/-SH groups present in ECL1, as well as the concentration of ECL1, might not have been determined accurately.

Another cause for the high number of sulfhydryl groups estimated might be the presence of contaminating 2-mercaptoethanol which has survived the purification step after the reduction of ECL1. Mather *et al.* (1990) reported an apparently too high number of sulfhydryl groups for a murine IgG when, similarly to ECL1, a 1000-fold molar excess of 2-mercaptoethanol was used, although the value obtained (~ 60 -SH groups) was not as high as the one obtained for ECL1 (500 -SH groups). Different purification methods for removing the excess of 2-mercaptoethanol were tested during the course of this work, and the results suggest that the best way to purify the reduced antibody is using a PD-10 desalting column followed by a Microcon centrifugal filter fitted with an Ultracel YM-10 membrane (data not shown). Since we have concentrated the fractions of reduced ECL1 eluted from the PD-10 with a Microcon filter, we believe that there was no remaining 2-mercaptoethanol on the reduced antibody after purification.

Even though there was an apparently excessive number of sulfhydryl groups, the work proceeded with the radiolabelling of ECL1 with ^{99m}Tc(I). In this direct radiolabelling procedure, the highest radiolabelling yield obtained was of 11% after 4 hours of incubation. Different radiolabelling conditions were tested, varying the proportions of antibody or ^{99m}Tc(I)-tricarbonyl precursor, but the radiolabelling efficiencies remained low. With the results of these experiments, we hypothesized that the concentration of the antibody could be the critical factor to take into account in the radiolabelling, since this procedure was performed with a solution with a low concentration of the ECL1 antibody.

As an alternative, the radiolabelling of ECL1 using ^{99m}Tc(IV) was performed. First, the radiolabelling conditions were optimized with another IgG, IOR-CEA1, and the experiments

with the highest radiolabelling yields reproduced using the ECL1 antibody, used at the same concentration as the tested IgG control. Unfortunately, however, this radiolabelling strategy also did not result, since we could not observe by ITLC-SG the radiolabelled ECL1, not even when the amount of ECL1 used in the radiolabelling was further increased.

A possible cause for the failure in this radiolabelling can be the fact that the antibody was reduced and stored for a few weeks at 4 °C, until it was radiolabelled with ^{99m}Tc(IV). The antibody was kept under a nitrogen atmosphere in order to prevent the oxidation of the sulfhydryl groups. However, there is the possibility that these groups may have oxidized, originating disulfide bonds, which prevent the radiolabelling by the direct method.

A comparison between the results obtained for the radiolabelling of ECL1 with ^{99m}Tc(I) and ^{99m}Tc(IV) is not possible, since the radiolabelling of ECL1 was too low (~ 11%) or barely inexistent using both strategies. However, in future work, the labelling with ^{99m}Tc(I) will continue to be the first option for the radiolabelling of the antibodies due to the reported high radiolabelling efficiencies for other IgGs,[51] the easiness of the procedure and the many advantages of the *fac*-[^{99m}Tc(CO)$_3$]$^+$ core.[40]

Although the main goal of the first part of the thesis, the development of radiolabelled imaging probes using the two anti-CFTR antibodies, was not fully achieved, all the results contributed to the optimization of the radiolabelling of ECL1 and will be useful in future radiolabelling experiments.

In the second part of the thesis, the main goal was the radiolabelling of the CFTR inhibitors **CFTR$_{inh}$-172a** and **GP$_{inh}$-5a** with the *fac*-[^{99m}Tc(CO)$_3$]$^+$ core using the bifunctional chelator approach, as well as the characterization of the resulting ^{99m}Tc-complexes.

Knowing that tridentate chelators form stable complexes with the *fac*-[^{99m}Tc(CO)$_3$]$^+$ core, a bifunctional chelator (**L1**), containing a pyrazolyl-diamine chelating unit with a spacer (propyl) and a terminal functional group (-NH$_2$) for conjugation to both CFTR inhibitors, was synthesized (**Scheme 3**).

The inhibitor **CFTR$_{inh}$-172a**, containing a terminal functional group (-COOH) was conjugated to **L1**, yielding the final bioconjugate **B1** (**Scheme 4**). **B1** was characterized by several techniques and the results compared with the obtained for the free **L1** and **CFTR$_{inh}$-172a**. In general, those results provided evidence of a successful conjugation, such as: different retention factor by TLC; chemical shift of some protons close to the site of conjugation in the ^{1}H-NMR spectrum; different retention time by RP-HPLC; and presence of its molecular peak by ESI-MS. Altogether, the data pointed to the successful synthesis of the bioconjugate **B1**.

Therefore, **B1** reacted with the *fac*-$[Re(CO)_3(H_2O)_3]^+$ and *fac*-$[^{99m}Tc(CO)_3(H_2O)_3]^+$ precursors, yielding complexes of the type *fac*-$[M(CO)_3(\kappa^3\text{-}\mathbf{B1})]^+$ (M = Re/^{99m}Tc, respectively) (**Scheme 6**). This was possible due to the *N*,*N*,*N* donor atom set of the pyrazolyl-diamine chelating unit of the **L1** moiety present in **B1**.

In the first case, the **Re1** complex was synthesized in order to identify and characterize the analogous ^{99m}Tc(I)-tricarbonyl complex, which would be obtained in a low concentration, as is the case for all ^{99m}Tc complexes. One-dimensional-NMR spectroscopic studies performed for **Re1** confirmed the tridentate coordination mode of the pyrazolyl-diamine chelating unit, since it was observed a diastereotopic pattern for the protons belonging to this unit. This behavior, considered an evidence of coordination to the metal, has already been observed in other Re(I)-tricarbonyl complexes synthesized by the RSG-IST/CTN group.[69-71] Another characteristic of **Re1** was the presence of three resonances due to the CO ligands coordinated to the rhenium.

Later, **B1** was radiolabelled with the *fac*-$[^{99m}Tc(CO)_3]^+$ core. As mentioned above, rhenium has been used as a non-radioactive surrogate of technetium since they are structurally similar. For that reason, we expected an identical chromatographic behavior between **Re1** and the analogous ^{99m}Tc(I)-tricarbonyl complex (**Tc1**) by RP-HPLC. However, unexpectedly, the ^{99m}Tc(I)-tricarbonyl complex obtained did not correspond to **Tc1**, since the retention time was considerably different of the obtained for **Re1**.

We hypothesized that the failure in the radiolabelling of **B1** could be related with its instability. A solution of **B1** was prepared a few weeks before the radiolabelling and stored at 4 °C. If, for some reason, **B1** is not stable in solution, it could suffer some degradation that could have been the cause for an unsuccessful radiolabelling. On the other hand, the temperature at which **B1** was subjected in the radiolabelling (100 °C) could also have contributed to its degradation. Then, it was of special interest to assess the stability of **B1**, in solution and at high temperature. However, due to the limitations in the amount of **B1** available, that was not possible. Therefore, we decided to assess the stability of the inhibitor **$CFTR_{inh}$-172a**, since we had previous evidence from the radiolabelling of compounds with the pyrazolyl-diamine chelating unit by the RSG-IST/CTN group, that **L1** was stable at 100 °C.[64]

The analysis of the stability of **$CFTR_{inh}$-172a** showed that degradation of **$CFTR_{inh}$-172a** tended to increase with the time of incubation at 100 °C. Per se, these results are not sufficient to conclude that the cause for the unsuccessful radiolabelling of **B1** was only and exclusively due to its degradation at high temperature. However, they help to understand that high temperature might contribute to degradation of **B1** and, consequently, to the failure in the

radiolabelling. Therefore, the radiolabelling temperature should be taken into account in future radiolabelling experiments of **B1**.

Relatively to the second CFTR inhibitor, **GP_{inh}-5a**, the aim was similar to the one for **$CFTR_{inh}$-172a**. We intended to conjugate **GP_{inh}-5a**, which also contains a terminal functional group (-COOH), to **L1,** giving **B2** (**Scheme 5**), and synthesize the complexes of the type *fac*-$[M(CO)_3(\kappa^3\text{-}\mathbf{B2})]^+$ (M = Re/^{99m}Tc).

Unfortunately, after several attempts of purification of **B2** by chromatography, the compound was not obtained in a pure form, mainly due to the difficulty in identifying the compound by TLC or RP-HPLC. Therefore, it was only possible to characterize the intermediate **B2-Boc** by NMR spectroscopy. In general, the chemical shifts as well as the multiplicities of the signals of **B2-Boc** were similar to those found for free **L1** and **GP_{inh}-5a**. As with the previous bioconjugate **B1**, it was observed a shift of two protons close to the site of conjugation in the ^{1}H-NMR spectrum, which constituted an evidence of conjugation of **GP_{inh}-5a** to **L1**.

Similarly to the first part of the thesis, the main goal of this second part, the radiolabelling of the two CFTR inhibitors with the *fac*-$[^{99m}Tc(CO)_3]^+$ core, using the bifunctional approach, was not fully achieved. However, as the development of the radiolabelled probes based on the CFTR inhibitors was divided in several sequential tasks, several milestones were successfully accomplished, namely: synthesis and characterization of the bifunctional chelator **L1**; synthesis and characterization of the bioconjugates **B1** and **B2-Boc**; and synthesis and characterization of rhenium complex **Re1**.

FUTURE PERSPECTIVES

Although the final goals of this thesis project have not been fully achieved, the results obtained will be helpful in future studies.

Relatively to the anti-CFTR antibodies, we will try the radiolabelling of the ECL1 antibody using a more concentrated solution, since radiolabelling optimization results showed that the radiolabelling yield increases with higher concentrations of antibody.

We also have in mind the purification of the MA1-935 antibody with a purification system suitable for IgMs, using immobilized mannan binding protein, which binds to IgMs. Once purified, we envisage the radiolabelling of the MA1-935 antibody based on previous reports in literature of radiolabelling of IgMs.

After obtaining the radiolabelled antibodies, their usefulness as molecular imaging radioprobes will be explored in cellular studies using human cell lines. In particular, we will assess the effect of the radiolabelling procedure on the intrinsic biological properties of the antibody, namely on the immunoreactivity and binding affinity to CFTR.

Relatively to the CFTR inhibitors, and fulfilling the purpose for which it was synthesized, we will use the **Re1** complex to assess the efficacy of the complex via functional assays of CFTR inhibition, through the iodide efflux technique in cells expressing the wt-CFTR protein. This will provide evidence if the metal complex of **$CFTR_{inh}$-172a** still maintain their ability to interact with CFTR at the PM.

In parallel, we also aim to obtain the final bioconjugate **B2** with high purity which, unfortunately, was not possible during the course of the work. The challenge is the identification of the compound by TLC and RP-HPLC, which will contribute to a successful purification.

We will optimize the radiolabelling temperature in order to prevent the degradation of the **$CFTR_{inh}$-172a** moiety. If we observe that **GP_{inh}-5a** is also unstable at 100 °C, that radiolabelling temperature will also be applied to this inhibitor. One of the important details to take into account in the future is also the preparation of fresh solutions of bioconjugates for the radiolabelling, in order to exclude factors such as instability in solution that might contribute to an unsuccessful radiolabelling.

However, in case the radiolabelling with ^{99m}Tc cannot be successfully accomplished, we envisage an alternative radiolabelling strategy for the CFTR inhibitors. We can test the alternative metal Gallium (Ga), which presents two radioisotopes with decay characteristics

that are suitable for either SPECT or PET imaging. ^{67}Ga is cyclotron produced, decays by γ-emission, and is used in SPECT imaging. ^{68}Ga is produced from the ^{68}Ge/^{68}Ga generator, decays by 89% β^+-emission, and is used in PET imaging. The utilization of Ga will imply the use of another bifunctional chelator and the conjugation to both inhibitors. Targeted Ga radiopharmaceuticals are dominated by polydentate bifunctional chelators, such as NOTA (1,4,7-triazacyclononane-1,4,7-triacetic acid) derivatives. The major advantage of the $^{67/68}$Ga is that the radiolabelling is performed at room temperature, which prevents the possible degradation that the bioconjugates might suffer.

In a long-term planning we also envisage to establish the proof-of-concept of this project by performing cellular studies in human bronchial epithelial cells expressing wt-CFTR or mutant F508del-CFTR. We will measure the amount of radiolabelled antibody or small molecule that can interact with the CFTR protein at the cell membrane. Moreover, the best-performing complexes (either based on the anti-CFTR antibodies or the CFTR inhibitors) will be tested as probes for detecting mutant-CFTR modulation.

REFERENCES

1. Lukacs, G.L., Verkman, A.S., CFTR: folding, misfolding and correcting the ΔF508 conformational defect. *Trends Mol Med* 2012, 18(2): 81-91.
2. Davis, P.B., Cystic fibrosis since 1938. *Am J Respir Crit Care Med* 2006, 173(5): 475-482.
3. Riordan, J.R., Rommens, J.M., Kerem, B., Alon, N., Rozmahel, R., Grzelczak, Z., Zielenski, J., Lok, S., Plavsic, N., Chou, J.L., *et al.*, Identification of the cystic fibrosis gene: cloning and characterization of complementary DNA. *Science* 1989, 245(4922): 1066-1073.
4. Hwang, T.C., Sheppard, D.N., Gating of the CFTR Cl^- channel by ATP-driven nucleotide binding domain dimerisation. *J Physiol* 2009, 587(Pt 10): 2151-2161.
5. Flume, P.A., Van Devanter, D.R., State of progress in treating cystic fibrosis respiratory disease. *BMC Med* 2012, 10: 88.
6. Accurso, F.J., Update in Cystic Fibrosis 2006. *Am J Respir Crit Care Med* 2007, 175(8): 754-757.
7. Derichs, N., Targeting a genetic defect: cystic fibrosis transmembrane conductance regulator modulators in cystic fibrosis. *Eur Respir Rev* 2013, 22(127): 58-65.
8. Cystic Fibrosis Mutation Database: Statistics.
   (at http://www.genet.sickkids.on.ca/cftr/StatisticsPage.html)
9. Rowe, S.M., Miller, S., Sorscher, E.J., Cystic Fibrosis *N Engl J Med* 2005, 352(19): 1992-2001.
10. Cheng, S.H., Gregory, R.J., Marshall, J., Paul, S., Souza, D.W., White, G.A., O'Riordan, C.R., Smith, A.E., Defective intracellular transport and processing of CFTR is the molecular basis of most cystic fibrosis. *Cell* 1990, 63(4): 827-834.
11. Denning, G.M., Anderson, M.P., Amara, J.F., Marshall, J., Smith, A.E., Welsh, M.J., Processing of mutant cystic fibrosis transmembrane conductance regulator is temperature-sensitive. *Nature* 1992, 358(6389): 761-764.
12. Dalemans, W., Barbry, P., Champigny, G., Jallat, S., Dott, K., Dreyer, D., Crystal, R.G., Pavirani, A., Lecocq, J.P., Lazdunski, M., Altered chloride ion channel kinetics associated with the delta F508 cystic fibrosis mutation. *Nature* 1991, 354(6354): 526-528.
13. Sharma M, Pampinella F, Nemes C, Benharouga M, So J, Du K, Bache KG, Papsin B, Zerangue N, Stenmark H, Lukacs GL. Misfolding diverts CFTR from recycling to degradation: quality control at early endosomes. *J Cell Biol* 2004, 164(6): 923-933.

14. Swiatecka-Urban, A., Brown, A., Moreau-Marquis, S., Renuka, J., Coutermarsh, B., Barnaby, R., Karlson, K.H., Flotte, T.R., Fukuda, M., Langford, G.M., Stanton, B.A., The short apical membrane half-life of rescued {Delta}F508-cystic fibrosis transmembrane conductance regulator (CFTR) results from accelerated endocytosis of {Delta}F508-CFTR in polarized human airway epithelial cells. *J Biol Chem* 2005, 280(44): 36762-36772.
15. Riordan, J.R., CFTR function and prospects for therapy. *Annu Rev Biochem* 2008, 77: 701-726.
16. Kim, S.J., Skach, W.R., Mechanisms of CFTR Folding at the Endoplasmic Reticulum. *Front Pharmacol* 2012, 3: 201.
17. Farinha, C.M., Amaral, M.D., Most F508del-CFTR is targeted to degradation at an early folding checkpoint and independently of calnexin. *Mol Cell Biol* 2005, 25(12):5242-5252.
18. Bertrand, C.A., Frizzell, R.A., The role of regulated CFTR trafficking in epithelial secretion. *Am J Physiol Cell Physiol* 2003, 285(1): C1-18.
19. Akabas, M.H., Cystic fibrosis transmembrane conductance regulator. Structure and function of an epithelial chloride channel. *J Biol Chem* 2000, 275(6): 3729-3732.
20. Li, M.S., Holstead, R.G., Wang, W., Linsdell, P., Regulation of CFTR chloride channel macroscopic conductance by extracellular bicarbonate. *Am J Physiol Cell Physiol* 2011, 300(1): C65-74.
21. Van Goor, F., Hadida, S., Grootenhuis, P.D., Burton, B., Stack, J.H., Straley, K.S., Decker, C.J., Miller, M., McCartney, J., Olson, E.R., Wine, J.J., Frizzell, R.A., Ashlock, M., Negulescu, P.A., Correction of the F508del-CFTR protein processing defect in vitro by the investigational drug VX-809. *Proc Natl Acad Sci U S A* 2011, 108(46):18843-18848.
22. Clancy, J.P., Rowe, S.M., Accurso, F.J., Aitken, M.L., Amin, R.S., Ashlock, M.A., Ballmann, M., Boyle, M.P., Bronsveld, I., Campbell, P.W., De Boeck, K., Donaldson, S.H., Dorkin, H.L., Dunitz, J.M., Durie, P.R., Jain, M., Leonard, A., McCoy, K.S., Moss, R.B., Pilewski, J.M., Rosenbluth, D.B., Rubenstein, R.C., Schechter, M.S., Botfield, M., Ordoñez, C.L., Spencer-Green, G.T., Vernillet, L., Wisseh, S., Yen, K., Konstan, M.W., Results of a phase IIa study of VX-809, an investigational CFTR corrector compound, in subjects with cystic fibrosis homozygous for the F508del-CFTR mutation. *Thorax* 2012, 67(1):12-8.
23. Flume, P.A., Liou, T.G., Borowitz, D.S., Li, H., Yen, K., Ordoñez, C.L., Geller, D.E., Ivacaftor in subjects with cystic fibrosis who are homozygous for the F508del-CFTR mutation. *Chest* 2012, 142(3): 718-724.
24. Vertex: Press release at February 26th, 2013 (Vertex Announces Initiation of Pivotal Phase 3 Program of VX-809 in Combination with Ivacaftor for the Treatment of People with Cystic Fibrosis Who Have Two Copies of the F508del Mutation.)

(at: http://investors.vrtx.com/releasedetail.cfm?ReleaseID=743425)

25. Kurdziel, K.A., Ravizzini, G., Croft, B.Y., Tatum, J.L., Choyke, P.L., Kobayashi, H., The evolving role of nuclear molecular imaging in cancer. *Expert Opin Med Diagn* 2008, 2(7): 829-842.
26. Chen, K., Chen. X., Design and development of molecular imaging probes. *Curr Top Med Chem* 2010, 10(12): 1227-1236.
27. Glunde, K., Pathak, A.P., Bhujwalla, Z.M., Molecular-functional imaging of cancer: to image and imagine. *Trends Mol Med* 2007, 13(7): 287-297.
28. James, M.L., Gambhir, S.S., A molecular imaging primer: modalities, imaging agents, and applications. *Physiol Rev* 2012, 92(2): 897-965.
29. Liu, S., The role of coordination chemistry in the development of target-specific radiopharmaceuticals. *Chem Soc Rev* 2004, 33(7): 445-461.
30. Weissleder, R., Pittet, M.J., Imaging in the era of molecular oncology. *Nature* 2008, 452(7187): 580-589.
31. Valk, P.E., Bailey, D.L., Townsend, D.W., Maisey, M.N., Positron Emission Tomography: Basic Science and Clinical Practice. *Springer* 2003.
32. Zolle, I., Technetium-99m Pharmaceuticals. *Springer* 2007.
33. Bartholomä, M.D., Louie, A.S., Valliant, J.F., Zubieta, J., Technetium and gallium derived radiopharmaceuticals: comparing and contrasting the chemistry of two important radiometals for the molecular imaging era. *Chem Rev* 2010, 110(5): 2903-2920.
34. Dilworth, J.R., Parrott, S.J., The biomedical chemistry of technetium and rhenium. ***Chem Soc Rev*** 1998, **27**: 43-55.
35. Liu, S., Bifunctional coupling agents for radiolabeling of biomolecules and target-specific delivery of metallic radionuclides. *Adv Drug Deliv Rev* 2008, 60(12): 1347-1370.
36. Alberto, R., Schibli, R., Egli, A., Schubiger, A.P., A novel organometallic aqua complex of Technetium for the labeling of biomolecules: synthesis of $[^{99m}Tc(OH_2)_3(CO)_3]^+$ from $[^{99m}TcO_4]^-$ in aqueous solution and its reaction with a bifunctional ligand. *J Am Chem Soc* 1998, 120(31): 7987-7988.
37. Alberto, R., Ortner, K., Wheatley, N., Schibli, R., Schubiger, A.P., Synthesis and properties of boranocarbonate: a convenient *in situ* CO source for the aqueous preparation of $[^{99m}Tc(OH_2)_3(CO)_3]^+$. *J Am Chem Soc* 2001, 123(13): 3135-3136.
38. Schibli, R., Schwarzbach, R., Alberto, R., Ortner, K., Schmalle, H., Dumas, C., Egli, A., Schubiger, P.A., Steps toward high specific activity labeling of biomolecules for therapeutic application: preparation of precursor $[^{188}Re(H_2O)_3(CO)_3]^+$ and synthesis of tailor-made bifunctional ligand systems. *Bioconjug Chem* 2002, 13(4): 750-756.

39. Lazarova, N., James, S., Babich, J., Zubieta, J., A convenient synthesis, chemical characterization and reactivity of $[Re(CO)_3(H_2O)_3]Br$: the crystal and molecular structure of $[Re(CO)_3(CH_3CN)_2Br]$. *Inorg Chem Commun* 2004, 7(9): 1023-1026.
40. Waibel, R., Alberto, R., Willuda, J., Finnern, R., Schibli, R., Stichelberger, A., Egli, A., Abram, U., Mach, J.P., Plückthun, A., Schubiger, P.A., Stable one-step technetium-99m labeling of His-tagged recombinant proteins with a novel Tc(I)-carbonyl complex. *Nat Biotechnol* 1999, 17(9): 897-901.
41. Schibli, R., Schubiger, P.A., Current use and future potential of organometallic radiopharmaceuticals. *Eur J Nucl Med Mol Imaging* 2002, 29(11): 1529-1542.
42. Reilly, R.M., Monoclonal Antibody and Peptide-Targeted Radiotherapy of Cancer. Chapter 2: The Radiochemistry of Monoclonal Antibodies and Peptides, *Wiley* 2010.
43. Hnatowich, D.J., Virzi, F., Winnard, P.Jr., Fogarasi, M., Rusckowski, M., Investigations of ascorbate for direct labeling of antibodies with technetium-99m. *J Nucl Med* 1994, 35(1): 127-134.
44. Mather, S.J., Ellison, D., Reduction-mediated technetium-99m labelling of monoclonal Abs. *J Nucl Med* 1990, 31(5): 692-697.
45. Gano, L., Fernandes, C., Cantinho, G., Santos, A.I., Pena, H., Vieira, R., Salgado, L., Patrício, L., Technetium-99m labelling of the IOR CEA 1 monoclonal antibody: evaluation of different methods. *Nuklearmed* 1997, 36(6): 205-212.
46. Klein, M., Cohen-Cymberknoh, M., Armoni, S., Shoseyov, D., Chisin, R., Orevi, M., Freedman, N., Kerem, E., ^{18}F-fluorodeoxyglucose-PET/CT imaging of lungs in patients with cystic fibrosis. *Chest* 2009, 136(5): 1220-1228.
47. Lindström, M., Camner, P., Falk, R., Hjelte, L., Philipson, K., Svartengren, M., Long-term clearance from small airways in patients with cystic fibrosis. *Eur Respir J* 2005, 25(2): 317-323.
48. Kastelik, J.A, Wright, G.A., Aziz, I., Davies, M., Avery, G.R., Paddon, A.J., Howey, S., Morice, A.H., A widely available method for the assessment of aerosol delivery in cystic fibrosis. *Pulm Pharmacol Ther* 2002, 15(6): 513-519.
49. Peters, K.W., Okiyoneda, T., Balch, W.E., Braakman, I., Brodsky, J.L., Guggino, W.B., Penland, C.M., Pollard, H.B., Sorscher, E.J., Skach, W.R., Thomas, P.J., Lukacs, G.L., Frizzell, R.A., CFTR Folding Consortium: Methods Available for Studies of CFTR Folding and Correction. *Methods Mol Biol* 2011, 742: 335-353.
50. Ellman, G.L., Tissue Sulfhydryl groups. *Arch Biochem Biophys* 1959, 82(1): 70-77.

51. Dias, C.R., Jeger, S., Osso, J.A.Jr., Müller, C., De Pasquale, C., Hohn, A., Waibel, R., Schibli, R., Radiolabeling of rituximab with ^{188}Re and ^{99m}Tc using the tricarbonyl technology. *Nucl Med Biol* 2011, 38(1): 19-28.
52. Morais, M., Subramanian, S., Pandey, U., Samuel, G., Venkatesh, M., Martins, M., Pereira, S., Correia, J.D.G, Santos, I., Mannosylated dextran derivatives labeled with *fac*-$[M(CO)_3]^+$ (M = ^{99m}Tc, Re) for specific targeting of sentinel lymph node. *Mol Pharmaceutics* 2011, 8(2): 609-620.
53. Saha, G.B., Fundamentals of Nuclear Pharmacy. *Springer* 2003, 5th edition, New York.
54. Cunnane, C.M., O'Brien, L.M., Waight, L.A., Millar, A.M., Determination of the radiochemical purity of 99mTc medronate injection by thin layer chromatography on iTLC-SG: effect of medronate concentration on the value measured. *J Label Compd Radiopharm* 2013, 56(5): 301-304.
55. Armarego, W.L.F., Perrin, D.D., Purification of Laboratory Chemicals. *Elsevier* 1996, 4th edition.
56. Pedemonte, N., Lukacs, G.L., Du, K., Caci, E., Zegarra-Moran, O., Galietta, L.J.V, Verkman, A.S., Small-molecule correctors of defective ΔF508-CFTR cellular processing identified by high-throughput screening. *J Clin Invest* 2005, 115(9): 2564-2571.
57. Routaboul, C., Norez, C., Melin, P., Molina, M.C., Boucherle, B., Bossard, F., Noel, S., Robert, R., Gauthier, C., Becq, F., Décout, J.L., Discovery of alpha-aminoazaheterocycle-methylglyoxal adducts as a new class of high-affinity inhibitors of cystic fibrosis transmembrane conductance regulator chloride channels. *J Pharmacol Exp Ther* 2007, 322(3): 1023-1035.
58. Bertrand, J., Boucherle, B., Billet, A., Melin-Heschel, P., Dannhoffer, L., Vandebrouck, C., Jayle, C., Routaboul, C., Molina, M.C., Décout, J.L., Becq, F., Norez, C., Identification of a novel water-soluble activator of wild-type and F508del CFTR: GPact-11a. *Eur Respir J* 2010, 36(2): 311-322.
59. Kofoed, T., Hansen, H.F., Orum, H., Koch, T., PNA synthesis using a novel Boc/acyl protecting group strategy. *J Pept Sci* 2001, 7(8): 402-412.
60. Cheng-yan, H., Heng-jun, Z., Zhong-min, S., Jin-song, Z., Hong, Y., Tong-hui, M., Synthesis and characterization of a small molecule CFTR chloride channel inhibitor. *Chem Res Chinese U.* 2004, 20(3): 334-337.
61. Sonawane, N.D., Verkman, A.S., Thiazolidinone CFTR inhibitors with improved water solubility identified by structure-activity analysis. *Bioorg Med Chem*. 2008, 16(17): 8187-8195.

62. Sonawane, N.D., Zegarra-Moran, O., Namkung, W., Galietta, L.J., Verkman, A.S., Alpha-aminoazaheterocyclic-methylglyoxal adducts do not inhibit cystic fibrosis transmembrane conductance regulator chloride channel activity. *J Pharmacol Exp Ther* 2008, 325(2): 529-535.

63. Alves, S., Paulo, A., Correia, J.D.G, Domingos, A., Santos, I., Coordination capabilities of pyrazolyl containing ligands towards the *fac*-$[Re(CO)_3]^+$ moiety. *J Chem Soc, Dalton Trans* 2002, (24): 4714-4719.

64. Oliveira, B.L., Raposinho, P.D., Mendes, F., Figueira, F., Santos, I., Ferreira, A., Cordeiro, C., Freire, A.P., Correia, J.D.G., Re and Tc tricarbonyl complexes: from the suppression of NO biosynthesis in macrophages to in vivo targeting of inducible nitric oxide synthase. *Bioconjugate Chem* 2010, 21(12): 2168-2172.

65. Askonas, B.A., Farthing, C.P., Humphrey, J.H., The Significance of Multiple Antibody Components in Serum of Immunized Rabbits. *Immunology* 1960, 3(4): 336-351.

66. Raju, M., Mäeorg, S., Tšubrik, O., Mäeorg, U., Efficient solventless technique for Boc-protection of hydrazines and amines. *Arkivoc* 2009, 2009(6): 291-297.

67. Mamat, C., Reinke, H., Langer, P., NMR studies and crystal structure determinations of CF_3 group-containing bicyclic phenolates. *Z Naturforsch* 2009, 64b: 423-426.

68. Lira, B.F., Miller, J., Simas, A.M., Filho, P.F.A, Dias, A.F., Silva, R.O., Oliveira, V.C., Synthesis and complete assignments of ^1H and ^{13}C NMR spectra of mesoionic 2-(p-trifluoromethylphenyl)-3-methyl-4-(*p*-tolyl)-1,3-thiazolium-5-thiolate and 2-(*p*-chlorophenyl)-3-methyl–4-(pisopropylphenyl)-1,3-thiazolium-5-thiolate, *Arkivoc* 2004, 2004(6): 12-21.

69. Morais, M., Raposinho, P.D., Oliveira, M.C., Pantoja-Uceda, D., Jiménez, M.A., Santos, I., Correia, J.D.G., NMR structural analysis of MC1R-targeted rhenium(I) metallopeptides and biological evaluation of ^{99m}Tc(I) congeners. *Organometallics* 2012, 31(16): 5929-5939.

70. Alves, S., Paulo, A., Correia, J.D., Gano, L., Smith, C.J., Hoffman, T.J., Santos, I., Pyrazolyl derivatives as bifunctional chelators for labelling tumor-seeking peptides with the fac-$[M(CO)_3]^+$ moiety (M = ^{99m}Tc, Re): synthesis, characterization, and biological behavior. *Bioconjug Chem* 2005, 16(2): 438-449.

71. Vítor, R.F., Alves, S., Correia, J.D.G., Paulo, A., Santos, I., Rhenium(I) and technetium(I) tricarbonyl complexes anchored by bifunctional pyrazole-diamine and pyrazole-dithioether chelators. *J Organomet Chem* 2004, 689(25):4764-4774.

ANNEXES

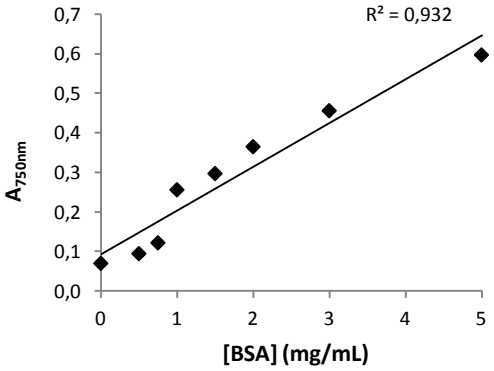

Figure 33: Standard curve describing the relation between A_{750nm} and the concentration of a series of BSA standards, used as reference for protein concentration determination.

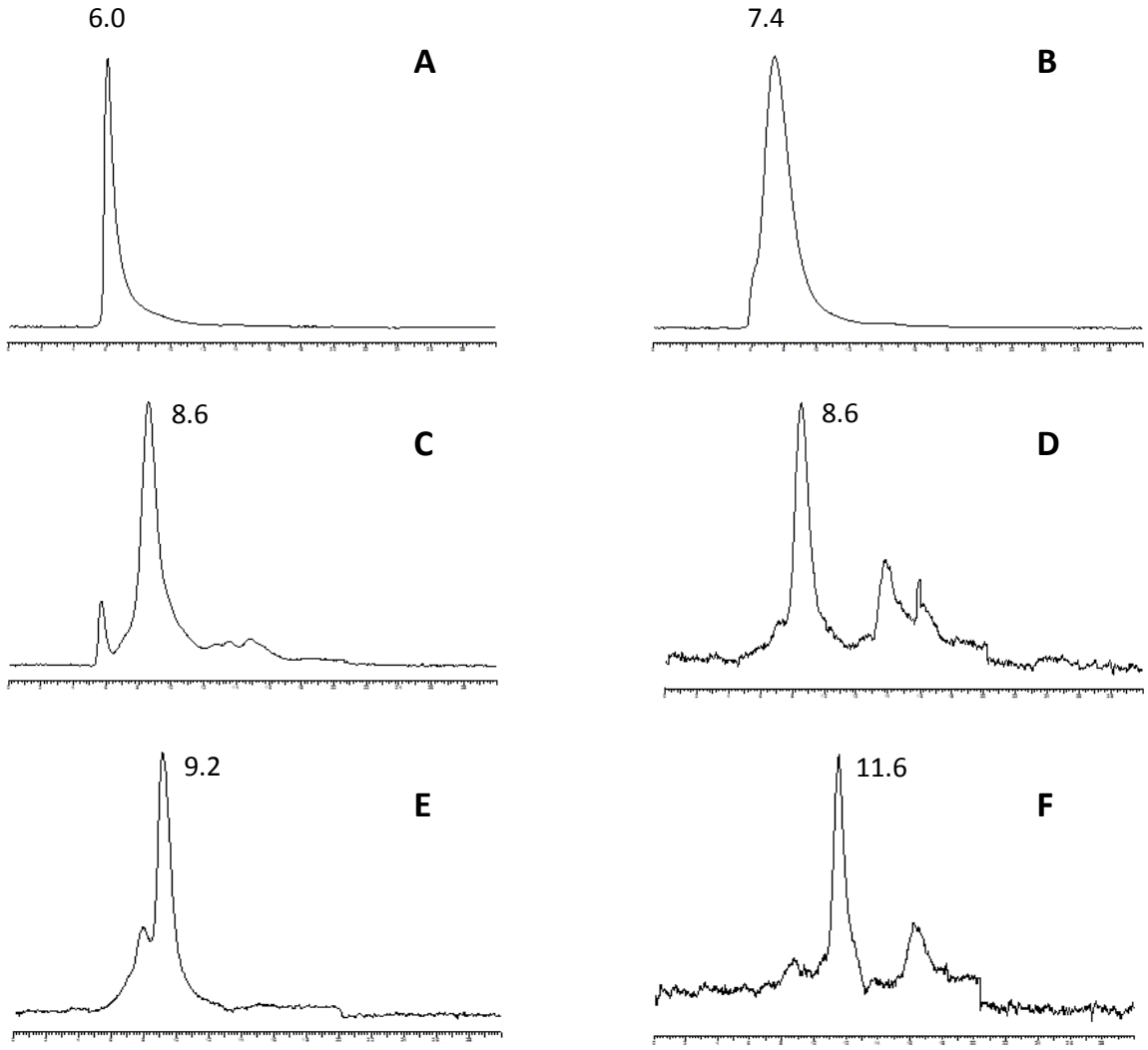

Figure 34: SE-HPLC profile of thyroglobulin (**A**), ferritin (**B**), catalase (**C**), aldolase (**D**), BSA (**E**) and ribonuclease A (**F**), using a TSK G3000SW column, with a flow rate of 1.0 mL/min and detection at 280 nm. 0.1 M Na_2SO_4 in 0.1 M phosphate buffer pH 7.0 was used as mobile phase.

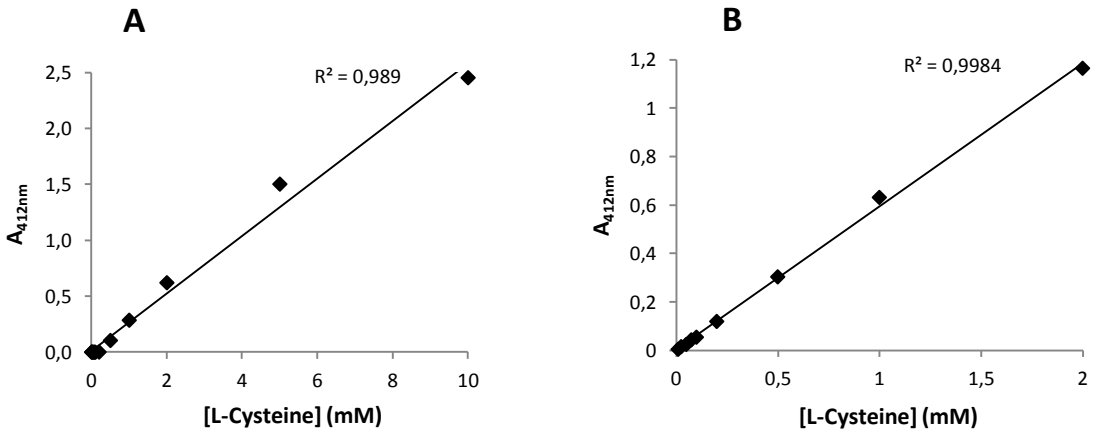

Figure 35: Standard curves describing the relation between A_{412nm} and the concentration of a series of L-cysteine standards, used as reference for determination of sulfhydryl groups. Absorbance was read using a Nanodrop 2000 (**A**) and a Varian DMS 80 (**B**) spectrophotometer.

Table 8: Values of A_{412nm} of a series of cysteine solutions obtained using two different spectrophotometers (Nanodrop 2000 and Varian DMS 80).

[L-cysteine] (mM)	A_{412nm}	
	Nanodrop 2000	**Varian DMS 80**
0.01	0.010	0
0.025	0.006	0.007
0.05	0.012	0.022
0.075	0.014	0.039
0.1	0.013	0.054
0.2	0.016	0.121
0.5	0.024	0.322
1	0.041	0.649
2	0.078	1.186
5	0.342	-
10	0.664	-

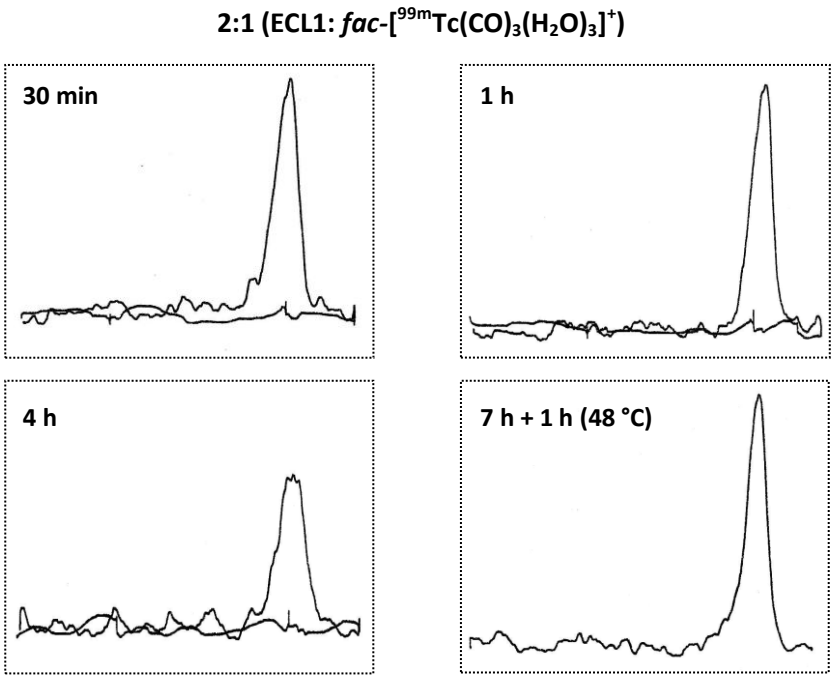

Figure 56: Analysis of the radiolabelling of ECL1 with ^{99m}Tc(I) by ITLC-SG at different incubation times, using ITLC-SG strips as stationary phase and 6 M HCl/MeOH (5/95) as mobile phase. 5 µL of a solution of *fac*-$[^{99m}Tc(CO)_3(H_2O)_3]^+$ were added to 10 µL of reduced ECL1 in PBS pH 7.4.The initial concentration of ECL1 was approximately 0.12 mg/mL.

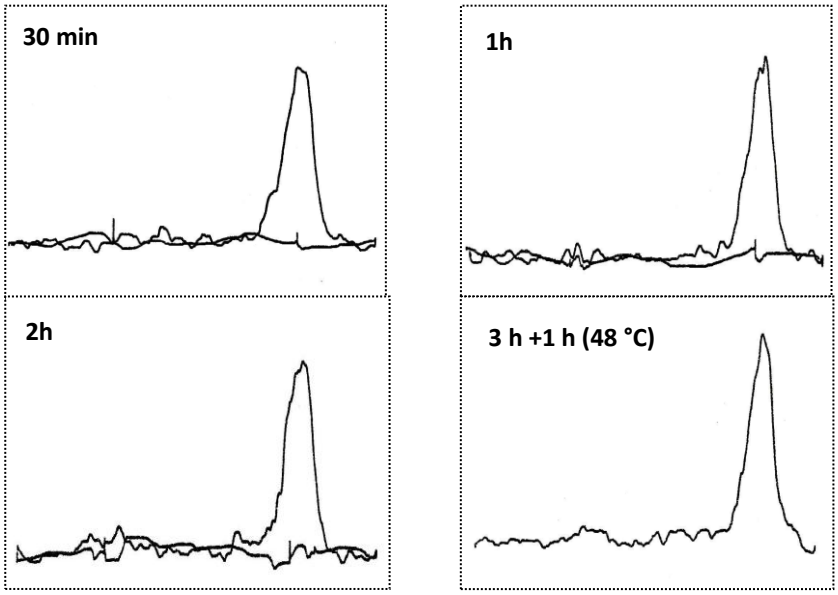

Figure 37: Analysis of the radiolabelling of ECL1 with ^{99m}Tc(I) by ITLC-SG at different incubation times, using ITLC-SG strips as stationary phase and 6 M HCl/MeOH (5/95) as mobile phase. 5 µL of a solution of *fac*-$[^{99m}Tc(CO)_3(H_2O)_3]^+$ were added to 15 µL of reduced ECL1 in PBS pH 7.4.The initial concentration of ECL1 was approximately 0.12 mg/mL.

^{1}H- and ^{13}C-NMR spectra of CFTR$_{inh}$-172a

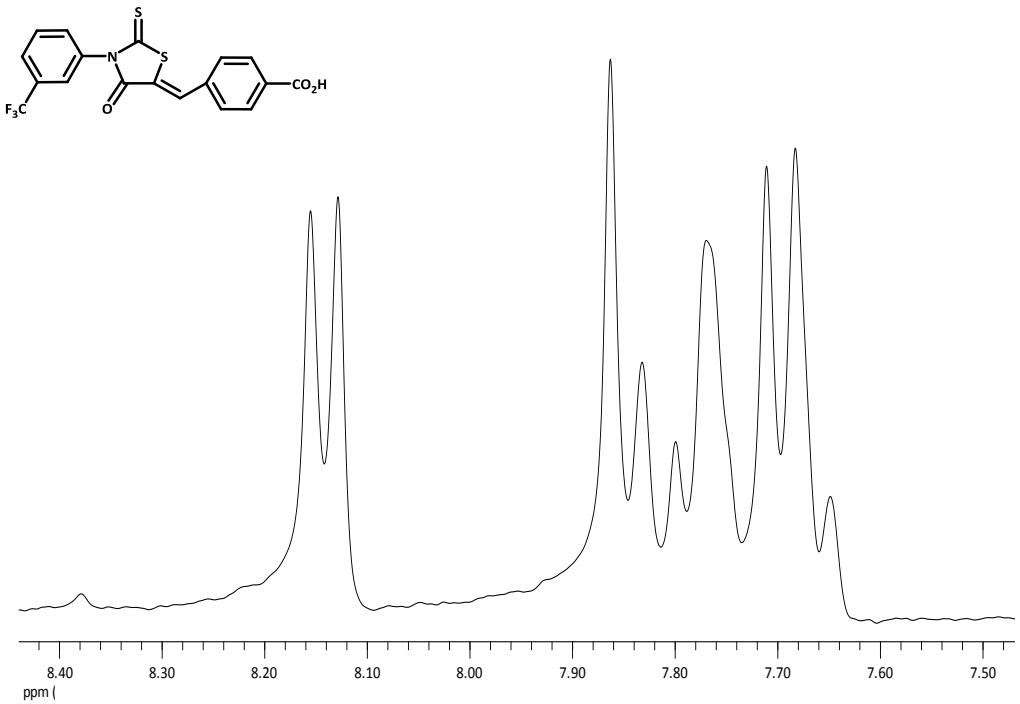

Figure 38: ^{1}H-NMR spectrum of **CFTR$_{inh}$-172a** in CD_3OD.

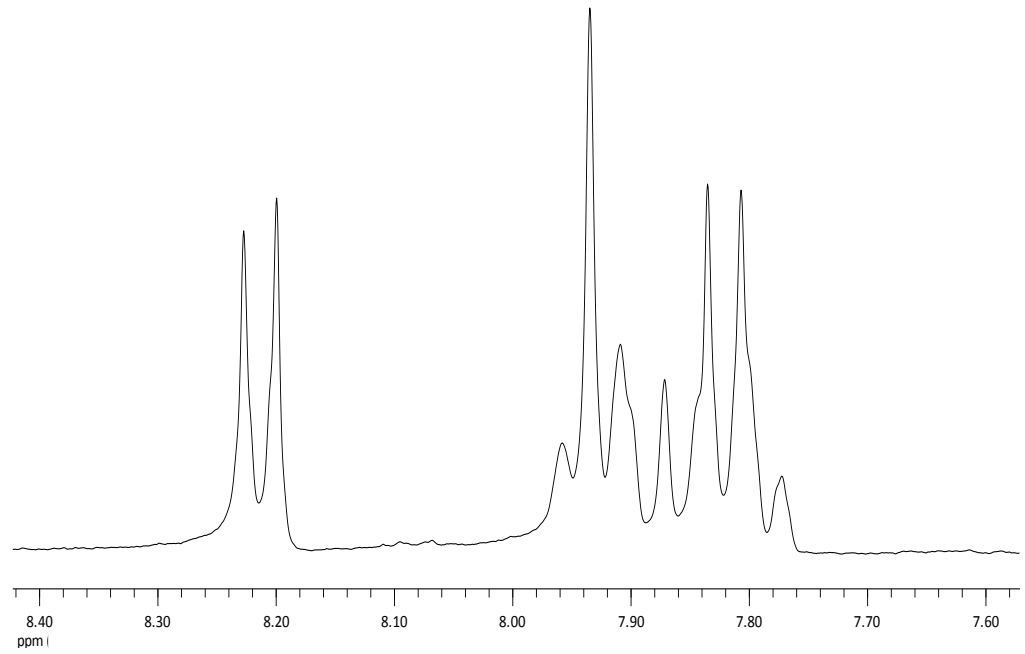

Figure 39: ^{1}H-NMR spectrum of **CFTR$_{inh}$-172a** in CD_3OD and DMSO-d_6.

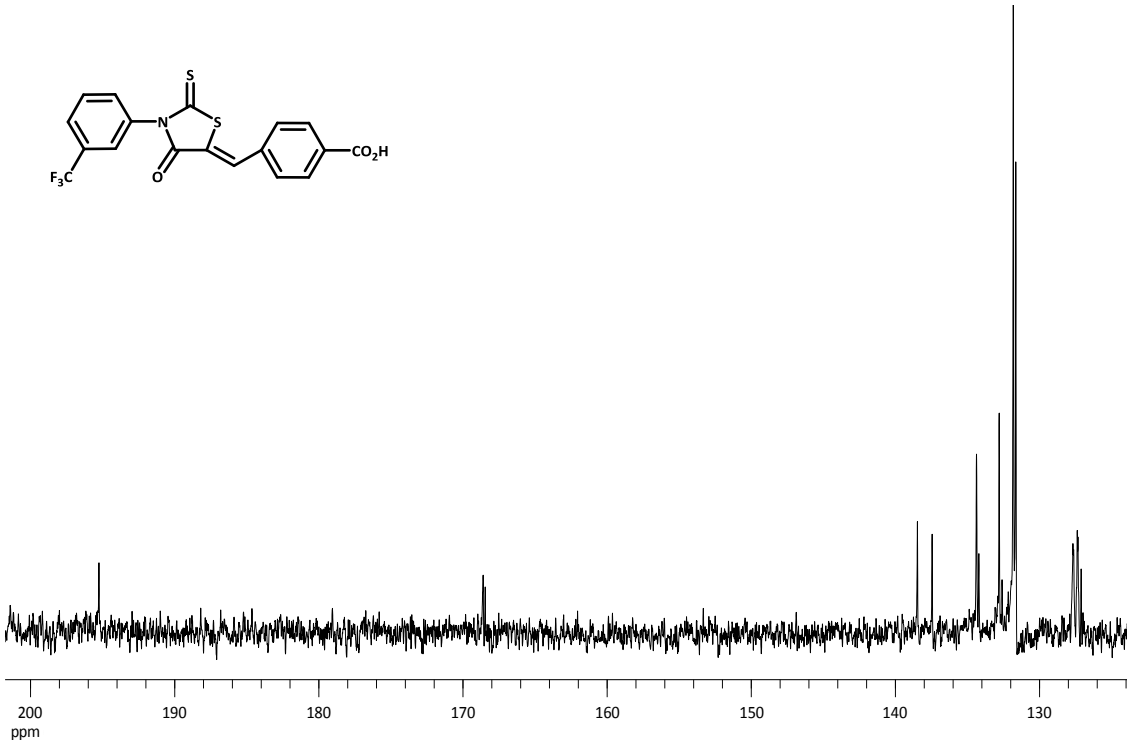

Figure 40: ^{13}C-NMR spectrum of **CFTR$_{inh}$-172a** in CD_3OD and DMSO-d_6.

^{1}H- and ^{13}C-NMR spectra of GP_{inh}-5a

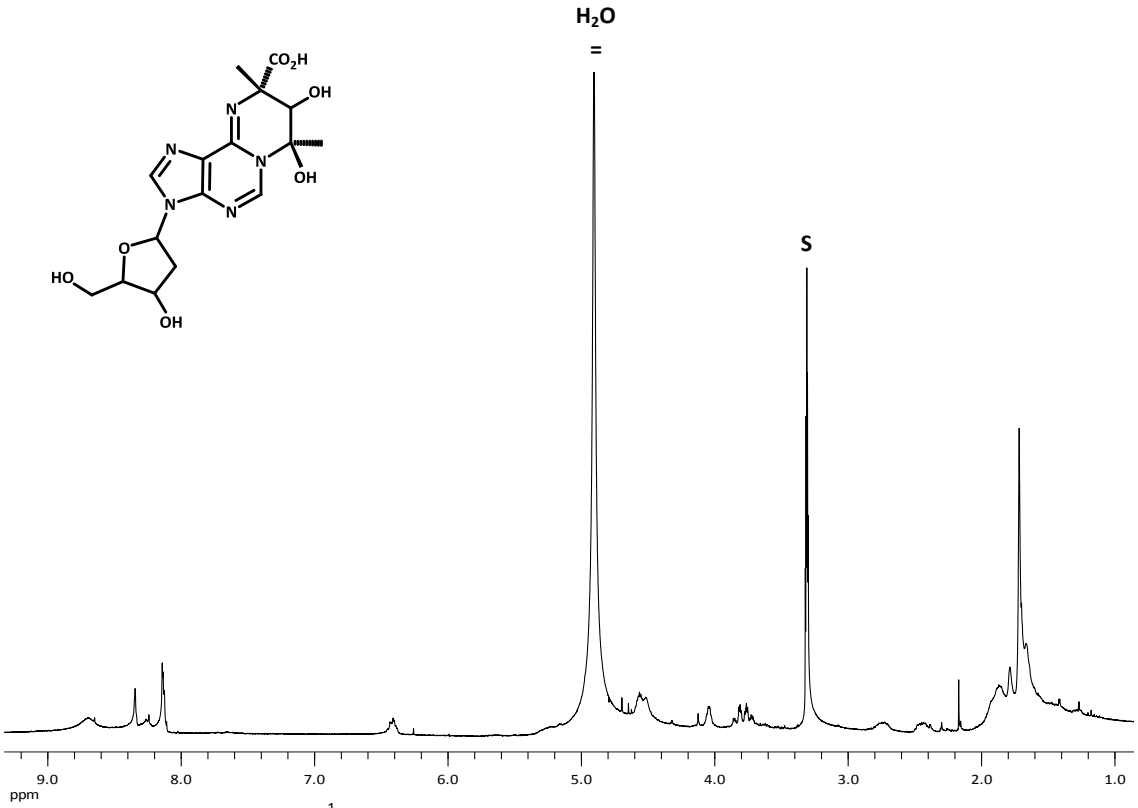

Figure 41: ^{1}H-NMR spectrum of **GP_{inh}-5a** in CD_3OD. S = residual MeOH.

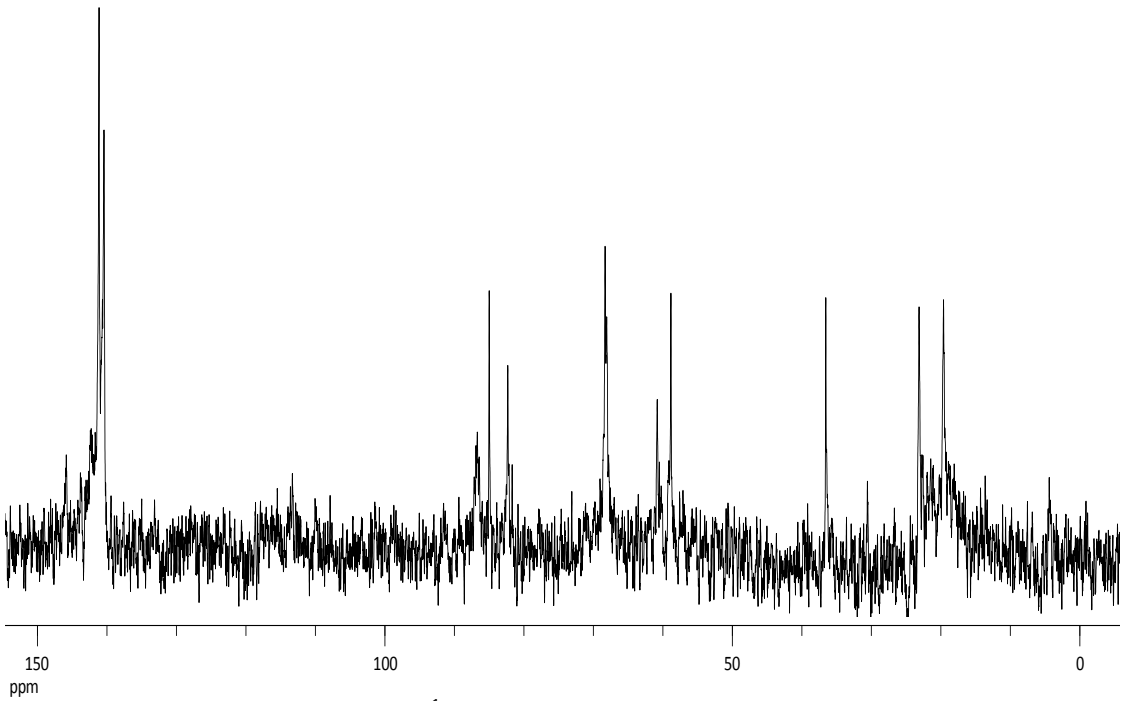

Figure 42: ^{1}H-NMR spectrum of **GP_{inh}-5a** in D_2O.

^{1}H-NMR spectra of intermediates of L1 synthesis

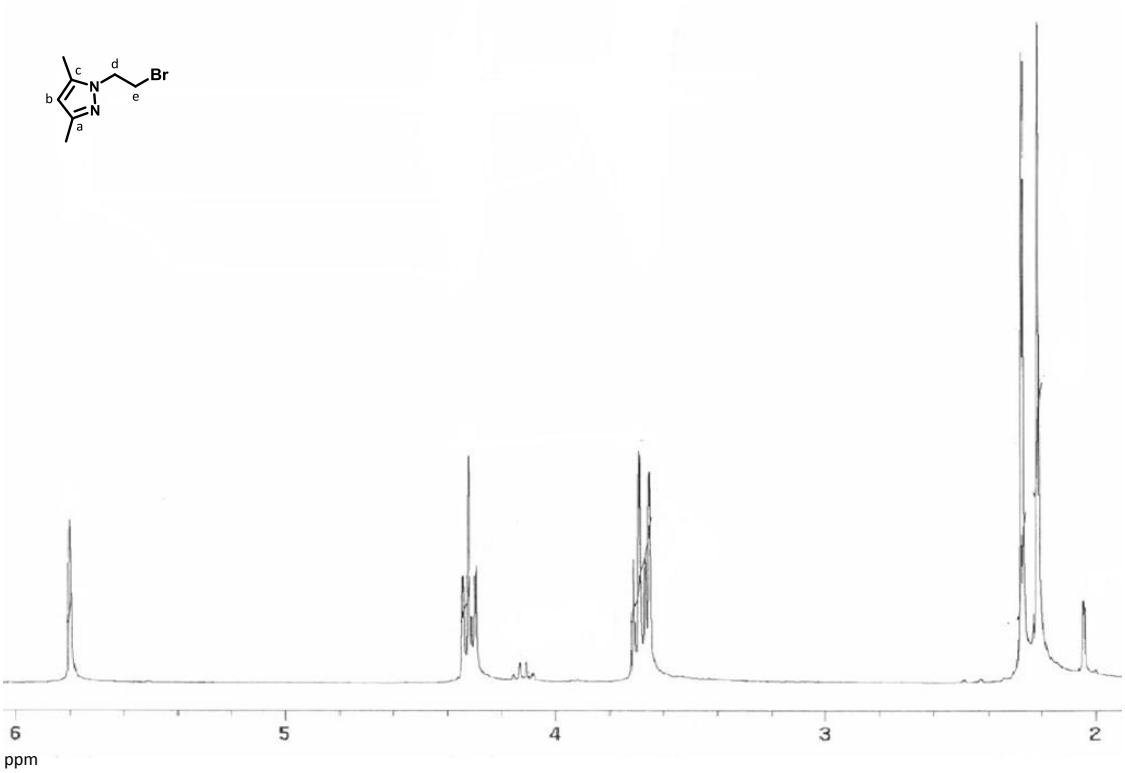

Figure 43: ^{1}H-NMR spectrum of intermediate **1** in $CDCl_3$.

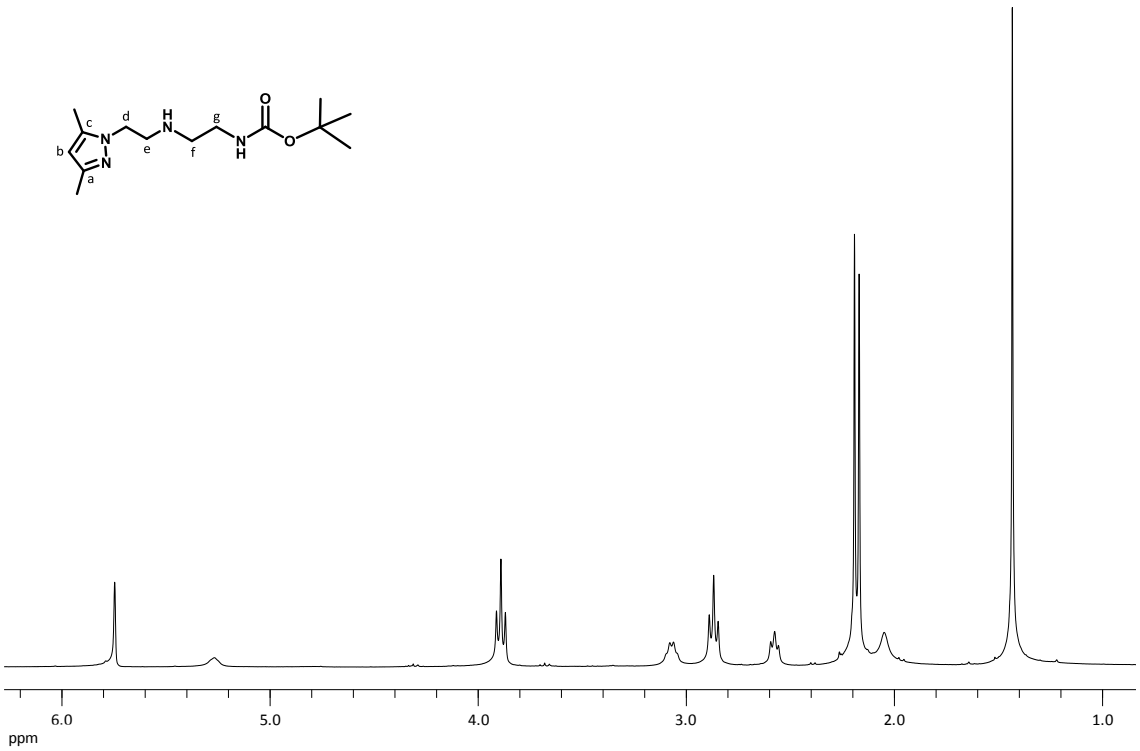

Figure 44: ^{1}H-NMR spectrum of intermediate **2** in $CDCl_3$.

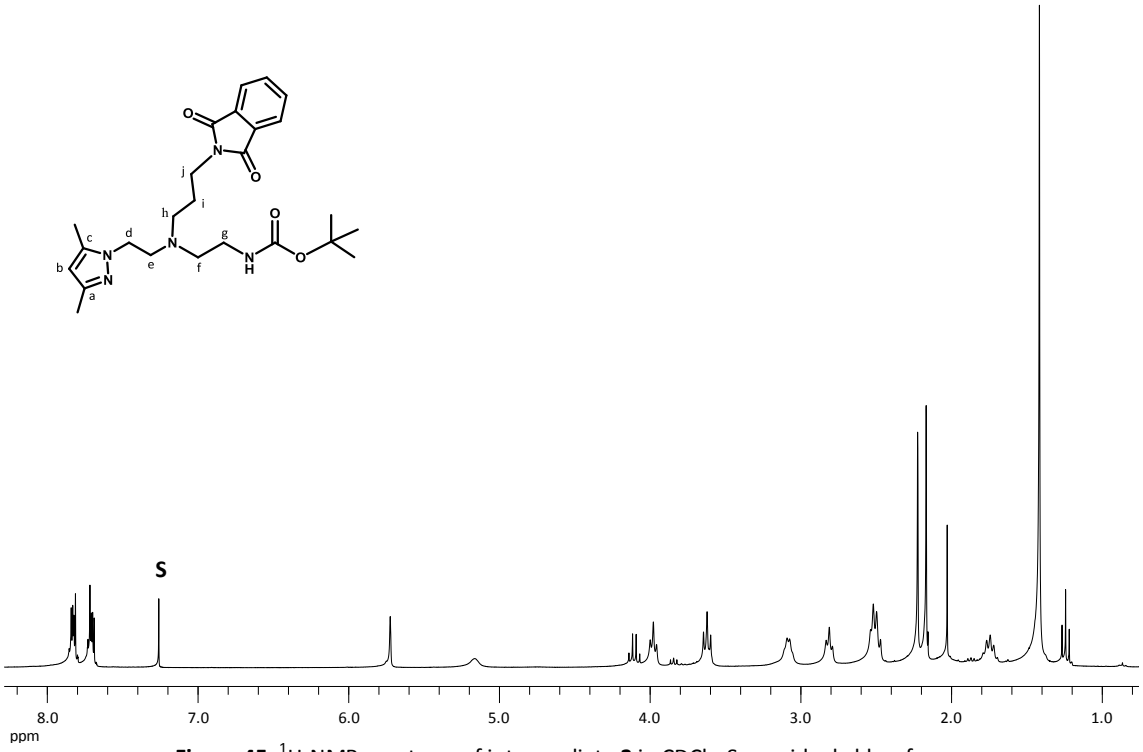

Figure 45: ^{1}H-NMR spectrum of intermediate **3** in $CDCl_3$. S = residual chloroform.

^{1}H-NMR spectrum of L1

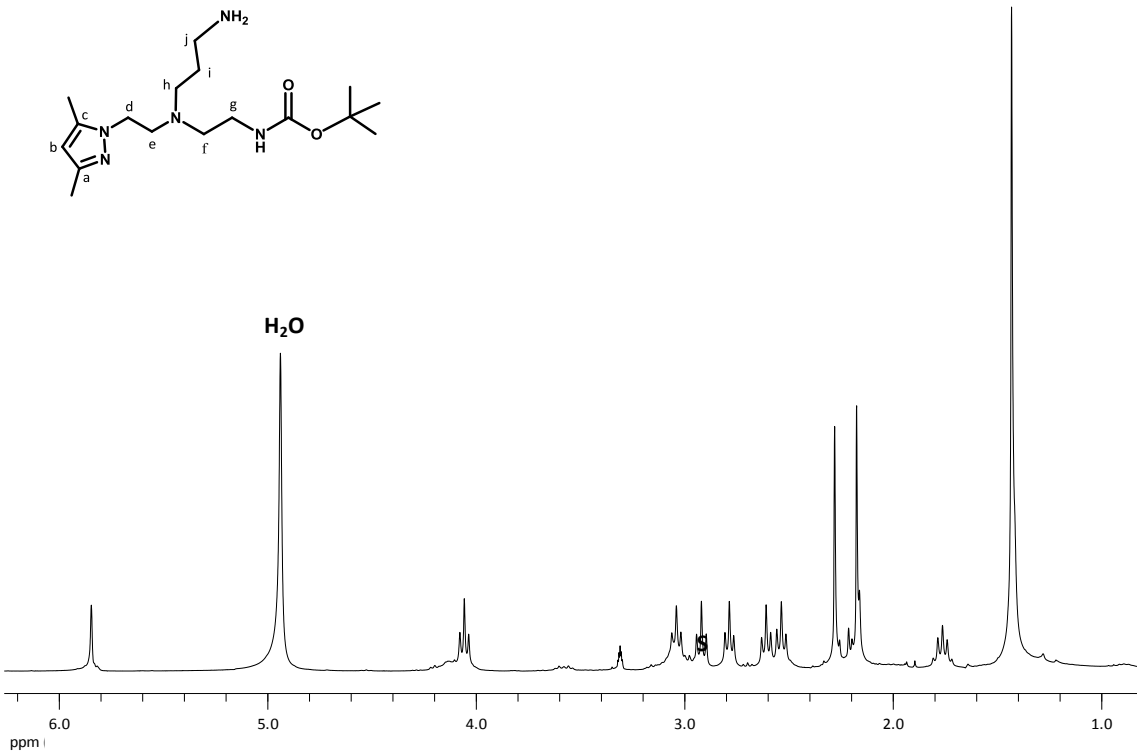

Figure 46: ^{1}H-NMR spectrum of **L1** in CD_3OD. S = residual MeOH.

^{1}H- and ^{13}C-NMR spectra of bioconjugate B1-Boc

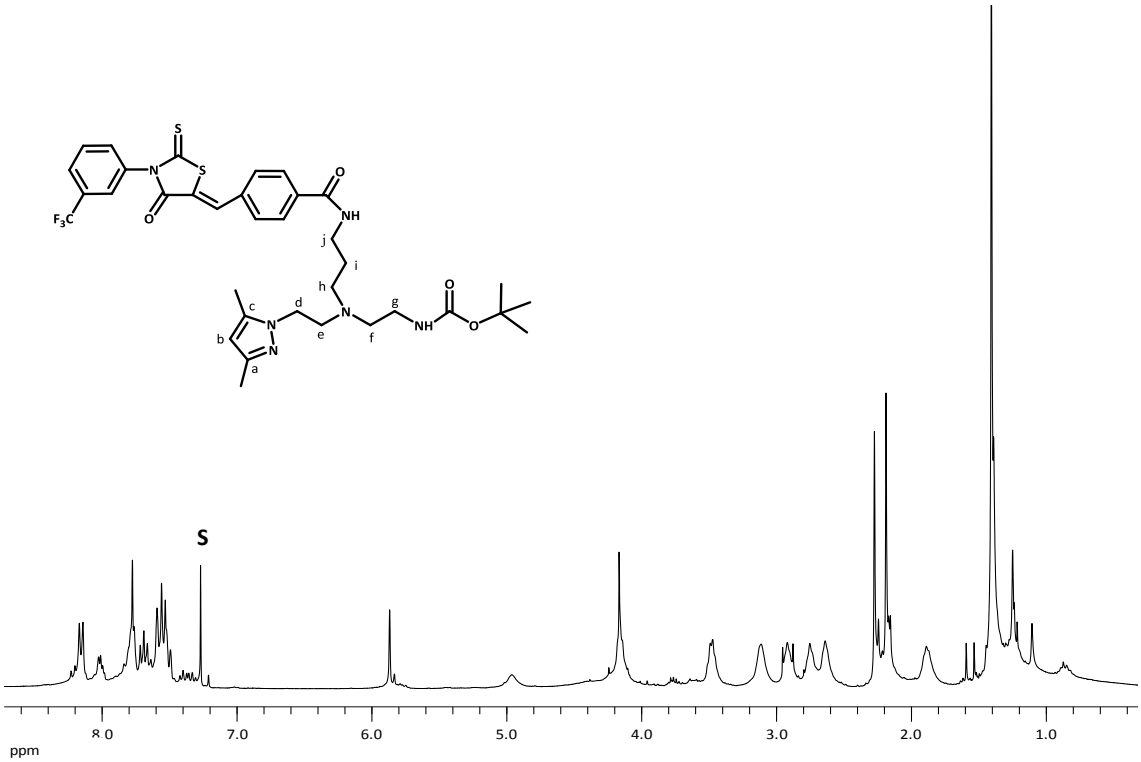

Figure 47: ^{1}H-NMR spectrum of **B1-Boc** in $CDCl_3$. S = residual chloroform.

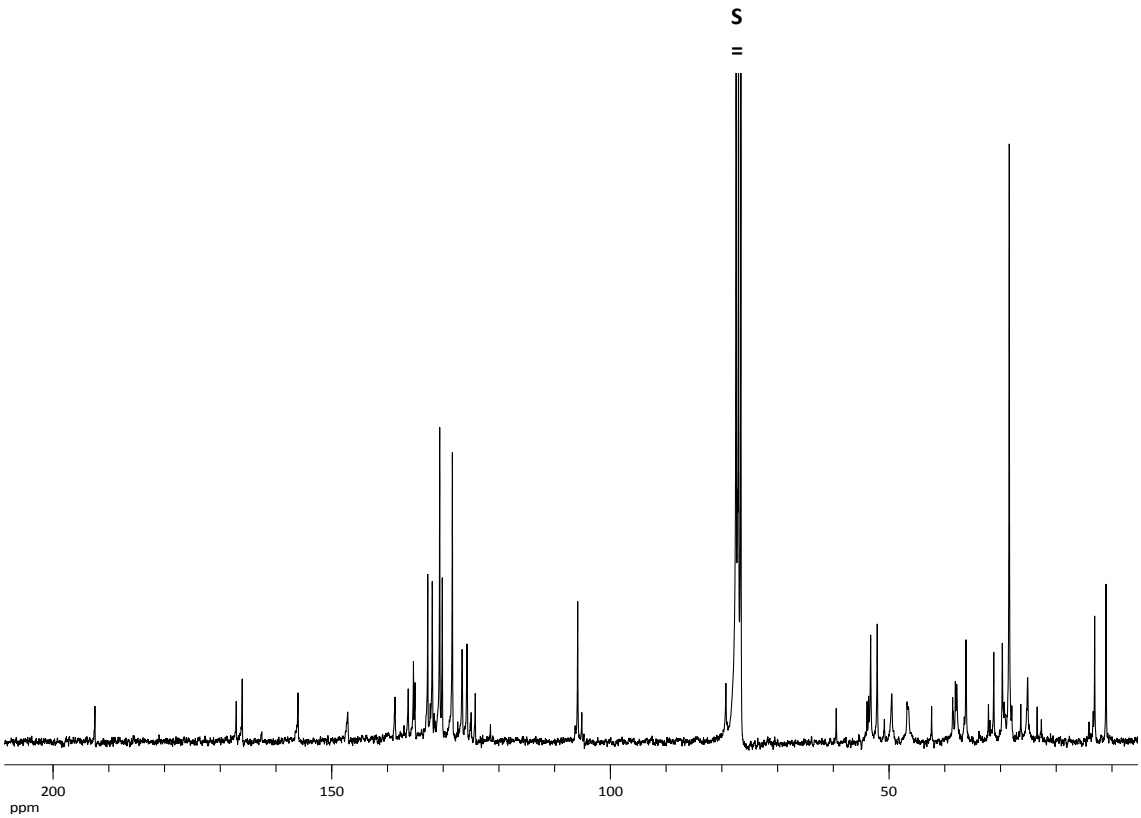

Figure 48: ^{13}C-NMR spectrum of **B1-Boc** in $CDCl_3$. S = residual chloroform.

^{13}C-NMR spectrum of bioconjugate B1

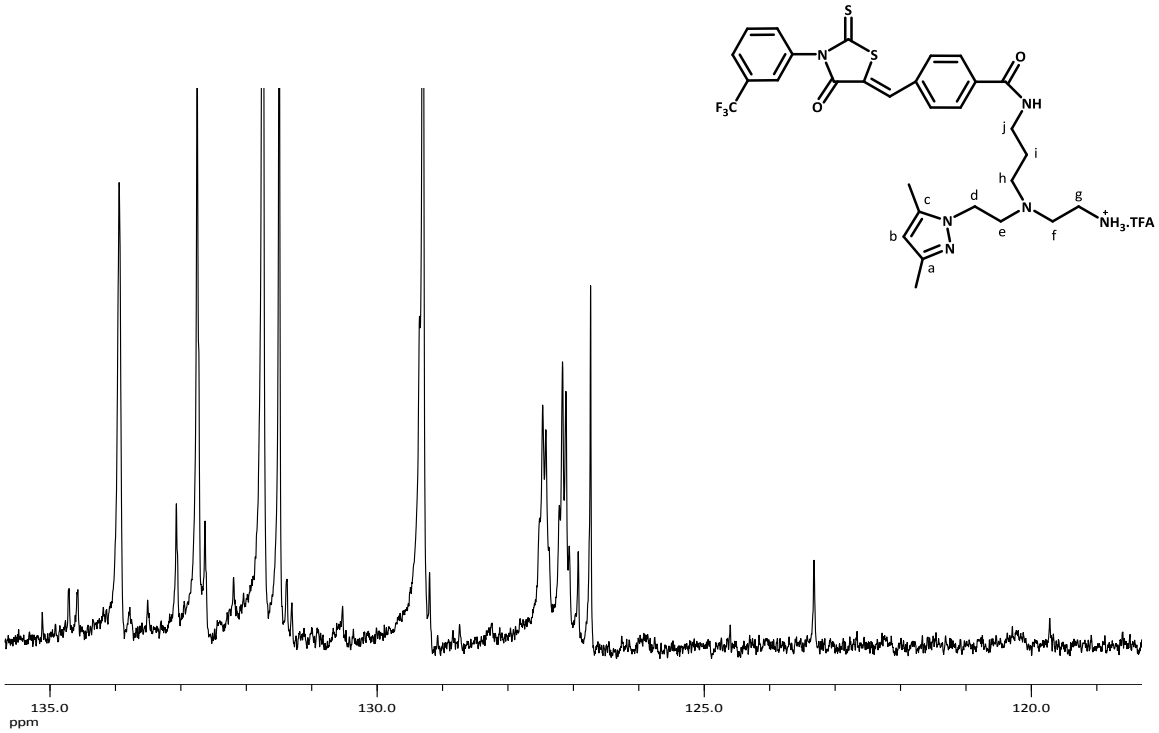

Figure 49: ^{13}C-NMR spectrum of **B1** in CD_3OD.

Table 9: Chemical shifts (ppm) of the peaks observed for the C-F coupling at one, two and three bonds distance observed in the ^{13}C-NMR spectrum of **B1**

	δ (ppm)	Mean δ (ppm)
$^{1}J_{CF}$ (272.03 Hz)	119.7	125.1
	123.3	
	126.9	
	130.5	
$^{2}J_{CF}$ (33.04 Hz)	132.2	132.9
	132.6	
	133.1	
	133.5	
$^{3}J_{CF}$ (3.80 Hz)	127.1	127.2
	127.1	
	127.2	
	127.2	
$^{3}J_{CF}$ (3.60 Hz)	127.4	127.5
	127.4	
	127.5	
	127.5	